POLITECNICO DI TORINO

Advanced numerical model for viscous friction between rough rubber and smooth ice

Master's Degree in Mechanical Engineering

Student:
Riccardo Leonardi

Academic Tutor:
ING. ALESSANDRO SCATTINA

Company Tutor:
ING. SALVATORE SCALERA

ANNO ACCADEMICO 2017-2018

Ringraziamenti

Alla mia famiglia, ai miei amici e al coraggio che dimostrate di avere nel continuare ad esserlo, nonostante tutto.

Abstract

In this work, the contact between a sliding rubber block and the ice was simulated. Both the thermodynamic and the hydrodynamic phenomena, as well as the phase change of the ice were considered in the model. The model was based on a contact theory proposed in the literature. To this aim, a FEM simulation containing a specific subroutine for the calculation of the friction coefficient, was developed. The subroutine works in parallel with a standard contact algorithm. The subroutine works starting from the value at the current time-step of the thermo-mechanical parameters e.g. the interface pressure, the nodal temperature and the sliding velocity. The subroutine gives as output of the model, step by step, the current value of the friction coefficient. The close interaction between the FEM model and the subroutine implies that, a variation of the thermo-mechanical phenomena affects also the contact friction and vice-versa. The comparison between the friction coefficient obtained with the numerical simulation and the coefficient obtained with the analytical solution proposed in the literature, showed good correlation. The accuracy of the developed numerical model was also confirmed by the comparison between the numerical results and some experimental results that can be found in the literature. The numerical model of the rubber-ice contact developed in this works is the base for the simulation of a full tire model rolling on an icy road.

Sommario

L'obiettivo di questo lavoro di tesi magistrale è stato principalmente quello di simulare il contatto di un blocco di gomma strisciante su di una superficie ghiacciata. Assieme al cambiamento di fase del ghiaccio, questo tipo di interazione porta a considerare effetti sia di natura termodinamica che di natura idrodinamica. Il modello sviluppato, pertanto, è basato su una formula per la previsione del coefficiente d'attrito ampiamente utilizzata in letteratura. Tale formula è stata poi implementata all'interno di una *subroutine* appositamente sviluppata. La *subroutine* funziona in parallelo con una simulazione termo-strutturale, in cui agisce un algoritmo di contatto standard. Al fine di fornire il valore corretto del coefficiente d'attrito, ad ogni passo, la *subroutine* necessita delle informazioni su dei parametri termo-meccanici quali ad esempio, la pressione di interfaccia, la temperatura nodale, la velocità di scorrimento. Tali informazioni provengono dalla simulazione termo-strutturale. La stretta interdipendenza tra questi due moduli, fa si che, ad esempio, una variazione delle caratteristiche termo-strutturali durante la simulazione vada ad influenzare il calcolo del coefficiente d'attrito e viceversa. Il confronto tra il coefficiente d'attrito, ottenuto con la soluzione numerica proposta in questo lavoro di tesi, e quello ottenuto con un modello analitico proposto in letteratura, mostra un buon livello di correlazione. Sulla base del modello di contatto gomma-ghiaccio proposto in questo lavoro di tesi, lo sviluppo futuro vuole essere quello di estendere questa metodologia al calcolo del coefficiente d'attrito per un intero pneumatico montato su ruota ed in contatto con una superfice ghiacciata.

Contents

1. INTRODUCTION 1

1.1. OBJECTIVES 1

1.2. OUTLINE OF THE THESIS 2

2. LITERATURE REVIEW 3

2.1. THEORY OF RUBBER FRICTION 3

2.2. RUBBER FRICTION ON ICE 4

2.2.1. Adhesive friction 5

2.2.2. Hysteresis friction 5

2.2.3. Viscous friction 6

2.2.4. Frictional effects related to the geometry of rubber block 6

2.3. RUBBER-ICE FRICTION MODELS 7

2.3.1. Microscopic model 7

2.3.2. Macroscopic model 7

2.4. FACTORS CONTRIBUTING TO THE FRICTION MECHANISM 10

2.4.1. Ambient temperature and ice conditions 10

2.4.2. Tire specifications 10

2.4.3. Vehicle specifications 11

3. MACROSCOPIC MODEL 12

3.1. INTRODUCTION 12

3.2. MODULE 2: TEMPERATURE RISE IN THE CONTACT PATCH 16

3.2.1. Effect of the operation parameters 18

3.2.2. Intermediate validation procedure 18

3.3. MODULE 3: THERMAL BALANCE ON THE CONTACT PATCH 20

4. MACROSCOPIC MODEL REPRODUCTION 23

4.1. INTRODUCTION 23

4.2. MONO-DIMENSIONAL MODEL: MODULE 1 24

4.3. MONO-DIMENSIONAL MODEL: MODULE 2 25

4.4. MONO-DIMENSIONAL MODEL: MODULE 3 26

4.5. BI-DIMENSIONAL MODEL: MODULE 1 28

4.6. BIDIMENSIONAL MODEL: MODULE 2 32

4.7. BIDIMENSIONAL MODEL: MODULE 3 34

4.8. CONCLUSION 36

5. MICROSCOPIC MODEL 39

5.1. INTRODUCTION 39

5.2. VISCOUS FORMULATION FOR RUBBER ON ICE 40

5.2.1. Thermodynamic model 43

5.2.2. Thermodynamic model with roughness effects 45

5.2.3. Hydrodynamic effects 46

5.2.4. Complete thermo-hydrodynamic formulation 52

5.2.5. Friction coefficient 52

5.3. SOLUTION OF THE THERMO-HYDRODYNAMICAL FORMULATION 54

5.3.1. Relative contact area 56

5.3.2. Average asperity diameter 57

5.3.3. Average free surface height 58

5.4. NUMERICAL RESULTS 59

5.4.1. Friction coefficient for 1 bar of nominal pressure 60

5.4.2. Friction coefficient for 5 bar of nominal pressure 61

5.5. VALIDATION PROCEDURE 63
5.5.1. Influence of nominal pressure 65
5.5.2. Influence of sliding velocity 66
5.5.3. Influence of the initial temperature of the ice 67
5.6. CONCLUSION 68
6. FINITE ELEMENT MODEL FOR RUBBER-ICE SLIDING FRICTION 69
6.1. INTRODUCTION 69
6.2. NUMERICAL FORMULATION 74
6.2.1. Discretization of phase 1 75
6.2.2. Discretization of phase 2 76
6.2.3. Discretization of phase 3 78
6.2.4. Numerical solution with Matlab 80
6.3. LS-DYNA MODEL ORGANIZATION 83
6.3.1. Geometry and material of the thermo-mechanical model 84
6.3.2. Contact condition 86
6.3.3. Load condition 88
6.4. LS-DYNA SUBROUTINE 89
6.4.1. User define variables and parameters 89
6.4.2. Stability condition 91
6.4.3. Subroutine code 92
6.5. SIMULATION RESULTS 96
6.5.1. Simulation with 1 bar of nominal pressure 97
6.5.2. Simulation with 5 bar of nominal pressure 100
6.5.3. Comparison between the LS-DYNA model and the Wiese model 104
7. CONCLUSION 109

BIBLIOGRAPHY **120**

List of Figures

Figure 1: Sketch of the rubber block sliding on the ice with a velocity v [5]. 4

Figure 2: flow chart of the macroscopic model. The green area on the left hand side represents the input section. Input parameters may come from the previous module or from an external source. The central blue area contains the three different modules. The red area on the right hand side is representative of the validation procedure 13

Figure 3: Simplified representation of the tire-ice contact patch at plane $\boldsymbol{z = 0}$. The different coloured areas represent different temperature-rise condition [4]..... 14

Figure 4: Results of the temperature rise simulation on the contact patch [4]. 18

Figure 5: Schematic representation of the results obtained with module 2 are shown in the blue area on the left hand side. The possibility of an intermediate rise temperature validation by using a thermo-camera is represented in the red area on the right hand side [4]. 20

Figure 6: on the left hand side, a schematic representation of the centreline of the tread of the contact patch obtained in [4] is showed. on the right hand side, the Gaussian pressure map on the centreline of the tread used in the mono-dimensional model is proposed. 25

Figure 7: comparison between the results in term of rise temperature. on the left hand side the rise temperature of the ice obtained with Matlab is shown. on the right hand side, the temperature rise distribution on the contact patch provided by Bhoopalam et al. [4] is shown. 26

Figure 8: Matlab GUI screen for the mono-dimensional model. 27

Figure 9: tire footprint [11]. 28
Figure 10: matrix representation of the rgb image. 29
Figure 11: on the left hand side is represented the grey-scale matrix representation is shown. On the right hand side of, the graphical representation of the matrix on the left is shown. 29
Figure 12:pressure map on the whole contact patch obtained by pre-processing the image provided by [11]. 31
Figure 13: zoom on the central zone of the contact patch. 31
Figure 14: refined zoom in the central area of the contact patch. 32
Figure 15: differences of contact and non-contact areas based on a graphical representation. 33
Figure 16: graphical representation of the matrix of the temperature. 35
Figure 17 Significative differences between temperature model's result of Bhoopalam et al. [3] and experimental measures are shown. 37
Figure 18: Sample of the tire with different levels of zoom. On the left hand side, a macroscopic sample of the tread is represented. On the centre of the image there is the rubber block subject of the thermodynamic formulation. On the right hand side of the image, the presence of the asperities is showed [5]. 41
Figure 19: Schematic representation of the geometry of the model whit the load condition and the sliding velocity [3]. 41
Figure 20: The comparison between the nominal contact area (on the left) and the real contact area (on the right) [5]. 42
Figure 21:the asperities are represented by cylinders. in the upper part, the plane Z,X is represented. in the lower part, plane X,Y is represented [5]. 47
Figure 22: Schematic representation of the squeeze-out effect [3]. 48

Figure 23: The occurrence of the saturation effect [3]. 50

Figure 24: on the left side, measurement with a contactless optical device of the rough rubber surface is shown. on the right side, the resulting 3D FEM meshed model [3]. 55

Figure 25: the relative contact area of the three rubber compounds as a function of the nominal pressure [3]. 56

Figure 26:contact pressure images from FEM contact simulation for the compound A [3]. 57

Figure 27: the average asperity diameter of the three rubber compounds as a function of the nominal pressure [3]. 58

Figure 28 the average surface height of the three rubber compounds as a function of the nominal pressure [3]. 59

Figure 29: on the left-hand side, the height of liquid layer is shown. on the right-hand side, the friction coefficient. the nominal pressure is 1 bar [3]. 61

Figure 30: on the left-hand side, the height of liquid layer is shown. on the right-hand side, the friction coefficient. the nominal pressure is 5 bar [3]. 63

Figure 31: the device used for the evaluation of the experimental friction coefficient, called High Speed Friction Tester [3]..... 63

Figure 32: The first two curves represent the operational parameters of the High Speed Friction Tester, the velocity $\boldsymbol{v(t)}$ and the normal load $\boldsymbol{FN(t)}$. The last two curves, instead, represents the output of the test, the frictional force $\boldsymbol{FR(t)}$ and the friction coefficient $\boldsymbol{\mu(t)}$ [3]. 64

Figure 33: the different value of the friction coefficient for different level of nominal pressure for the rubber compound b [3]. 66

Figure 34: the different value of the friction coefficient for different value of the sliding velocity for the rubber compound b [3]. 66
Figure 35: the different value of the friction coefficient for different value of the initial temperature of the ice for the rubber compound b [3]. 67
Figure 36: LS-DYNA simulation scheme. 70
Figure 37: the three different stages of the pre-load phase. on the left hand side, the initial condition is shown. in the centre, the apllication of the normal load is shown. on the right hand side, the sliding simulation are represented. 71
Figure 38: on the left hand side, the initial condition of the simulation is shown. On the right hand side, the deformed shape of the rubber block reached at the equilibrium is shown. 71
Figure 39: bending of the rubber block during the sliding simulation 72
Figure 40: comparison between two different level of deformation of the rubber block with different value of friction coefficient. the friction coefficient for the image on the left side is 0.12 while on the right side is 0.04. 73
Figure 41: on the left hand side, the Matlab results is shown. on the right hand side, the results obtained in [3]. Both of these plots are referred to 1 bar of nominal pressure. 81
Figure 42: the average height of the squeezed-out water obtained with Matlab for 1 (bar) of nominal pressure. 81
Figure 43: on the left hand side, the Matlab results is shown. on the right hand side, the results obtained in [3]. Both of these plots are referred to 5 bar of nominal pressure. 82
Figure 44: the average height of the squeezed-out water obtained with Matlab for 5 bar of nominal pressure. 82

Figure 45: schematic representation of the whole LS-DYNA model, with the loop between the LS-DYNA thermo-mechanical simulation and the customized subroutine for the calculation of the frictional coefficient. 83
Figure 46: geometry of the LS-DYNA model in the initial condition. The rubber block is in blue while the ice block is in red. 85
Figure 47: graphical difference between the original two blocks condition and the modified condition with shell elements. on the left hand side, the rubber and the ice block in the original configuration. on the right hand side the rubber and the ice block covered by the shell elements. 87
Figure 48: rigid plate for the load application in the initial condition. 88
Figure 49: chosen nodes for the stability condition on the leading edge of the rubber block. 92
Figure 50 friction coefficient as a function of the displacement with a nominal pressure of 1 bar 98
Figure 51: in the upper part the friction coefficient in function of the displacement is shown, in the lower part the rubber block deformed at the beginning and at the end of the simulation is shown. The condition with the squeeze-out effect for a nominal pressure of 1 bar is considered. 99
Figure 52: in the upper part the friction coefficient in function of the displacement is shown, in the lower part the rubber block deformed at the beginning and at the end of the simulation is shown. The condition with the squeeze-out effect and the melting of the ice for a nominal pressure of 1 bar is considered. 100
Figure 53: friction coefficient as a function of the displacement with a nominal pressure of 5 bar 101

Figure 54: in the upper part the friction coefficient in function of the displacement is shown, in the lower part the rubber block deformed at the beginning and at the end of the simulation is shown. The condition with the squeeze-out effect for a nominal pressure of 5 bar is considered 102
Figure 55: in the upper part the friction coefficient in function of the displacement is shown, in the lower part the rubber block deformed at the beginning and at the end of the simulation is shown. The condition with the squeeze-out effect and the melting of the ice for a nominal pressure of 5 bar is considered 103
Figure 56: in the upper part the friction coefficient in function of the displacement is shown, in the lower part the rubber block deformed at the beginning and at the end of the simulation is shown. The condition with the saturation effect for a nominal pressure of 5 bar is considered 104
Figure 57: friction coefficient versus time for 1 bar of nominal pressure obtained with LS-DYNA..... 105
Figure 58: overlapping of the ls-dyna model's results curve (in red) and the wiese's results (in blue) [3] for 1 bar of nominal pressure. 106
Figure 59: friction coefficient versus time for 5 bar of nominal pressure obtained with LS-DYNA..... 107
Figure 60: overlapping of the ls-dyna model's results curve (in red) and the wiese's results (in blue) [3] for 5 bar of nominal pressure. 108

List of Tables

Table 1: thermal properties of ice and tire's rubber [4]. 24

Table 2: operational parameters used in the tests conducted by Bhoopalam et al. [4]... 24

Table 3: Elastic moduli of the three different rubber compounds. 54

Table 4: user defined friction parameters with symbol, numbering and the indication of the numerical value with the relative unit system. 90

Table 6: operational parameters for the LS-DYNA simulation 96

Table 7: material parameters for medium rubber compound 97

Table 8: contact parameters for the LS-DYNA simulation with 1 bar of nominal pressure. 97

Table 9: contact parameters for the LS-DYNA simulation with 5 bar of nominal pressure 100

Nomenclature

(X, Y, Z)	Coordinates of the heat source
(x, y, z)	Coordinates of the point of the heat rise
α	Thermal diffusivity (m^2/s)
ΔT	Temperature rise (°C)
η_{water}	Viscosity of the water $(Pa\ s)$
λ	Thermal conductivity for the microscopic model $(W/m\ K)$
μ	Friction coefficient
τ	Viscous shear stress (Pa)
A	Generic contact area (m^2)
d	Depth of heat penetration (m)
D_{asp}	Diameter of the asperity (m)
F_{Shear}	Shear force (N)
F_Z	Normal load (N)
h	Height of liquid layer (m)
H_s	Average height of squeezed-out water (m)
H_V	Average height of the free rubber surface (m)
k	Thermal conductivity for the macroscopic model $(W/m\ K)$
k	Relative contact area
L_{ice}	Latent heat of the ice (J/kg)
p	Pressure (Pa)
p_{nom}	Nominal pressure (Pa)

Q	Instantaneously generated heat (J)
R	Rolling radius of the tire (m)
S	Longitudinal slip ratio
V	Longitudinal velocity for the macroscopic model (m/s)
v	Longitudinal velocity for the microscopic model (m/s)

Chapter 1

1. Introduction

Nowadays, safety drive on icy road conditions is one of the most important challenges in the tire industry. Under these conditions, the frictional behaviour between the car and the road is characterized by the lowest value of the friction coefficient. The lower the value of friction coefficient, the higher the probability of losing control of the car so, it is clear the importance that developing new methods to improve grip performance could have. A clearer understanding of the contact phenomena which occurs in rubber-ice interface, could be very helpful in winter tire design. Numerical prediction of rubber-ice friction in different environment conditions and for different rubber compounds could be a very useful tool in tire design. Unfortunately, the number and the physics of the phenomena involved as well as the dimensions of the problem, until this moment, did not allow to develop a unified solution for the problem, at least in the numerical simulation area.

1.1. Objectives

The aim of this Master Thesis' project is the development of a tool which allows to predict the friction coefficient of rubber-ice sliding contact. The theoretical formulation used is based on a widely-used formula, [3]. Thermodynamic effects as the melting of the ice, and the related hydrodynamic effects are taken into account. In particular, the developed tool consists in a subroutine written by using a commercial code LS-DYNA. Thinking about a whole vehicle simulation, could be possible to have a better degree of

comprehension about the influence of the operational parameters as normal pressure on the tire, car speed, tire and vehicle specification but also ambient and ice temperature. Trough the integration of this results in a complete and experimental-matching model, should be possible to develop different strategies for the winter tire industry.

1.2. Outline of the thesis

This Master Thesis' work is organized as follow. Chapter 2 presents a general literature review on the tire-ice contact theory and on the developed predictive models. Starting from the rubber contact theory on a generic hard surface, the main topic of the sliding contact of the rubber on ice are discussed. Two different approach of study are presented. The macroscopic one, whit the goal to predict the friction coefficient considering the whole contact patch of the tire on ice. The microscopic one which is focused on the phenomenological study of the interaction between the rubber and the ice. Chapter 3 contains a description of the macroscopic model developed by Bhoopalam et al. [4, 9] whereas, in chapter 4 a reproduction of the same model performed with Matlab is presented. The microscopic model based on the viscous formulation, developed by Wiese et al. [3], is described in Chapter 5. The FEM model developed by using the commercial code *LS-DYNA* is presented in Chapter 6. The customized subroutine for the calculation of the friction coefficient based on the theory proposed in [3] is also described in Chapter 6. Finally, in Chapter 7 the conclusion in term of quality of the results obtained and possible future developments are detailed.

Chapter 2

2. Literature Review

2.1. Theory of rubber friction

Rubber friction is characterized by a completely different behavior in comparison of other materials. The reasons of these significant differences can be found in the very low elastic modulus of rubber and in the high internal friction exhibited by the rubber over a wide frequency region. The main studies about the contact and the friction theory were made by B. Persson, [1, 2, 6, 7].

The general Persson's friction theory starts with a contact between the rubber and a rough surface. Under these conditions, the frictional behavior of a sliding rubber block on a hard surface, is characterized by different mechanisms that are classified as follows:

- Hysteresis friction, due to viscoelastic energy losses; during sliding the asperities of the rough substrate exert oscillating forces on the rubber surface, leading to a cyclic deformation of the rubber, and to an energy dissipation via the internal damping of the rubber [1, 2, 3].
- Adhesive friction, due to the atomic scale interaction [1, 3].
- Viscous friction, due to the presence of a liquid layer in the gap between the surfaces [1, 2, 3].
- Frictional effects related to the geometry of the rubber block [3].

However, the role of each previous phenomena can be specified for the rubber-ice contact.

2.2. Rubber friction on ice

Sliding contact between rubber and ice is characterized by a completely different interaction of the physical phenomena that generally occur during the contact between rubber and other (hard) common solid material. The most significant difference is the presence of the *premelting* phenomenon for which, at the rubber-ice interface, there is a thin liquid water layer, even in the absence of sliding. As said by Persson [1], considering the microscopic rough surface of rubber, the large thermal movement which affects the rubber molecules, leads to break up any icelike structure at the interface. For this reason, it is plausible that a thin liquid layer does not exist when ice is in contact with a hard, high energy solid surface, such as glass, metal, stone, etc.

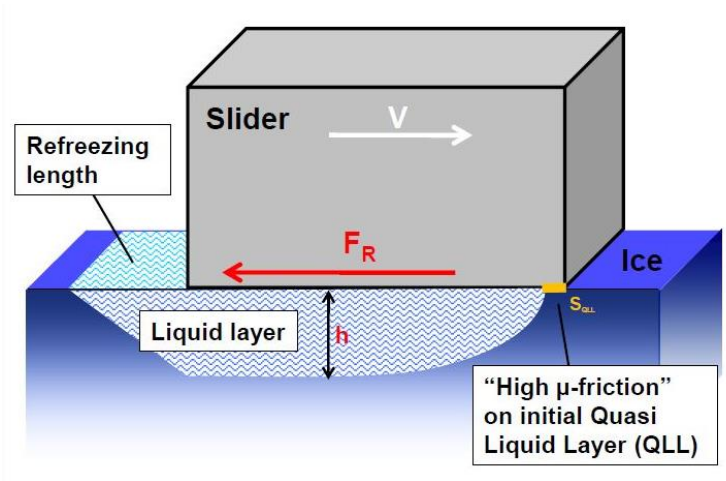

FIGURE 1: SKETCH OF THE RUBBER BLOCK SLIDING ON THE ICE WITH A VELOCITY V [5].

2.2.1.Adhesive friction

The adhesive contribution results from the real contact area that rubber and ice share during the sliding. Unfortunately, the evaluating of this area is a very hard task because of the roughness on very wide distribution of length scale, deformation of both solid in contact, relative motion between rubber and ice.

However, it is also important to consider that, for detecting a tangible contribution of the adhesion force, it is necessary to have completely flat surfaces in contact. For example, the adhesive friction can be neglected in rubber-ice contact, where at least the rubber surface has a micro-roughness. [1, 3]. Moreover, as showed in [8], the adhesive rate to the friction coefficient is directly proportional to the frictional shear stress that, in case of meltwater film between rubber and ice surface (considering also the *premelitng* phenomena), decreases considerably, leading to a negligible value of adhesive friction with respect the other phenomenon.

2.2.2. Hysteresis friction

A lot of studies were made on the hysteresis friction by Persson et al., [1, 2, 7], where, a theory for predicting a viscoelastic contribution to the friction coefficient was proposed. In this theory, the energy that comes from the cyclic deformation of the rubber, caused by the asperities of the road, can produce a significant friction force. The friction force depends on the nature of the substrate surface roughness and on the sliding velocity. The modelling of surface roughness is made considering the length scale and the corresponding frequencies distributions. In particular, Persson found that *"surface roughness of different length scale contribute equally to the friction force if the ratio between the amplitude and wavelength is constant",* [1]. Consequently, the studying of

the roughness effect, for all length scales, can be very important. For this reason, the study of Persson was extended to a general *"Multiscale physics of rubber-ice friction"*, [2], where ice surface topography is analyzed under linear friction test with a rubber slider. Although this is a very characteristic and specific phenomenon on rubber friction, considering a sliding contact between viscoelastic solid with a rough surface (rubber) on a rigid solid with smooth surface (ice), *"no hysteresis friction is generated during the sliding interaction"*, [1, 3, 7]. The contribution of the hysteresis to the friction is negligible until the transient behavior becomes relevant.

2.2.3.Viscous friction

According to [3, 5], considering a microscopic sample of rubber block, the microscopic contact mechanic is mainly determined by the viscous friction in the thin layer of melted water under the microscopic contact patches. Under sliding, the frictional shear force is determined partly by using general Coulomb friction law and partly considering the Newton law for viscous friction. The heat from shear stress leads to a continuous melting on the ice surface.

2.2.4.Frictional effects related to the geometry of rubber block

All macroscopic effects like geometrical block characteristics are neglected both in viscous model and in viscoelastic model. This comes from the experimental observation that the real microscopic contact area, instead of the nominal contact area, has a considerable influence on the resulting friction coefficient. However, considering macroscopic models, the effect of the geometry of rubber block becomes very important for the determination of the friction coefficient in contact patch.

2.3. Rubber-ice friction models

Overall, it is possible to distinguish between microscopic model and macroscopic model. Both types of model are based on contact theory proposed by Persson. The main differences are in the fact that while the macroscopic one is referred to the whole contact patch of the tire leading to an average friction coefficient, the microscopic considers only a sample of a rubber block to reproduce the frictional phenomena.

2.3.1.Microscopic model

The purpose is to obtain a qualitative prediction of the friction coefficient according to the physics of the problem; it is possible to consider all the previously mentioned phenomena, or just the ones that, in the particular studying scenario, it is thought to be more representative. The result is, in general, a non-stationary value of friction coefficient that is different, point by point, in the geometry of the problem.

2.3.2.Macroscopic model

The macroscopic model allows to predict the average friction coefficient based on empirical information and, in general, operational parameters, e.g. mechanical property of the tire, inflation pressure, pressure and temperature map on contact patch etc.

This procedure is very useful, especially for practical applications related to the tire development, when there is a large possibility of experimental testing directly on the tire in different conditions. Anyway, the numerical simulation of rubber friction on ice, e.g., by means of finite element method, remain a very challenging task, considering the complexity of the physical processes. The solution proposed in [8] is to use the result of friction experiments as input for the numerical simulation. This can be possible by using

empirical friction formulas, with the aim to interpolate experimental results between the different tested situations. For example, Macnabb et al. [9], developed a relation to predict the friction coefficient as a function of velocity and stopping distance of the vehicle, based experimental data. The equation (1.1) shows this relation.

$$\mu = V^2/(254 \cdot d) \tag{1.1}$$

Where, V is the vehicle speed in $\left(\frac{km}{h}\right)$ and d is the stopping distance in (m).

The model developed by Navin et al. [9], considers the effect of the aggregate and ambient temperature on friction coefficient. From tests conducted with different vehicle, the formula obtained is the (1.2).

$$f_x = 0.11 - 0:0052T + 0:0002A, A < 1000 \ \ (g/m^2) \tag{1.2}$$

Where A is the aggregate application in $\left(\frac{g}{m^2}\right)$ and T is the temperature in (°C).

Other models consider a friction law based on the difference between wet and dry area on the contact patch. According to Hayhoe and Sahpley [9], the friction coefficient is a function of the heat generated by fluid friction and the heat conducted into the tire. Formula (1.3) shows this relationship.

$$\frac{dh}{dx} = \frac{A}{h} - \frac{B}{\sqrt{x}} \tag{1.3}$$

Where:

$$A = \frac{Friction\ Flux}{Melt\ Flux} \cdot h \tag{1.4}$$

$$B = \frac{Conduction\ Flux}{Friction\ Flux} \cdot \sqrt{x} \tag{1.5}$$

And, h is the height of water film in (m) and x is the longitudinal dimension of the contact patch in (m).

The traction model proposed by Peng [9], is also based on thermal balance in contact patch. It is necessary to setup the model to distinguish between elliptical, showed in formula (1.6) or rectangular contact patches showed in formula (1.7). By using mass conservation, energy conservation and momentum conservation laws, the friction coefficient can be estimated as follow:

$$f_m = \eta \cdot \frac{U_s}{h} \cdot \frac{1}{p_0} \cdot \frac{x_m \cdot y_m \cdot 2}{\pi \cdot l} + f_d \cdot \left(\frac{(l - x_m)\,(\pi - 2 \cdot y_m)}{\pi \cdot l} \right) \tag{1.6}$$

$$f_m = \eta \cdot \frac{U_s}{h} \cdot \frac{1}{p_0} \cdot \frac{x_m^2}{\pi \cdot l} + f_d \cdot \left(1 - \frac{x_m}{\pi \cdot l}\right) \tag{1.7}$$

Where f_m is the average friction coefficient on the contact patch, f_d is the coefficient of dry friction, h is the height of melted water in (m), p_0 is the average pressure across the contact patch in (Pa), l is the length of contact patch in (m), U_s is the sliding velocity in $\left(\frac{m}{s}\right)$ and x_m is the length of dry area in (m).

2.4. Factors contributing to the friction mechanism

Considering tire-ice interface, there are numerous factors that affect the frictional behavior with direct effects on the performance, [9, 4]. It is possible to distinguish:

- Ambient temperature and ice conditions
- Tire specifications
- Vehicle specifications and type

2.4.1.Ambient temperature and ice conditions

Temperature has considerable influence on tire performance. In particular, the lower the temperature is, the higher the friction force was observed, [9]. One reason for this could be found in the fact that, for cold ice surface (about -10°C), high adhesion level was observed. Changing in the ambient temperature alters property on ice surface, especially when the temperature increases its value close to 0°C with the beginning of the phase-changing. Temperature affect also ice crystal size and, experimentally, it has been observed higher value of friction coefficient for ice with larger crystal size, [9]. Moreover, the presence of impurities affects also the traction behavior on ice in different ways. Initially, the friction coefficient is increased as well as the rate of melting of the ice and so, the formation of water film that reduces traction force, [9].

Others important parameters are the age and the texture of the ice, [9].

2.4.2.Tire specifications

Clearly the tire itself is another crucial factor that is necessary to take into consideration in friction studying. For instance, the effects of tread pattern and compound are very

important. Experimentally, it was seen that the addition of hard aggregate, which works as small studs, improves both tractive and braking performance under icy conditions as well as the possibility to increase the glass transition temperature of the tread compound, [9]. The tire normal pressure has also a substantial influence for traction on ice surface, in particular it affects the dimension and the shape of the contact patch. A lot of tests demonstrate that, the lower the value of the normal pressure the higher the friction coefficient, [9]. In conclusion, it is possible to say that a rectangular shaped contact patch leads to a better traction condition than the elliptical shaped interface, [9].

2.4.3.Vehicle specifications

The type and the condition of the vehicle, as well as the presence of safety system as traction control or ABS, are crucial for the determination of the friction coefficient on ice. In general, from experimental tests results that cars are more safety than trucks, at least on ice condition. This is showed in [9], and it also can be considered as a confirm of the theoretical consideration about the role of the normal pressure. Considering also electric vehicle, the fact that the rolling resistance in this kind of vehicle is generally 30 % lesser in comparison to a conventional vehicle, leads to a worse traction behaviour than the conventional endothermic-engine vehicle, [9].

Chapter 3

3. Macroscopic model

3.1. Introduction

Macroscopic models usually are developed in relationship with the experimental facilities available. In general, the subject of the study is the whole geometry of the problem and, the theoretical results are developed through empirical considerations. So, in tire-ice contact literature, frequently the macroscopic models proposed consist in a formula that comes from an interpolation procedure of experimental data. In this work a specific macroscopic model was replicated [4, 9], at least mathematically, in order to obtain the same theoretical procedure.

First of all, in this model there is a development of a friction theory, principally based on thermodynamic considerations. The most particular aspect of this model is the modular structure. The model is made up of three different modules. In figure 2 is schematically shown the model's organization. Theoretically, each module needs input variables that comes from the previous module and gives output results which work as input for the next module (green area on the left of the image). However, the user has completely freedom of choosing the best way to insert the input parameters for each module. The central part of the image, in blue, contains the sequence of the modular structure, thus obtained to reflect of all the theoretical procedures used in order to obtain final results. Moreover, a relative simple experimental procedure, was also proposed in the intermediate module, in order to validate both final result (friction coefficient) and the

middle input/output module's information. In particular, as shown in the right side of the image with red colour, there are two validation parameters:

- The temperature in the contact patch - intermediate
- The friction coefficient - final

On one side, the aim of this procedure is, to have a better comprehension of the relative influence of each intermediate result. On the other side, the procedure refines the matching level between the final output and the experimental measure.

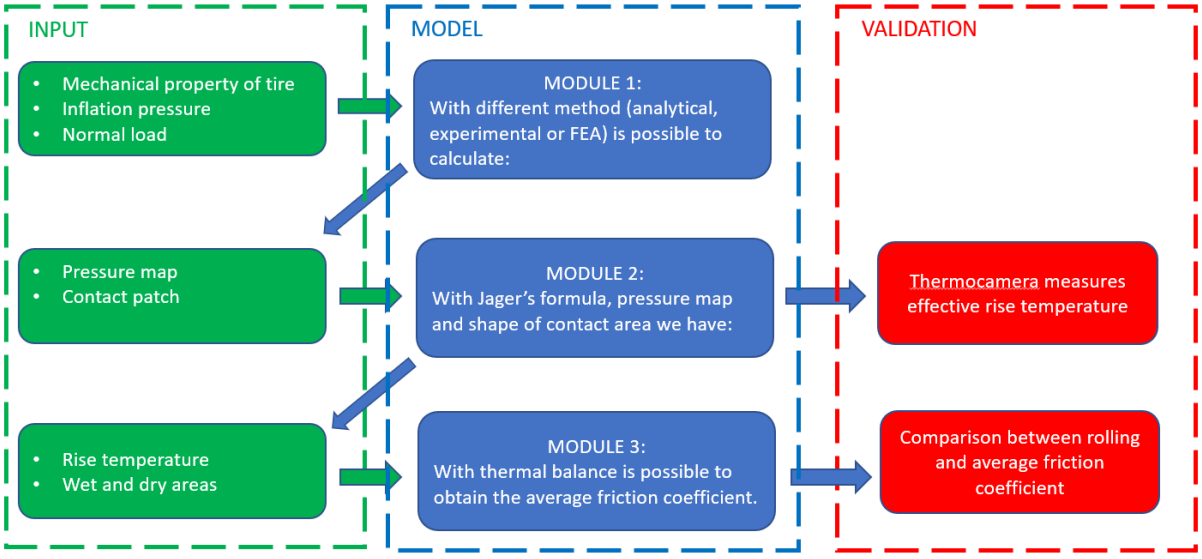

FIGURE 2: FLOW CHART OF THE MACROSCOPIC MODEL. THE GREEN AREA ON THE LEFT HAND SIDE REPRESENTS THE INPUT SECTION. INPUT PARAMETERS MAY COME FROM THE PREVIOUS MODULE OR FROM AN EXTERNAL SOURCE. THE CENTRAL BLUE AREA CONTAINS THE THREE DIFFERENT MODULES. THE RED AREA ON THE RIGHT HAND SIDE IS REPRESENTATIVE OF THE VALIDATION PROCEDURE

The purpose of this module is to provide the shape and the dimensions of the contact patch with the relative pressure distribution. These entities are mainly influenced by:

- The mechanical properties of the tire
- The inflation pressure
- The normal load

As previously mentioned, the modular structure of the model allows the user to choose the more suitable method to obtain the pressure distribution and the contact patch. For instance, it can be possible to use FE analysis as well as analytical procedure or, where available, experimental measures. The model proposed in [4, 9] uses an image that represents the pressure distribution on tire footprint obtained with experimental test showed in figure 3.

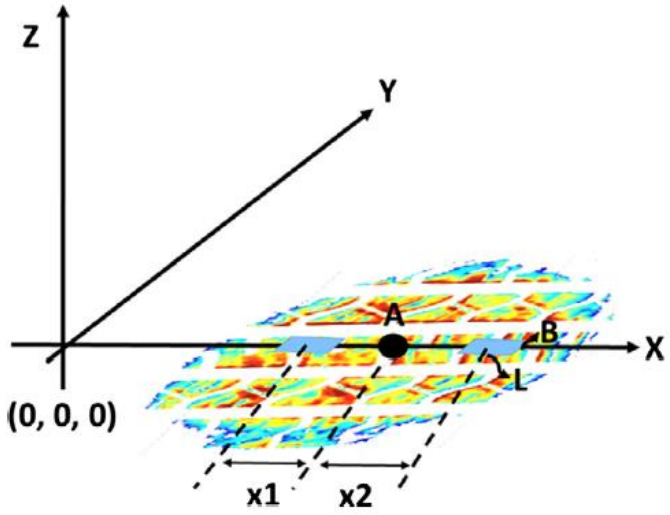

FIGURE 3: SIMPLIFIED REPRESENTATION OF THE TIRE-ICE CONTACT PATCH AT PLANE $z = 0$. THE DIFFERENT COLOURED AREAS REPRESENT DIFFERENT TEMPERATURE-RISE CONDITION [4].

A pre-processing phase on the picture is required in order to obtain numerical information from a graphical data. First of all, the contact patch image has to be converted in a matrix which dimensions depends on the resolution of the image. Each element of the matrix is a number which derives from the RGB numerical conversion. After that,

considering that at each colour corresponds a pressure value, it is possible to associate to the contact patch, another matrix which contains the pressure value for each pixel. An approximation of the contact patch as a grid of pixels is available for the computation. Consequently, the linked pressure distribution with matrix representation. Clearly, the quality of the image has direct influence on the accuracy of the results. In addition, it is necessary to specify that this whole procedure has another degree of approximation. Usually, the longitudinal velocity of the vehicle is different from the value of the product between rotational velocity of the tire and tire radius. Theoretically there should not be any different but, actually there is a certain degree of longitudinal slip, especially on icy roads. A parameter that take into account this difference is the slip ratio, defined as follow in equation (3.1):

$$S = 1 - \frac{\omega \cdot R}{V} \tag{3.1}$$

From equation (3.1) it is easy to understand that, if there is not any kind of longitudinal slip, the velocity of the vehicle V is equal to the product $\omega \cdot R$ and the value of the slip ratio will be zero. Otherwise, the higher is the value of the sliding velocity, the nearer to 1 is the value of the slip ratio.

High values of S introduce shearing effects at the contact interface, which relevant effects on the pressure distribution on the contact patch. Consequently, the pressure data obtained from the previous pre-processing procedure of the image, are a good approximation of the real situation just in case of low value of slip ratio.

3.2. Module 2: temperature rise in the contact patch

In order to be coherent with the theoretical formulation used for the calculation of the rise temperature in the contact patch, the following assumptions were made by [3, 9]:

- The contact interface between tire and ice is located at $z = 0$.
- The heat generated at the interface is equal to the frictional work.
- The heat is generated only at the tread-ice interface.
- The generation of the heat is assumed to be uniformly distributed in the contact interface.
- The temperature of the ice is equal to the temperature of the tread at the contact interface.
- For the temperature computation, only the effects of two tread blocks are considered in the point of interest.
- The pixels are assumed to be uniform rectangles.
- The ice surface is considered completely flat.
- The tread of the tire is assumed to be in complete contact with the ice surface.
- There is only longitudinal slip of the tread (x-direction); lateral slippage of the tread is neglected (y-direction).
- The computation of the temperature rise is considered only in longitudinal segments; there is no lateral temperature rise effect.

The target of this module is to associate a temperature-rise map to the previous contact patch, in order to distinguish between wet and dry areas in the contact interface. The contact can, in fact, directly affect rubber and ice but, in some areas, it is possible to find water which comes from the melting of the ice. This difference is strictly related to the

different amount of frictional heat generated in different portions of the contact patch. In order to evaluate these differences, which lead to completely different thermal balance equation, the following procedure is developed. A matrix representation of the tire footprint was obtained from module 1, through pixelization of the image. At this point, the next step is the calculation of the amount of the frictional heat which affects the temperature of each portion of the contact area. So, it can be possible to obtain the heat distribution applying the formula (3.2) suggested by Bhoopalam et al. [4, 9], to each element of the pressure matrix:

$$Q = \mu_{st} \cdot p \cdot V \cdot S \tag{3.2}$$

Now, all the necessary elements for the evaluation of the temperature rise are available. The Jaeger's (Jaeger, 1942) temperature rise formulation, chosen for the calculation by [4, 9], can be generally written as follow in equation (3.3):

$$\Delta T = \frac{Q\alpha}{8k(\pi\alpha t)^{3/2}} \cdot \exp\left(-\frac{(X-x)^2 + (Y-y)^2 + (Z-z)^2}{4\alpha t}\right) \tag{3.3}$$

Now, the evaluation of the temperature at a point (x, y, z) can be made by knowing the heat source at another point with coordinates (X, Y, Z).

Thus, considering the initial temperature of the ice, it is possible to understand which areas will be affected by the melting of the ice and which ones remain in a dry condition. Image 4 represents a graphical output of the previous procedure. Just by looking at this image, it is possible to detect where wet areas are located into the contact patch. If the known initial temperature of the ice is sufficiently high, certain value of the rise temperature in certain areas lead to reach the melting temperature.

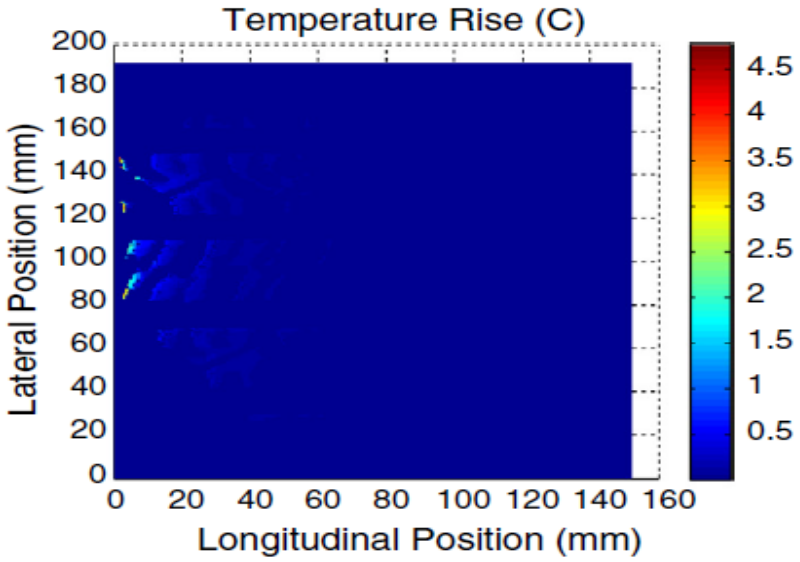

FIGURE 4: RESULTS OF THE TEMPERATURE RISE SIMULATION ON THE CONTACT PATCH [4].

3.2.1.Effect of the operation parameters

The normal load on the tire has a significative influence on the pressure distribution and, as showed in (9) and (10), for this reason affects directly the rise temperature value. The higher is the value of the normal load, the higher the value of the pressure in contact patch and so, the greater the amount of the temperature rise. The same behaviour is observed, by experiments [4, 9], if the wheel torque is increased from 0 $N \cdot m$ to 448 $N \cdot m$ whereas, for higher value of the torque results a lower temperature rise. The reason of this difference could be found in the fact that, the higher the value the torque, the lower the value of the contact time on ice surface.

3.2.2.Intermediate validation procedure

To arrive at the intermediate validation of the rise temperature map, in the work [4, 9] a measurement procedure for detecting experimental data which can be compared to the

simulation's result is proposed. The temperature measure is made using a thermo-camera. It is impossible to do an instantaneous measure on the contact patch because of the tire rolling. Therefore, the comparison between experimental data and model's results is made on the leading edge and on the trailing edge of the tire. The result can be synthetized considering that the trailing edge's temperature is higher than the leading edge's temperature. The higher the pressure value, the higher the difference between the edge's temperature values. For the classification of the areas in the contact patch a very simple procedure is showed. Starting from the initial temperature of the ice, if the rise temperature leads to obtain a value greater than 0°C, it means that the ice is melted and the area will be considered as wet. In the other case the rise is not sufficient to melt the ice, and the area will be considered as dry. A border zone is also considered due to the presence of the impurities in the contact area. If the temperature is between -2°C to 0 °C, the interested area will be considered as a dry-wet zone. In figure 5 is graphically showed the procedure proposed by [4, 9]. Starting from the temperature rise map, a correlation between contact patch and the position of the wet/dry areas is developed. From this result, through a comparison with the image obtained with the thermo-camera measurement, it is possible to evaluate the differences between the model's result and the experimental data.

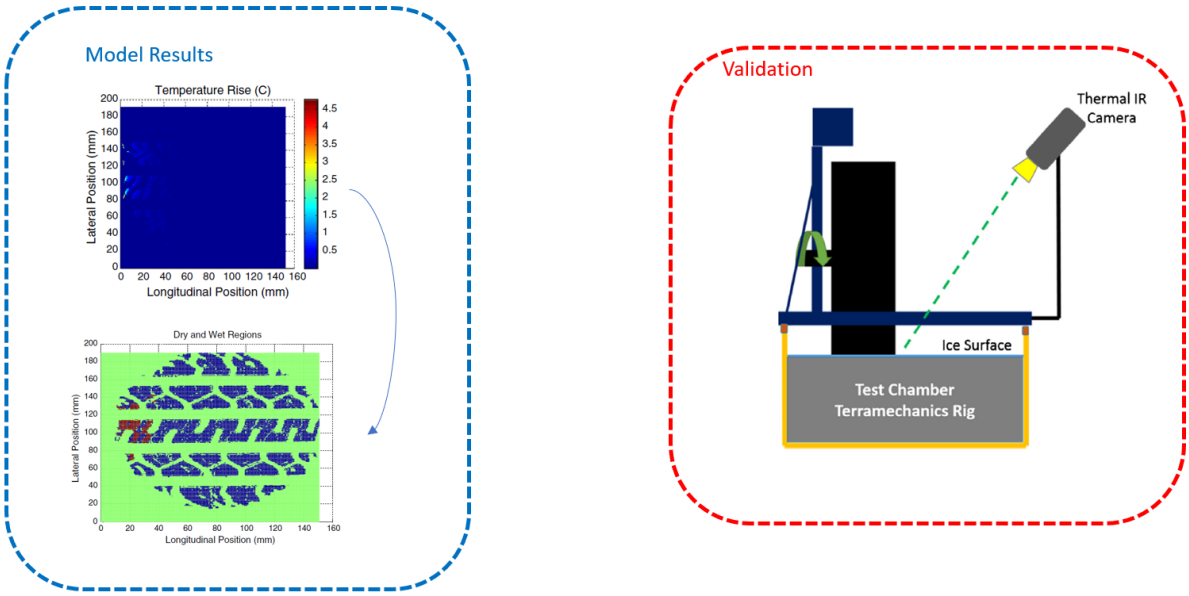

FIGURE 5: SCHEMATIC REPRESENTATION OF THE RESULTS OBTAINED WITH MODULE 2 ARE SHOWN IN THE BLUE AREA ON THE LEFT HAND SIDE. THE POSSIBILITY OF AN INTERMEDIATE RISE TEMPERATURE VALIDATION BY USING A THERMO-CAMERA IS REPRESENTED IN THE RED AREA ON THE RIGHT HAND SIDE [4].

3.3. Module 3: thermal balance on the contact patch

With the aim to apply the first principle of the thermodynamic, the considerations about the different possible aggregation states of the ice in the contact interface have a fundamental importance. The variety of the heat exchange mechanisms and the different thermal properties have to be taken into account in the writing of the energy balance. Anyway, the heat source is the friction mechanism between tire and ice. It is important here to specify that the considered quantities are averaged on the whole contact patch. Thus, the formula (3.4) allows to calculate the amount of the generated frictional energy.

$$q_{generated} = \mu_{av} \cdot p_{av} \cdot V \cdot S \cdot A_{tot} \tag{3.4}$$

Where the various term are:

- μ_{av} the average of the friction coefficient on the contact patch

- p_{av} the average of the pressure value on the whole contact patch
- V represents the longitudinal (x-direction) velocity of the wheel
- S is the slip ratio
- A_{tot} is the whole contact area

This energy amount can be divided in three different ways. In the first possibility represented by equation (3.5), considering dry areas, the heat is conducted through the ice surface.

$$q_{ice} = \frac{k_{ice}}{d} \cdot A \cdot (\Delta T) \tag{3.5}$$

Where k_{ice} is the thermal conductivity, d is the penetration deep of the heat, A is the dry area (in this case) and ΔT represents the temperature rise.

In the second possibility the heat comes through the conduction to the tire. This energy amount can be calculated using the equation (3.6).

$$q_{tread} = \frac{k_{tread}}{d} \cdot A \cdot (\Delta T) \tag{3.6}$$

The quantities used in this last formula have the same meaning of the previous but referred to another material.

The remaining heat is assumed to be transferred by conduction to the liquid layer between the tread and the ice. The equation (3.7) allows to evaluate this entity.

$$q_{water} = \frac{k_{water}}{d} \cdot A \cdot (\Delta T) \tag{3.7}$$

Thus, the general thermal balance can be written as showed in equation (3.8):

$$q_{generated} = q_{tred} + q_{ice} + q_{water} \tag{3.8}$$

Where, the only unknown variable is the average friction coefficient μ_{av} considering the equation (3.8).

The average friction coefficient is obtained experimentally by the ratio between the longitudinal force and the normal force. In the tests, a longitudinal tractive force is applied to the centre of the tire by using a beam. In addition, to monitoring the slip ratio, a torque is also applied to the wheel using an electric engine. The rolling friction coefficient wherewith is possible to make the comparison with the model friction coefficient is finally obtained.

Chapter 4

4. Macroscopic model reproduction

4.1. Introduction

As mentioned before, in this work a reproduction of the theoretical procedure of the macroscopic model proposed in [4, 9] is proposed. To this aim, two different kind of model are developed. The first one is a simplified mono-dimensional model, which was useful to take confidence with the amplitude of the unknown parameters such as the slip ratio, the depth of heat penetration, the period of the simulation time and so on. By a better comprehension of these quantities, a more complex bidimensional model was then developed. This second attempt tries to be faithful, as much as possible, to the original work proposed in [4, 9].

Considering the impossibility to have experimental data, the module 2 and the module 3 were developed starting from experimental data obtained from the literature. Moreover, for the same reason, validation methods suggested in the modular model [4, 9] are not developed. In order to fill this lack of information, a qualitative comparison between the results showed in [4, 9] and the ones obtained in this work is made. Table 1 contains thermal properties of the ice and the tire's rubber. All values come from [4].

Material	Density $\left(\frac{kg}{m^3}\right)$	Thermal conductivity $\left(\frac{W}{m\,K}\right)$	Specific heat $\left(\frac{kJ}{kg\,K}\right)$
Tire's rubber	940	0.19	1.500
Ice	917.8	2.22	2.020

TABLE 1: THERMAL PROPERTIES OF ICE AND TIRE'S RUBBER [4].

The operational parameters used in the model are shown in table 2:

Velocity $\left(\frac{m}{s}\right)$	Static friction coefficient [10]	Slip ratio	Initial temperature $(°\,C)$	Heat penetration deep (m)
3	0.1	1e-5	-4	1e-4

TABLE 2: OPERATIONAL PARAMETERS USED IN THE TESTS CONDUCTED BY BHOOPALAM ET AL. [4].

4.2. Mono-dimensional model: Module 1

At first, for the evaluation of the pressure map on the contact patch, the centreline of the tread on the x-axis was only considered, as shown in the left side of figure 6. The reason of this choice is in the geometrical symmetry of the problem for which, the condition of the centreline of the tire footprint can be representative of the whole contact patch. Moreover, a Gaussian curve was adopted instead of a constant pressure distribution, in order to have a better picture of the different areas that could be present at the tire-ice interface. In the right side of figure 6, the chosen Gaussian distribution of the pressure on the centreline of tread is showed.

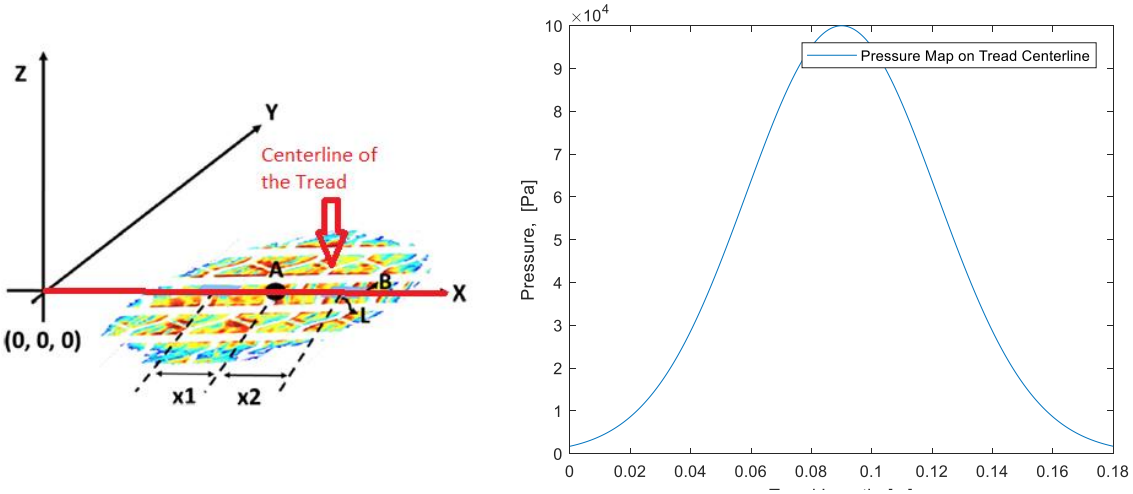

FIGURE 6: ON THE LEFT HAND SIDE, A SCHEMATIC REPRESENTATION OF THE CENTRELINE OF THE TREAD OF THE CONTACT PATCH OBTAINED IN [4] IS SHOWED. ON THE RIGHT HAND SIDE, THE GAUSSIAN PRESSURE MAP ON THE CENTRELINE OF THE TREAD USED IN THE MONO-DIMENSIONAL MODEL IS PROPOSED.

4.3. Mono-dimensional model: Module 2

With these information, the amount of frictional heat can be evaluated by using equation (3.2). Considering a mono-dimensional problem the Jaeger's formulation (3.3) can be written as showed in equation (4.1).

$$\Delta T = \frac{Q\alpha}{8k(\pi\alpha t)^{3/2}} \cdot \exp\left(-\frac{(X-x)^2}{4\alpha t}\right) \tag{4.1}$$

From the comparison between the numerical result of the simplified model developed in this work and the image of the contact patch preformed via a thermo-camera in [4, 9], it is possible to see a good matching level. This comparison is made by considering the left and right hand side of figure 7 which represent respectively, the plot of the rise temperature on the centreline of the tread obtained with the mono-dimensional model and the result of the temperature rise computation in [4, 9]. The maximum value of the rise temperature in the mono-dimensional model is very similar to the one showed in the

image (respectively 5 °C and 4.5 °C). An acceptable result seems to be reached, considering also the area in which the peak is reached.

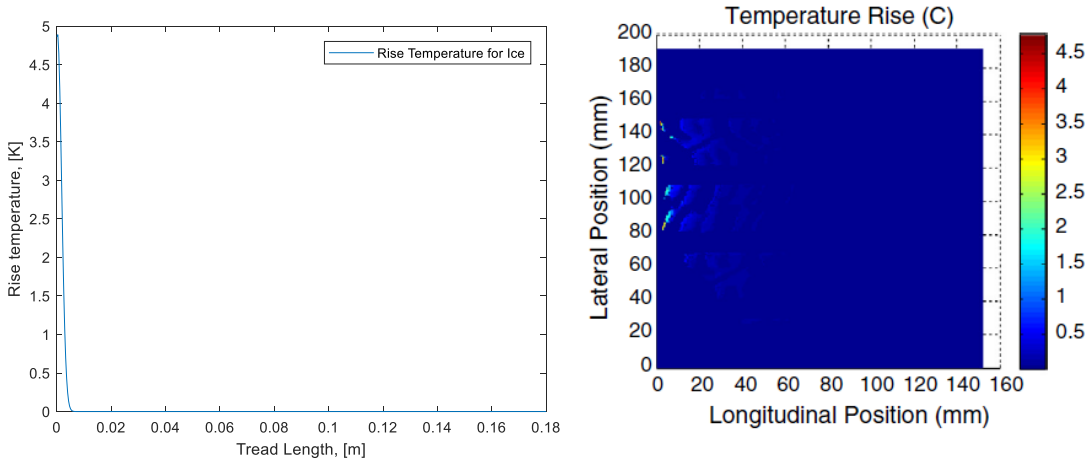

FIGURE 7: COMPARISON BETWEEN THE RESULTS IN TERM OF RISE TEMPERATURE. ON THE LEFT HAND SIDE THE RISE TEMPERATURE OF THE ICE OBTAINED WITH MATLAB IS SHOWN. ON THE RIGHT HAND SIDE, THE TEMPERATURE RISE DISTRIBUTION ON THE CONTACT PATCH PROVIDED BY BHOOPALAM ET AL. [4] IS SHOWN.

4.4. Mono-dimensional model: Module 3

Now it is possible to distinguish between wet and dry areas on the centreline of the tread. Consequently, the correct equation of the heat balance, for each particular aggregation state of the ice which affects differently the contact condition in different areas of the contact patch, can be written. The numerical result match also in this case the friction coefficient obtained in the reference paper [4]. A GUI, as showed in figure 8, was developed with the aim of speeding up the operations of the analysis of the influence of the parameters on the problem. This tool allows to change the input parameters much faster giving a better understanding of the links between the various intermediate results and the input data.

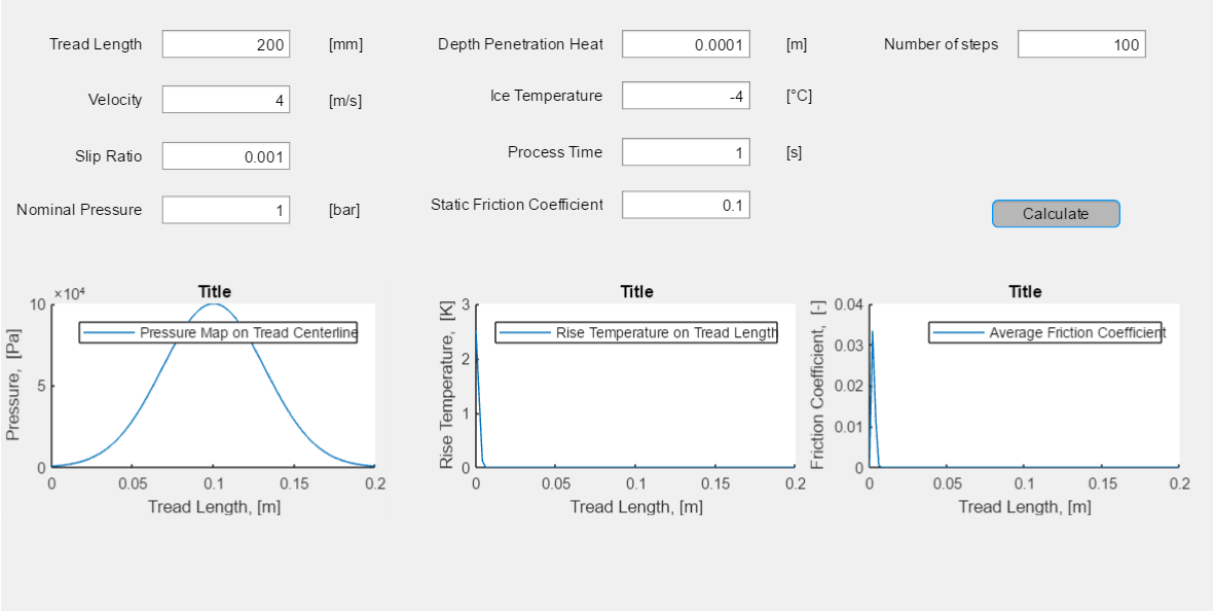

FIGURE 8: MATLAB GUI SCREEN FOR THE MONO-DIMENSIONAL MODEL.

4.5. Bi-dimensional model: Module 1

The information about the dimensions and the shape of the contact patch, as well as the pressure map, comes from an optical footprint measurement made by Smithers Rapra [11]. This particular image, represented in figure 9, was chosen mainly for reason related to the quality and the availability of a colour-bar legend. Another important aspect of this picture is the clear indication of the dimensions in x and y directions.

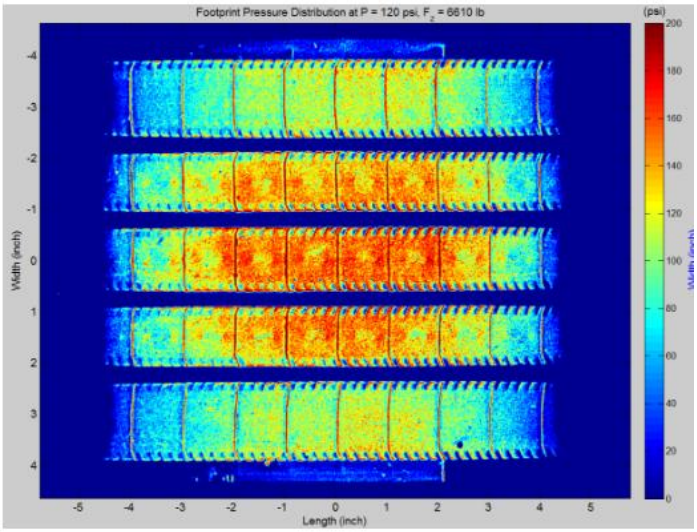

FIGURE 9: TIRE FOOTPRINT [11].

The first step is the pre-processing of the image. The aim is to obtain the data necessary in the correct format for the simulation. This is made by using the Matlab "Image Toolbox". Once the image is imported in Matlab a symbolic 3-dimensional matrix is obtained as result. The dimensions of this object are directly dependent on the resolution of the image in term of number of pixels used in each direction. Every space of the 3-dimensional matrix represents a colour of RGB scale (Red, Green or Blue) as showed in figure 10.

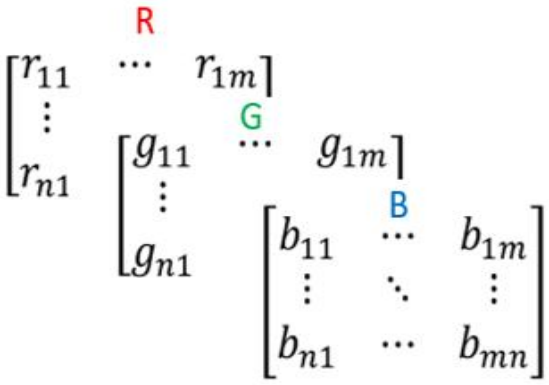

FIGURE 10: MATRIX REPRESENTATION OF THE RGB IMAGE.

A grey-scale matrix can be used to have a numerical description of the contact patch because the interest is in the numerical value and not in the graphical representation. The next necessary operation is to convert the format of the data (uint8 to double) in order to make possible the application of the mathematics operators. Figure 11 shows the relationship between the matrix representation and the graphical output obtained with Matlab.

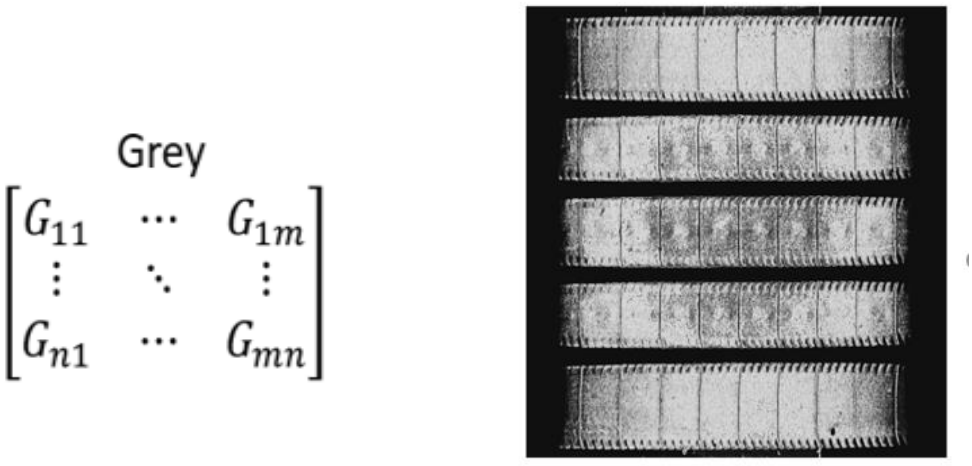

FIGURE 11: ON THE LEFT HAND SIDE IS REPRESENTED THE GREY-SCALE MATRIX REPRESENTATION IS SHOWN. ON THE RIGHT HAND SIDE OF, THE GRAPHICAL REPRESENTATION OF THE MATRIX ON THE LEFT IS SHOWN.

At this point, a new matrix was built. In this matrix, each element represents the pressure value linked to that pixel. This is possible considering that the greyscale, as well as the RGB scale, consists to associate in a numeric way a value belonging to the interval 0-255. The higher the RGB scale value, the higher the pressure value. More in detail, the following relationships can be written. In equation (4.2), a generic element of the grey-scale matrix is associated to the maximum pressure level. In equation (4.3) the same thing is done with the minimum level of pressure which represents the non-contact situation.

- $$G_{mn} = 255 \longrightarrow Pmax \tag{4.2}$$

- $$G_{nm} = 0 \longrightarrow Pmin \longrightarrow no\ contact \tag{4.3}$$

Consequently, a generic P value can be obtained using equation (4.4).

$$P = \frac{G_{mn}}{Pmax} \tag{4.4}$$

The following three images, figure 12, figure 13 and figure 14, show the graphical result of this procedure. Only in the last image, figure 14, it is possible to clearly see a little portion of the shape of the contact patch. This is because, in figure 12 and figure 13, the high number of pixel makes impossible to distinguish between different colours. These figures are putted in sequence of zoom refinement. While figure 12 represents the whole contact patch, figures 13 and 14 show a more detailed information about the central part of the tread, about the y-dimension interval $0.08\ mm - 0.1\ mm$.

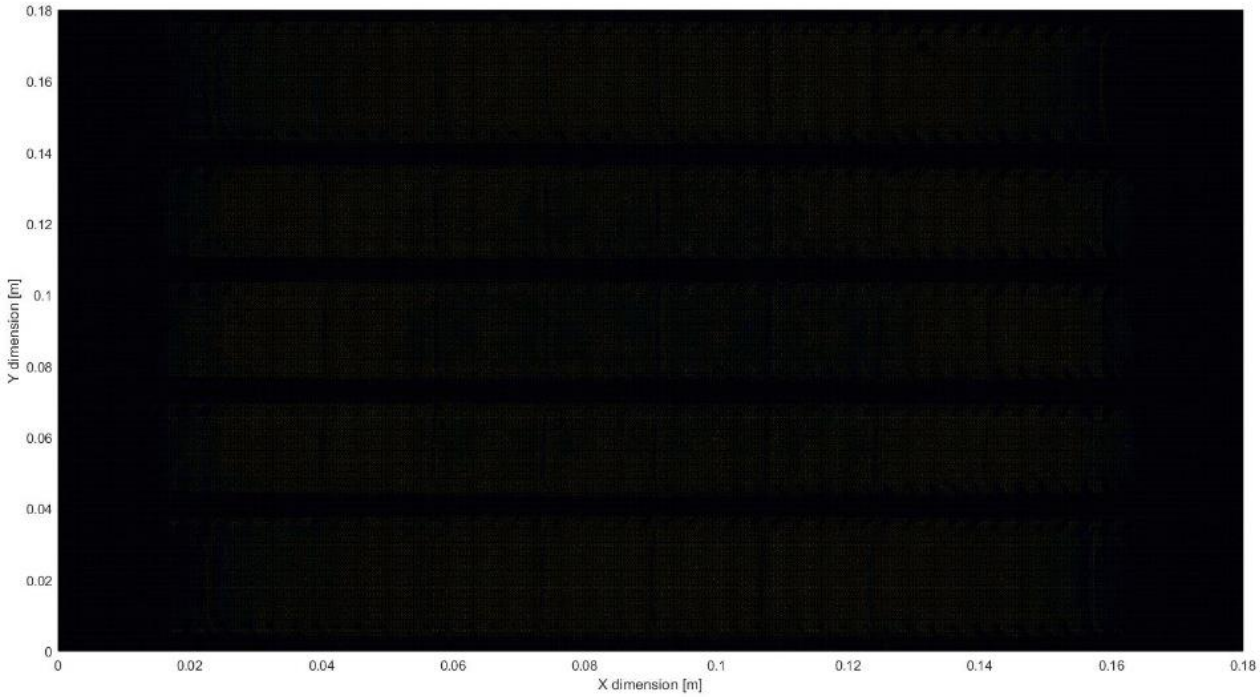

FIGURE 12:PRESSURE MAP ON THE WHOLE CONTACT PATCH OBTAINED BY PRE-PROCESSING THE IMAGE PROVIDED BY [11].

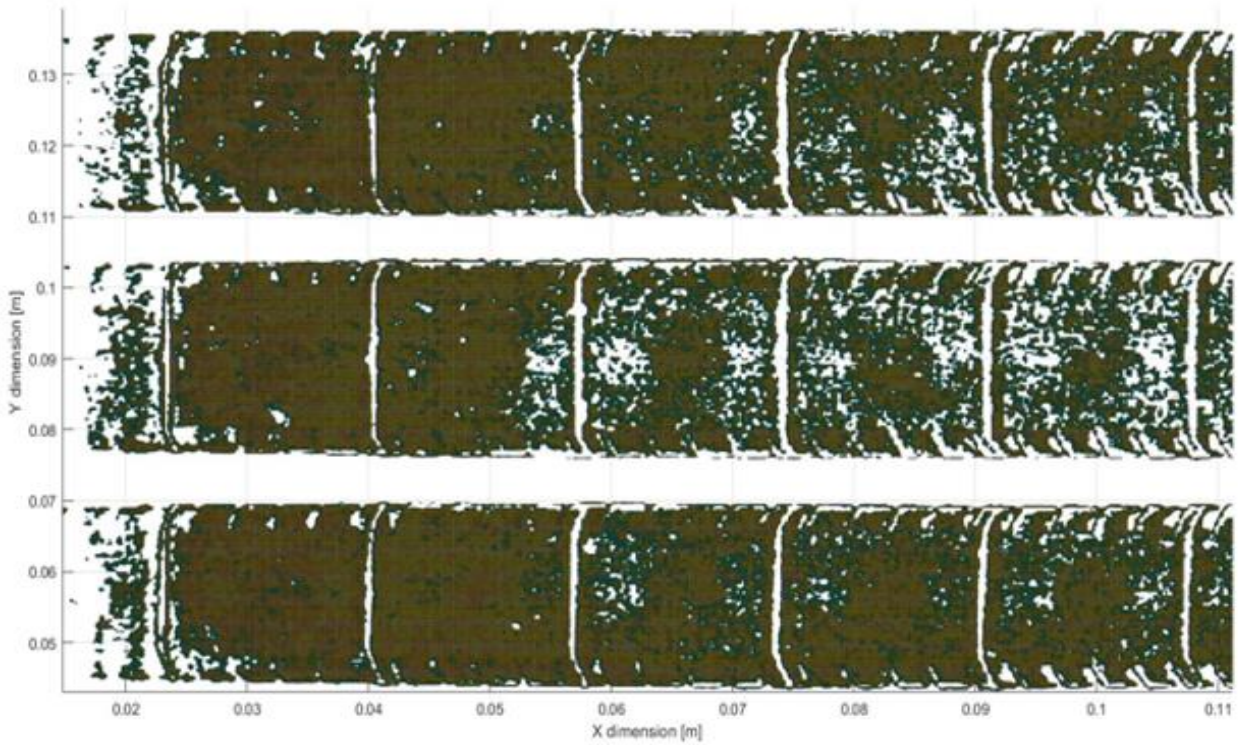

FIGURE 13: ZOOM ON THE CENTRAL ZONE OF THE CONTACT PATCH.

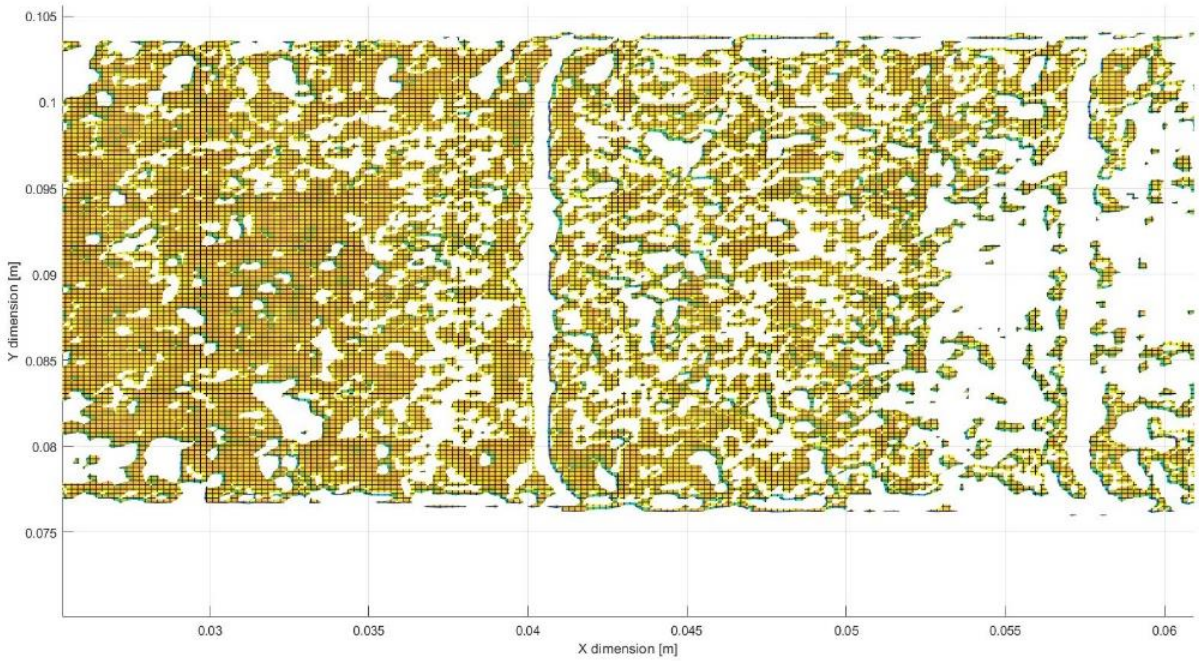

FIGURE 14: REFINED ZOOM IN THE CENTRAL AREA OF THE CONTACT PATCH.

4.6. Bidimensional model: Module 2

Now it is possible to calculate the amount of frictional heating that can be associated to the pressure matrix by using the formula (3.2). Knowing these quantities, it is possible to use the Jaeger's formula (3.3). In particular, as mentioned below, only the effect of the "next" longitudinal pixel has been considered in the calculation of the rise temperature. For this reason, two vectors have been created:

- the first vector, $\boldsymbol{x_i}$ represents the point affected by the heat that comes from the "next" longitudinal point;
- the second vector, $\boldsymbol{X = x_{i+1}}$ represents the next longitudinal pixel considered as the heat source;

Thus, using these conditions, the rise of the temperature on the whole contact patch is obtained. The next step is to distinguish between wet and dry areas. However, before, it is necessary to calculate the real contact area. As showed in figure 15, which is a further zoom of figure 14, not all pixels are representative of a contact situation. Considering the particular geometry of the tread, it is possible to understand the reason of this. White coloured portion represent non-contact area while other coloured pixels are effectively in contact with the tire surface.

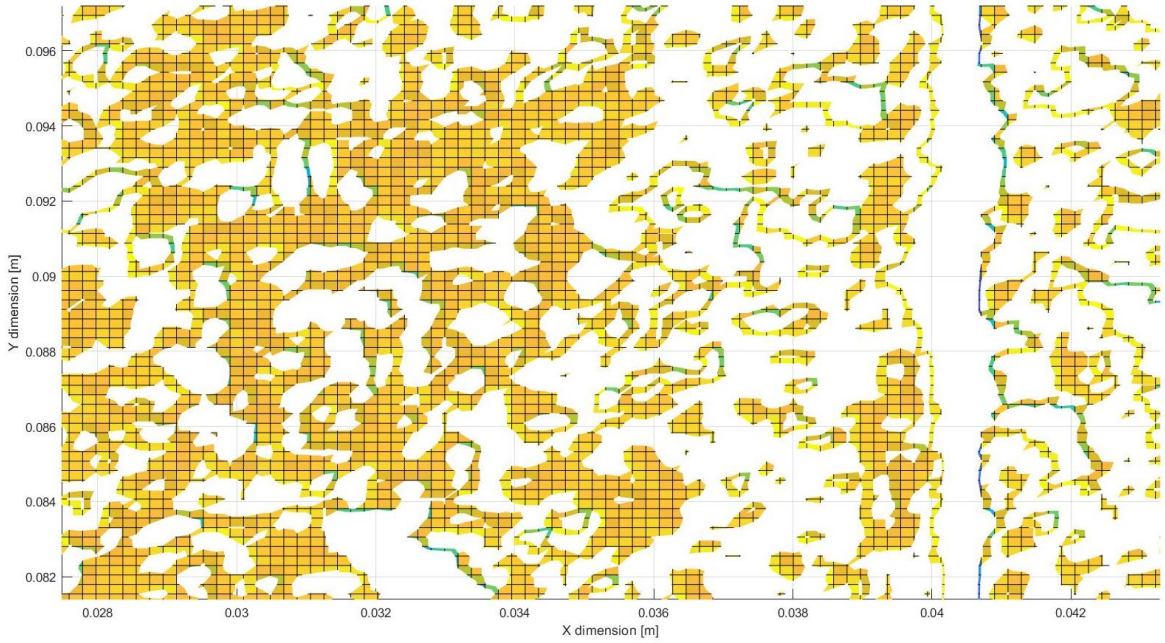

FIGURE 15: DIFFERENCES OF CONTACT AND NON-CONTACT AREAS BASED ON A GRAPHICAL REPRESENTATION.

The dimensions of the pixel can be obtained by dividing the physical length of the contact patch by the dimension of the representative matrix. The x dimension of the pixel is assumed equal to the y dimension, therefore the area of each pixel is calculated using equation (4.5).

$$A_{pixel} = x_{length}^2 \tag{4.5}$$

To estimate the correct value of the whole area of the footprint the value of A_{pixel} has to be multiplied for the number of pixels. However, as mentioned before, not every pixel is representative of the contact patch. Practically this means that the value of the RGB scale is 0 in the zones where there is no contact between the tread and the ice. In order to consider this condition into the computation of the entire contact area, an algorithm for counting all the non-zero elements of the matrix was developed. Therefore, the total area of the tread in contact with the ice is expressed by equation (4.6).

$$A_{tot} = A_{pixel} \cdot N_{contact\ pixel} \tag{4.6}$$

4.7. Bidimensional model: Module 3

Through a simple for-cycle condition, it is possible to detect which areas have to be considered as wet and which ones as dry. Scanning all elements in the matrix of the temperature rise and taking into account in which position the temperature is representative of a melting status, it is possible to apply the correct equation (3.5), (3.6) or (3.7) for the thermal balance (3.8). Figure 18 represents the matrix of the temperature which contains the generic element T_{ij}, representative of the thermal condition of that particular pixel.

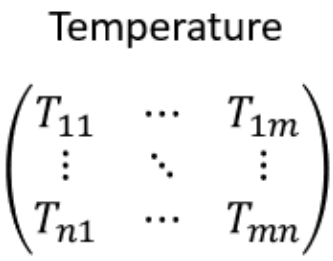

FIGURE 16: GRAPHICAL REPRESENTATION OF THE MATRIX OF THE TEMPERATURE.

By considering the numerical value of the element T_{ij} it is possible to choose which equation has to be used in order to properly describe the thermal balance. The logical condition in the Matlab script establishes that:

- $if\ T_{ij} < -2\ °C$, then:
  - $q_{generated} = q_{tred} + q_{ice}$ so, the friction coefficient is:

$$\mu_{av} = \left(\frac{(k_{tread} + k_{ice})}{d} \cdot A \cdot (\Delta T)\ + \right) / p_{av} \cdot V \cdot S \cdot A_{tot} \tag{4.7}$$

- $if\ -2°C \leq T_{ij} < 0°C$, then:
  - $q_{generated} = q_{tred} + q_{ice} + q_{water}$ so, the friction coefficient is:

$$\mu_{av} = \left(\frac{(k_{tread} + k_{ice} + k_{water})}{d} \cdot A \cdot (\Delta T)\ + \right) / p_{av} \cdot V \cdot S \cdot A_{tot} \tag{4.8}$$

- $if\ T_{ij} > 0°C$, then:
  - $q_{generated} = q_{tred} + q_{water}$ so, the friction coefficient is:

$$\mu_{av} = \left(\frac{(k_{tread} + k_{water})}{d} \cdot A \cdot (\Delta T) \; + \right) / p_{av} \cdot V \cdot S \cdot A_{tot} \tag{4.9}$$

At the end of this last procedure, a new matrix which collects the values of the friction coefficients on the contact patch is created. Each pixel has a different value for the friction coefficient and, by plotting this last matrix on the contact patch, a graphical evaluation of the tractive performances in different areas of the contact interface is finally possible. This last result has a great relevance, especially considering the importance of understanding how different geometries of the tread could affect the behaviour of the vehicle. However, for the validation procedure, just an average value for the friction coefficient is necessary, in order to make possible the comparison with the rolling experimental friction coefficient.

4.8. Conclusion

To sum up, it is possible to say that the macroscopic procedure for the evaluation of the friction coefficient presents for sure some advantages. A simple and intuitive theoretical method is strictly linked to an experimental procedure which allow to avoid a lot of uncertainties about both, input and output data of each module. Moreover, the modular structure could be very useful especially considering also the opportunities to develop new ways for detecting experimental input parameters. Thinking also about the possibility to obtain new validation procedures, the accuracy of the average frictional coefficient could be increased more and more. However, considering the lack of information such as the available material properties, the source of the tire footprint image and pressure map, the goal of this work is to obtain an own model which allow to predict the rubber-ice frictional behaviour focusing on the phenomenological aspects. Excepted

for the thermodynamic aspects, the other physical phenomena which occur during the sliding contact between rubber and ice, are not considered in this model. Thus, the model's theorical base is uncomplete and, as said before, missing the experimental part that could fill the theoretical gaps, the predicted frictional coefficient via macroscopic procedure can't be assumed satisfactory.

Moreover, in the original model there are also differences between the experimental results and the model's results (as shown in [4, 9]) which cannot be neglected, as shown in figure 9.

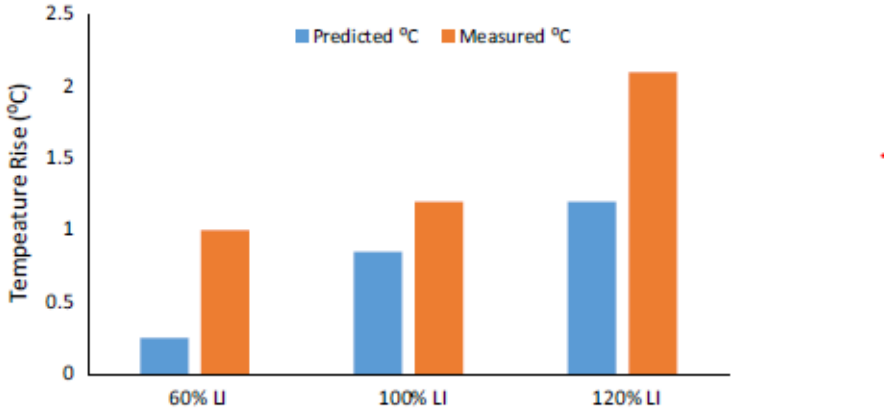

FIGURE 17 SIGNIFICATIVE DIFFERENCES BETWEEN TEMPERATURE MODEL'S RESULT OF BHOOPALAM ET AL. [3] AND EXPERIMENTAL MEASURES ARE SHOWN.

Another uncertainty aspect concerns the evaluation of some parameters, such as the heat penetration deep d. As said in [4, 9], "*The depth of penetration was initially assumed to compute the average friction; the depth value was further modified to match the friction from simulation and from the indoor test program*". Considering again this work's available means, a further matching modification of the parameters is not possible. For all these reasons, the following part of this master thesis work is focused on the

development of microscopical-based model, in which the phenomenological considerations are fundamental and the comparison between the literature results and model's results are easier and more accurate.

Chapter 5

5. Microscopic Model

5.1. Introduction

The basic idea for the microscopic model is to reproduce, as close as possible, all the phenomena which occur in the sliding contact between rubber and ice. The same purpose is shared by the works of Persson et al. [1] and K. Wiese et al. [5], where a theory based on viscous friction formulation was widely developed. During this contact situation between the rubber and the ice, the main friction mechanism is represented by the viscous friction. This means that, beyond thermodynamic effects, there are also hydrodynamic effects which have a significant influence on the rubber frictional behaviour (e.g. aquaplaning phenomenon). Moreover, these two different aspects are strictly related to each other in the friction formulation. It is impossible to consider hydrodynamic effects without taking into account the thermo-mechanical conditions which lead to have a relevant volume of liquid layer at the rubber-ice interface. For this reason, the friction coefficient is a time-dependent parameter. The higher the frictional heat generated, the higher the amount of water that is due to the ice melting. On the other hand, the frictional energy is directly dependent on the deformation work of the rubber, which is also a time-dependent quantity being a direct consequence of the friction coefficient itself.

Thus, the formula which allows to describe the interaction between these two materials, depends on several parameters. The material properties, both mechanical and thermal, as well as the sliding velocity and the normal pressure applied on the rubber are needed to

solve the constitutive equation of the problem. All these physical aspects are connected together, therefore, in this work, a model divided in two parts was built . The first part is the thermo-mechanical simulation of a rubber block sliding on an ice surface. This thermo-mechanical simulation was done using the finite elements method. The information obtained with the finite element model were used as input for a second numerical model used to calculate the value of the friction coefficient. This second part of the model was developed in Fortran language. The interaction between these two models leads to a complete finite element model, in which the viscous interaction between the rubber and the ice during the sliding contact is showed. By studying the model's results, the effects of the operational parameters and of the material properties become clearer. Moreover, it becomes easier to understand which changes could be more appropriate to improve the frictional performance of the rubber.

5.2. Viscous formulation for rubber on ice

The main problems in tire-ice contact, mainly defined by the loss of adhesion, occur when the pure rolling is lost and the sliding phenomenon starts. Considering that the viscous model is also based on a microscopic formulation, the subject of this study is not the whole tire but a small sample of it. The Figure 19 shows three different scenarios of the problem. The first one, on the left hand side is the macroscopic scenario, in which the geometry of the tread is important to analyse the macroscopic effects such as the so called *water wiping* The central part of the image is a small cubic sample of the whole tread with completely flat surface. The contact interface is represented in the figure. It is useful for the thermodynamic analysis. On the right hand side of the image, the roughness of the rubber block is also considered. The roughness is necessary to take into account the hydrodynamic effects.

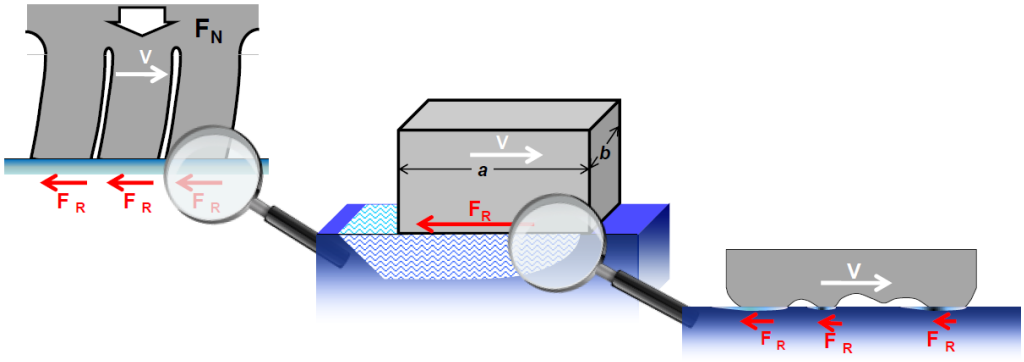

FIGURE 18: SAMPLE OF THE TIRE WITH DIFFERENT LEVELS OF ZOOM. ON THE LEFT HAND SIDE, A MACROSCOPIC SAMPLE OF THE TREAD IS REPRESENTED. ON THE CENTRE OF THE IMAGE THERE IS THE RUBBER BLOCK SUBJECT OF THE THERMODYNAMIC FORMULATION. ON THE RIGHT HAND SIDE OF THE IMAGE, THE PRESENCE OF THE ASPERITIES IS SHOWED [5].

The geometry of the model developed in this work and the setup of the finite element simulation are taken from the work [1,5]. Figure 19 shows the axes orientation and the geometrical properties of the bodies which are in contact.

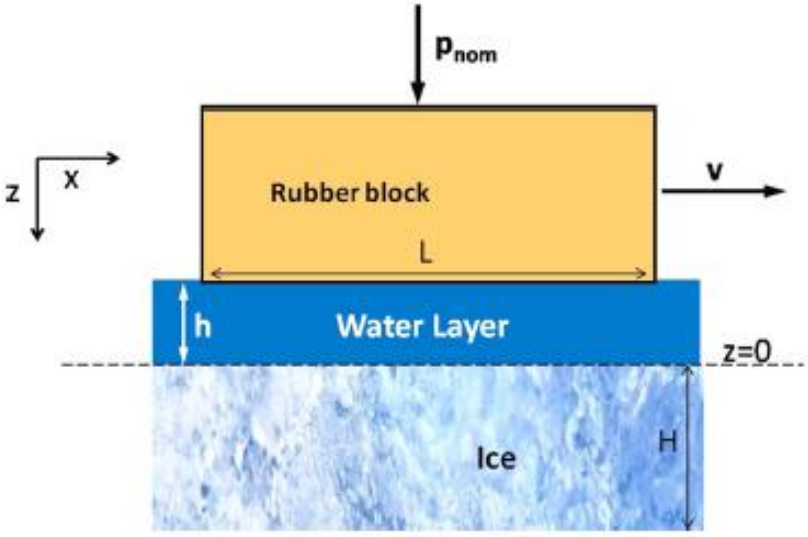

FIGURE 19: SCHEMATIC REPRESENTATION OF THE GEOMETRY OF THE MODEL WHIT THE LOAD CONDITION AND THE SLIDING VELOCITY [3].

In order to simulate the rubber-ice sliding interaction, a rubber block of length L is considered. The direction of the motion is on the x-axis whereas, the load is applied on z-axis. The nominal contact pressure is obtained by the equation (5.1).

$$p_{nom} = F_z / A_{nom} \tag{5.1}$$

Where, F_z is the load in z-direction and A_{nom} is the nominal contact area, which does not consider the roughness of the rubber surface. If a certain roughness level is introduced in this contact problem, the real contact area and not the nominal contact area should be considered. While the nominal contact area is equal to the lower surface of the rubber block, the real contact area is the sum of the contact areas of each single asperity. In the Figure 20 it is possible to appreciate this difference.

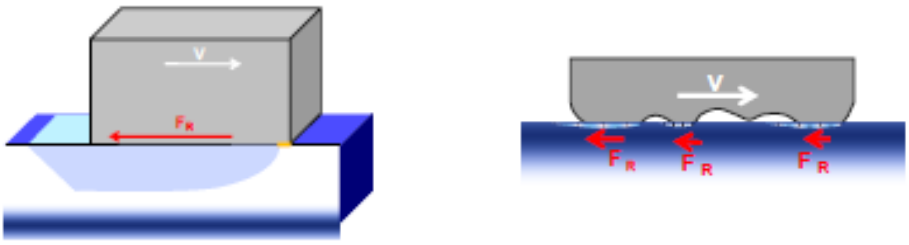

FIGURE 20: THE COMPARISON BETWEEN THE NOMINAL CONTACT AREA (ON THE LEFT) AND THE REAL CONTACT AREA (ON THE RIGHT) [5].

The contact interface between the rubber and the ice is located on a plane with $z = 0$. H is the height of the ice block whereas h is the height of the liquid layer at the rubber-ice interface. Under the normal load in z-direction and velocity applied in x-direction previously defined, a rubber block sliding on the ice surface exhibits a frictional behaviour mainly dependent on the viscous shear stress at the interface with this liquid

layer [1]. The liquid layer is considered a time-dependent variable. Therefore, the model is based on a differential equation for the evaluation of the height of the liquid layer. By knowing that quantity, through the Newton's viscous law, it is possible to obtain the friction coefficient. First, a simplified thermodynamic model is proposed and after, a complete thermo-hydrodynamical model will be obtained.

5.2.1.Thermodynamic model

In order to make the basic thermodynamic considerations it is possible to assume that both the surfaces in contact are completely smooth. The roughness of the rubber block will be further considered in the extended model for the hydrodynamic effects. So, when a rubber block is sliding on an ice surface, a frictional shear stress can be represented using Newton's law [3], assuming that the velocity of the liquid layer is the same of the rubber block. The Newton's law is showed in the equation (5.2).

$$\tau_{shear}(t) = \eta_{water} \frac{v}{h(t)} \tag{5.2}$$

Where η_{water} is the viscosity of the water and $h(t)$ is the height of the liquid layer at the time t. A dependency of $h(t)$ from coordinate x can be neglected being the rubber surface completely smooth. Starting from the equation (5.2), the resulting frictional energy due to the shear stress can be written as showed in equation (5.3)

$$\dot{E}_{shear}(t) = \eta_{water} \frac{v^2}{h(t)} \tag{5.3}$$

where $\dot{E}_{shear}(t)$ is expressed in $\left(\frac{W}{m^2}\right)$. Clearly, for the building of the thermodynamic model is necessary to have a thermal balance condition. The energy generated will be distributed in two terms which are respectively, the energy necessary for the phase transition from ice to water (5.4) and the heat which is flowing into the ice (5.5).

$$\dot{E}_{melting}(t) = \rho_{ice}\, L_{ice}\, \frac{dh(t)}{dt} \cdot \mathcal{X}_{\{T_{ice(0,t)}=T_m\}} \tag{5.4}$$

The term represented by equation (5.4) is present only if the value of the ice temperature at the interface ($z = 0$) is equal to the melting temperature T_m. Mathematically, this condition is represented by the term $\mathcal{X}_{\{T_{ice(0,t)}=T_m\}}$ which is equal to one if the temperature at $z = 0$ is equal to T_m, and it is zero if $T < T_m$.

$$\dot{E}_{iceflux}(t) = \lambda_{ice} \cdot \partial_z T_{ice}(z,t)_{|z=0} \tag{5.5}$$

Where λ_{ice} represents the thermal conductivity of the ice. As discussed in [5], the heat transfer to rubber is neglected. When the melting temperature is reached, the heat equation (5.5) admit the solution represented in equation (5.6)

$$\dot{E}_{iceflux}(t) = \lambda_{ice} \cdot \frac{T_m - T_0}{\sqrt{\pi \cdot \alpha \cdot t}} \tag{5.6}$$

Where T_0 is the initial temperature of the ice and α is the thermal diffusivity. It is also reasonably assuming that the temperature of the ice surface cannot overcome the melting temperature. Therefore, the equilibrium can be generally written as showed in equation (5.7).

$$\dot{E}_{shear} = \dot{E}_{melting}(t) + \dot{E}_{iceflux}(t)$$

$$\eta_{water}\frac{v^2}{h(t)} = \rho_{ice}\, L_{ice}\, \frac{dh(t)}{dt} \cdot \mathcal{X}_{\{T_{ice(0,t)}=T_m\}} + \lambda_{ice} \cdot \partial_z T_{ice}(z,t)_{|z=0} \tag{5.7}$$

In particular, the object of this formulation is the unknown height of the liquid layer as time-dependent quantity. For this reason, starting from the (5.7), the constitutive equation for the thermodynamic model is:

$$\frac{dh(t)}{dt} = \frac{1}{\rho_{ice}\, L_{ice}}\left(\eta_{water}\frac{v^2}{h(t)} - \lambda_{ice} \cdot \partial_z T_{ice}(z,t)_{|z=0}\right) \cdot \tag{5.8}$$

$$\mathcal{X}_{\{T_{ice(0,t)}=T_m\}}, \quad for\ t > 0$$

and the initial condition for the water height is:

$$h(0) = h_0, \quad for\ t = 0 \tag{5.9}$$

5.2.2. Thermodynamic model with roughness effects

Starting from a completely smooth situation, a further step concerns the study of the contact between a rough elastic surface (rubber) and a still smooth rigid surface. It is also clear that a distinction between nominal contact area and real contact area is necessary. The equation (5.8) cannot be assumed true for all the *x* value but just for the ones which belong to the real contact area. For this reason, a new constitutive equation is obtained:

$$\frac{\partial h(x,t)}{\partial t} = \frac{1}{\rho_{ice}\, L_{ice}}\left(\eta_{water}\frac{v^2}{h(x,t)} \cdot \mathcal{X}_{\{x \in A_{real}\}} - \lambda_{ice} \cdot \partial_z T_{ice}(x,z,t)_{|z=0}\right) \cdot \mathcal{X}_{\{T_{ice(0,t)}=T_m\}} \tag{5.10}$$

$$for\ t > 0$$

A new characteristic function is introduced to consider only the x values which belong to A_{real}. It is possible to reduce the number of the independent variables of the equation (5.10). The spatial dependence can be overcome considering an integral average. For the whole contact area, equation (5.11) can be written as follow:

$$h(t) = \frac{1}{A_{nom}} \int_{A_{nom}} h(x,t)\, dx \tag{5.11}$$

By introducing the parameter *k* which represents the relative contact area contribution:

$$k = \frac{A_{real}}{A_{nom}} \tag{5.12}$$

The equation (5.10) can be written as follow:

$$\frac{dh(t)}{dt} = \frac{1}{\rho_{ice}\, L_{ice}} \left(k\, \eta_{water} \frac{v^2}{h(t)} - \lambda_{ice} \cdot \partial_z T_{ice}(z,t)_{|z=0} \right) \tag{5.13}$$

$$\cdot\, \mathcal{X}_{\{T_{ice(0,t)} < T_m\}}, \quad for\ t > 0$$

the height of the liquid layer is again obtained with a time-dependent differential equation.

5.2.3.Hydrodynamic effects

Roughness on the rubber surface leads also to develop a new formulation in which the hydrodynamic effects can be considered. In particular, there are two different hydrodynamic effects: the *squeeze-out* and the *saturation* effect. To explain how these two phenomena affect the height of the liquid layer is necessary to remember the

roughness formulation. It is possible to assume that, each asperities of the rough surface of the rubber block can be modelled as a smooth cylinder of diameter D_{asp}, as shown in the Figure 21.

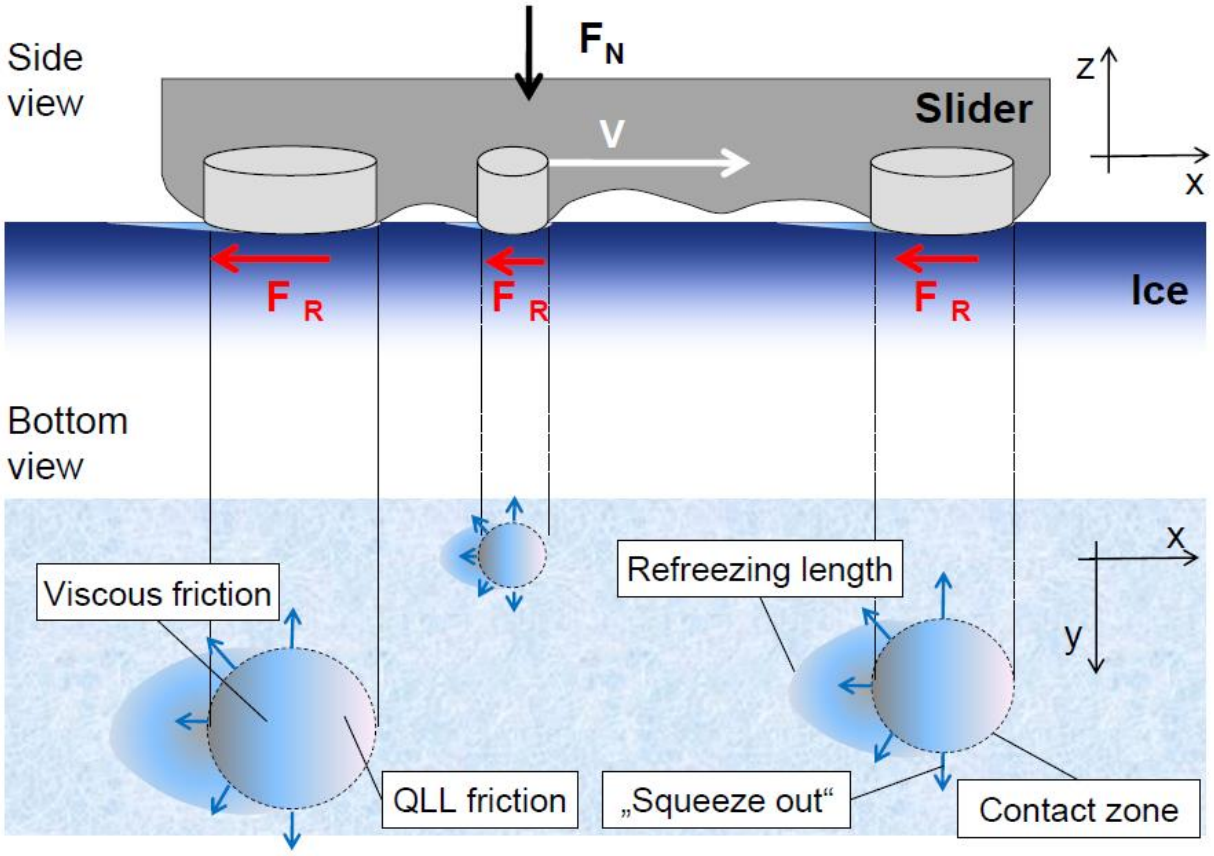

FIGURE 21:THE ASPERITIES ARE REPRESENTED BY CYLINDERS. IN THE UPPER PART, THE PLANE Z,X IS REPRESENTED. IN THE LOWER PART, PLANE X,Y IS REPRESENTED [5].

On the upper surface of the rubber block a normal pressure is applied. The rubber block is in sliding motion. This phenomenon leads to an amount of *squeezed-out* water carried away by the cylinders from the thin liquid layer at the rubber-ice interface. Consequently, this first hydrodynamic effect reduces the height of the water leading to an increasing value of the friction coefficient. To obtain the height of the water from a numerical point

of view it is necessary to focus first on a single asperity with diameter D_{asp}. The local pressure for each single asperity is p_{asp}. This pressure is applied on the ice surface. Assuming that $h_{asp} \ll D_{asp}$, the variation along the time of the height of the liquid layer due to the "squeeze-out" effect can be written with the equation (5.14) as follow:

$$\frac{dh_{asp}(t)}{dt} = -\frac{8}{3\,\eta_{water}} \frac{p_{asp}}{D_{asp}^2} h_{asp}(t)^3\,, \qquad t > 0 \tag{5.14}$$

the average of the local pressure can be written as follow (5.15):

$$\langle p_{asp} \rangle = \frac{F_z}{A_{real}} = A_{nom} \cdot \frac{p_{nom}}{A_{real}} = \frac{p_{nom}}{k} \tag{5.15}$$

Moreover, considering the average of the asperities diameter $\langle D_{asp} \rangle$ the formula (5.14) can be modified, as shown below (5.16):

$$\frac{dh_{asp}(t)}{dt} = -\frac{8}{3\,\eta_{water}} \frac{p_{nom}/k}{\langle D_{asp} \rangle^2} h_{asp}(t)^3\,, \qquad t > 0 \tag{5.16}$$

In figure 22 the squeeze-out effect is graphically represented.

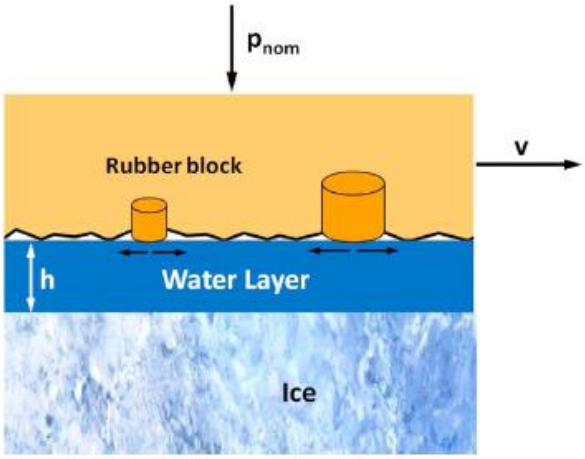

FIGURE 22: SCHEMATIC REPRESENTATION OF THE SQUEEZE-OUT EFFECT [3].

The next step is to consider the effect on the whole contact area. Therefore, it is necessary to assert that the *squeeze-out* occurs only in the points of the real contact area. The equation used to describe the phenomenon on the whole contact area is obtained multiplying the equation for the relative contact area k, as in the equation (5.17).

$$\frac{dh_{asp}(t)}{dt} = -\frac{8}{3\,\eta_{water}}\,\frac{p_{nom}}{\langle D_{asp}\rangle^2}\;h_{asp}(t)^3\,, \qquad t > 0 \tag{5.17}$$

The water trapped in the layer of the interface liquid is stored in the rough rubber surface. Admitting the presence of the rubber asperities at the contact surface a free volume exists. When all the free volumes of the rubber are filled by the *squeezed-out* water the saturation effect is reached. In the saturation condition the *squeeze-out* effect is no more possible. This last phenomenon becomes more probable over the time. In fact, when the melting temperature is reached, a new amount of water, which is added to the existing one, can be squeezed-out, filling the available volume on the rubber surface more quickly. The saturation has a considerable negative effect on the friction coefficient. In fact, when saturation occurs, there is a very rapid growth of the height of liquid layer with a consequent huge drop in the value of the friction coefficient. Graphically, this phenomenon is shown in figure 23.

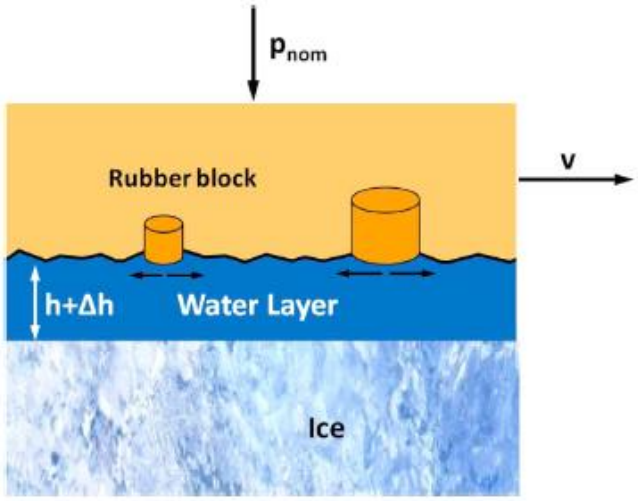

FIGURE 23: THE OCCURRENCE OF THE SATURATION EFFECT [3].

To describe this phenomenon from a mathematical point of view, it is necessary to consider two quantities:

- The free surface volume V
- The squeezed-out water volume at time t, $V_S(t)$

the saturation effect does not occur if:

- $V_S(t) \leq V, \ for \quad t \geq 0$

The same relation can be written in terms of water height and nominal contact area considering, respectively, the average height of the free rubber surface H_V:

$$H_V = \frac{V}{A_{nom}} \tag{5.18}$$

and the average of the squeezed-out water height at time t $H_S(t)$:

$$H_S(t) = \frac{V_S(t)}{A_{nom}} \tag{5.19}$$

So, the saturation effect is not present when:

$$H_S(t) \leq H_V, \qquad for\ t \geq 0 \tag{5.20}$$

The evaluation of the of the average height of the squeezed-out water is made considering, first the height of the squeezed-out water of a single asperity $H_{asp,S}(t)$, (5.14) and then, applying the integration procedure over the time, as follow (5.21):

$$H_S(t) = k \cdot H_{asp,S}(t) = \frac{8}{3\,\eta_{water}} \frac{\langle p_{nom} \rangle}{\langle D_{asp} \rangle^2} \int_0^t h(t)^3 \, dt, \qquad t \geq 0 \tag{5.21}$$

k is the relative contact area and $H_{asp,S}(t)$ refers to the real contact area whereas $H_S(t)$ is referred to the nominal contact area. The condition which distinguishes between the squeeze-out phenomenon and the saturation phenomenon can be written as follow (5.22):

$$H_S(t) = \frac{8}{3\,\eta_{water}} \frac{p_{nom}}{\langle D_{asp} \rangle^2} \int_0^t h(t)^3 \, dt \leq H_V, \qquad t \geq 0 \tag{5.22}$$

If the (5.22) is true, there is no saturation effect and the squeeze-out phenomenon is the only one present. Otherwise, if $H_S(t)$ becomes equal to the value of H_V, all the available free space in the rubber surface is filled by the water and no more saturation effect is possible. For this reason, a parameter $\mathcal{X}_{\{H_S(t)<H_V\}}$, is introduced in this formulation. The value of this parameter can be 0 or 1. This parameter activates or deactivates the term expressed in equation (5.17):

- If $H_S(t) < H_V$, $\mathcal{X}_{\{H_S(t)<H_V\}} = 1$
- If $H_S(t) = H_V$, $\mathcal{X}_{\{H_S(t)<H_V\}} = 0$

5.2.4.Complete thermo-hydrodynamic formulation

The complete formula for the evaluation of the height of the liquid layer, considering a rough rubber block that slides on a smooth ice surface, can be written with the equation (5.23):

$$\frac{dh(t)}{dt} = \frac{1}{\rho_{ice}\, L_{ice}} \left(k\, \eta_{water} \frac{v^2}{h(t)} - \lambda_{ice} \cdot \partial_z T_{ice}(z,t)_{|z=0} \right) \cdot \mathcal{X}_{\{T_{ice(0,t)} < T_m\}} - \frac{8}{3\, \eta_{water}} \frac{p_{nom}}{\langle D_{asp} \rangle^2}\ h_{asp}(t)^3 \cdot \mathcal{X}_{\{H_S(t) < H_V\}}, \quad for\ t > 0 \tag{5.23}$$

With the initial condition (5.24):

$$h(0) = h_0, \quad for\ t = 0 \tag{5.24}$$

5.2.5.Friction coefficient

The height of the liquid layer, due to the thermo-hydrodynamic interaction between the rubber block and the ice is obtained solving the equation (5.23). The next step is the calculation of the value of the friction coefficient. In general, the friction coefficient can be described as a time-dependent quantity using the Coulomb's formulation, as done by Wiese et al. [3]. The friction coefficient is defined as the ratio between the reaction force in the opposite direction of the motion $F_{shear}(t)$ and the normal load F_z. More in detail, it is possible to write:

$$\mu(t) = \frac{F_{shear}(t)}{F_z} \tag{5.25}$$

considering that the reaction force in the opposite direction of the motion is:

$$F_{shear}(t) = \tau_{shear} \cdot (t)\, A_{nom} \tag{5.26}$$

and that the normal load can be defined as:

$$F_z = p_{nom} \cdot A_{nom} \tag{5.27}$$

if the loads are both applied on the same area, the formula (5.25) for the evaluation of the friction coefficient can be written in terms of pressure and shear stress (5.28):

$$\mu(t) = \frac{\tau_{shear}}{p_{nom}} \tag{5.28}$$

The value of the viscous shear stress can be obtained with Newton's law [3] equation (5.2).

$$\tau_{shear}(t) = \eta_{water}\ \frac{v}{h(t)} \tag{5.2}$$

However, the friction force is applied on the real contact area, hence a further modification of the equation (5.29) has to be made introducing the relative contact area k:

$$\tau_{shear}(t) = k\ \eta_{water}\ \frac{v}{h(t)} \tag{5.29}$$

Therefore, considering the equations (5.28) and (5.29), the final expression of the friction coefficient is expressed by the equation (5.30):

$$\mu(t) = k\ \frac{\eta_{water}}{p_{nom}}\ \frac{v}{h(t)} \tag{5.30}$$

5.3. Solution of the thermo-hydrodynamical formulation

The easiest way for solving the equation (5.23) is using numerical methods. To define a numerical procedure it is necessary to define all the parameters of the equations. To solve the thermo-hydrodynamical equation (5.23), the following parameters have to be defined:

- The relative contact area k
- The average asperity diameter $\langle D_{asp} \rangle$
- The average free surface height H_V

These contact parameters are strictly related to the material characteristics and to the level of the load applied to the rubber as demonstrated by Wiese et al. in [3], where three different rubber compounds are evaluated, varying the value of the pressure applied. The difference between these rubber compounds concern the stiffness. Compound A is the softest, compound C is the hardest while compound B has intermediate characteristics. The elastic modulus of each compound, representative of the mechanic properties of that particular material tested by Wiese et al. [3], are shown in table 3:

A	B	C
1.10 MPa	1.64 MPa	2.04 MPa

TABLE 3: ELASTIC MODULI OF THE THREE DIFFERENT RUBBER COMPOUNDS.

The three contact parameters are a consequence of the contact characteristics between the rubber and the ice. Therefore, a model of the roughness of the lower rubber surface is necessary. The method proposed in [3] consists in a measurement with a contactless optical device of the rough rubber profile in order to obtain a 3D geometrical model of

the contact surface. The geometry obtained with the experimental measurement was used to build a FEM model of the rubber block. A contact area of 1 mm^2 was considered. The highest possible resolution (17.5 μm in this case) was chosen to discretize the rubber block with a regular mesh and without losing information about the roughness. The material model used for the rubber is the Mooney-Rivlin model [3, 14]. The reason of this choice is in the high deformation level of the rubber block under the application of the normal load with a consequent strong non-linear behaviour. The next step for the evaluation of the contact parameters is a static FE simulation. In this simulation the rubber block is pressed on the ice surface with different values of pressure. In this analysis the static friction coefficient was assumed 0.1. The results of the FE simulation allow to obtain the parameters k, D_{asp} and H_V. In figure 24 the model developed in [3] and the results of the profile of the contact interface are shown.

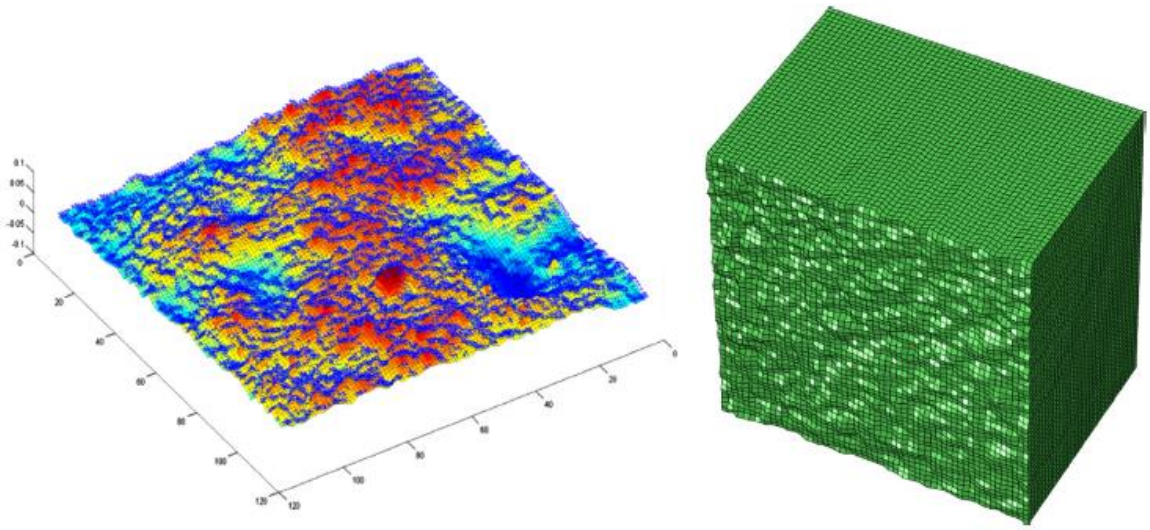

FIGURE 24: ON THE LEFT SIDE, MEASUREMENT WITH A CONTACTLESS OPTICAL DEVICE OF THE ROUGH RUBBER SURFACE IS SHOWN. ON THE RIGHT SIDE, THE RESULTING 3D FEM MESHED MODEL [3].

5.3.1.Relative contact area

Wiese et al. [3] were able to calculate the value of the relative contact area studying the 3D contact surface obtained with the static simulation. In more details, the number of the nodes in contact between the two parts were counted. This number, divided by the total number of the nodes on the lower surface, gives a qualitatively value of k. The absolute value of the relative contact area cannot be evaluated due to the resolution level of the contact image. The real contact area is a decreasing function of the length scale as suggested by Persson [1]. For this reason, the real contact area has to be lower that the predicted one and, in order to overcome this inaccuracy, the contact area was reduced by 25%. In figure 25 the results obtained by Wiese et al. [3] are shown. Three different rubber compounds are tested. The relative contact area is directly dependent on the nominal pressure. The higher the value of the nominal pressure, the higher the real contact area. The curve of the relative contact area for the compound A is the highest one because it has the lowest value of stiffness. Summarizing, the higher the stiffness value, the lower the real contact area.

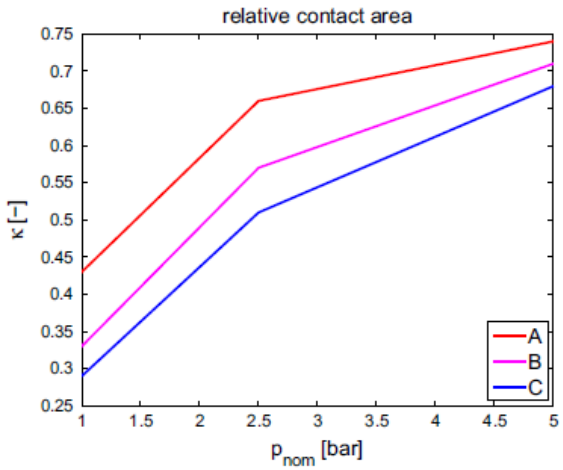

FIGURE 25: THE RELATIVE CONTACT AREA OF THE THREE RUBBER COMPOUNDS AS A FUNCTION OF THE NOMINAL PRESSURE [3].

5.3.2.Average asperity diameter

For the evaluation of the average diameter of the asperity, it is necessary to obtain, as done by Wiese et al. [3], a contact picture from the FEM simulation. Figure 26 shows three different contact images for the compound A. The three images differ for the level of the pressure applied to the rubber. The same procedure was also applied to the other compounds.

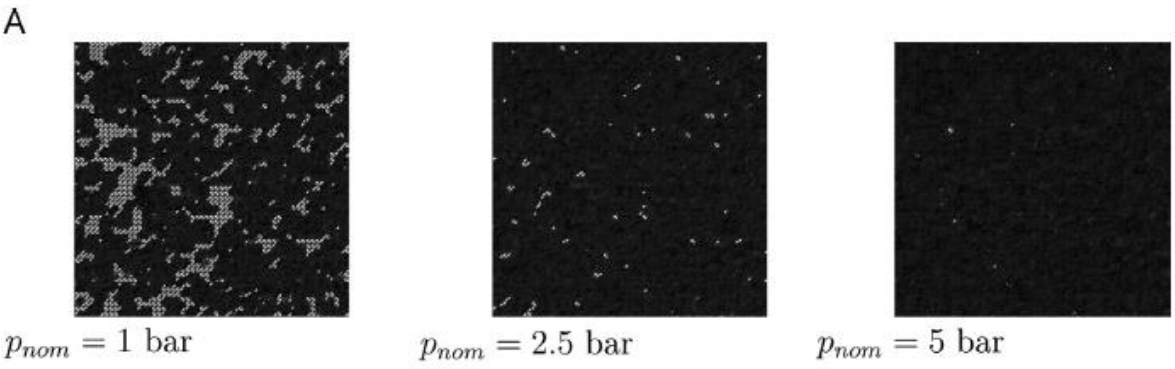

FIGURE 26:CONTACT PRESSURE IMAGES FROM FEM CONTACT SIMULATION FOR THE COMPOUND A [3].

The connected intervals of the contact pixel can be counted on these images, as suggested by Wiese et al., [3]. This operation was made both in x- and y-direction. The entity so called "contact length" is the results of this operation. The average asperity diameter was obtained as the median of all the determined contact lengths. The Figure 27 shows the results of this procedure for the three compound and for the different levels of the nominal pressure. The average diameter of the asperity is an increasing function of the pressure. Moreover, softer compounds have higher value of $\langle D_{asp} \rangle$.

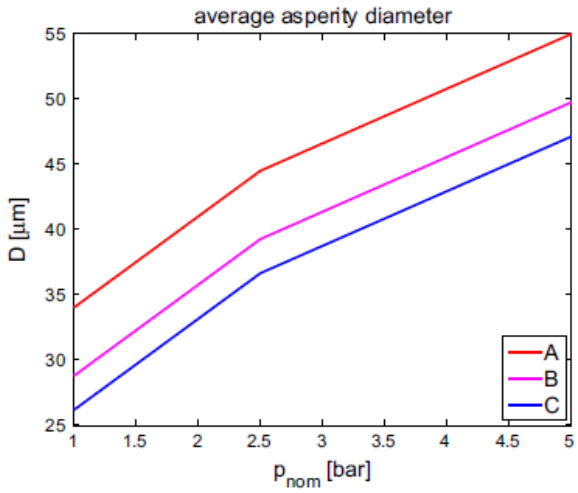

FIGURE 27: THE AVERAGE ASPERITY DIAMETER OF THE THREE RUBBER COMPOUNDS AS A FUNCTION OF THE NOMINAL PRESSURE [3].

5.3.3.Average free surface height

For the average height of the free surface, the evaluation procedure was made studying the results of the FEM simulation, as proposed by Wiese et al. [3]. The normal distance between all the non-contact nodes between the ice surface and the rubber surface $d(x)_{x\notin A_{real}}$ has to be measured. By averaging this quantity and by multiplying it with the complementary of the relative contact area, the average of free surface height H_V is obtained:

$$H_V = (1-k)\cdot \langle d(x)\rangle_{x\notin A_{real}} \tag{5.31}$$

The average height of the free surface decreases for higher values of pressure as shown in Figure 30. Softer compound has, in general, lower values of H_V.

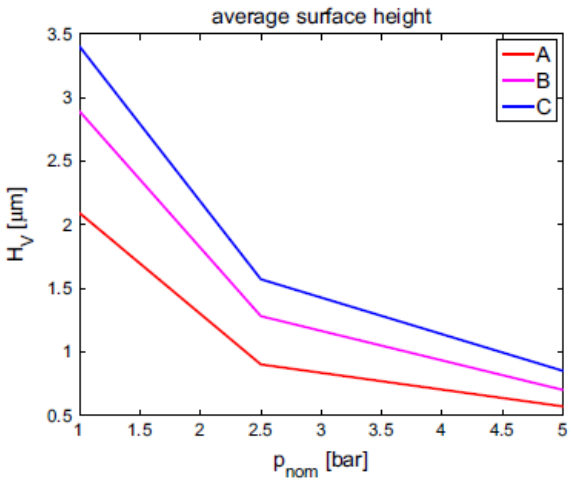

FIGURE 28 THE AVERAGE SURFACE HEIGHT OF THE THREE RUBBER COMPOUNDS AS A FUNCTION OF THE NOMINAL PRESSURE [3].

5.4. Numerical results

A time-dependent friction coefficient is obtained solving the equation (5.23) coupled with the equation (5.30). The effects related to the rubber compound as well as the dependence of the load condition and the sliding velocity are taken into account. Wiese et al. [3] proposes two different solutions of the non-stationary friction coefficient for two different levels of the nominal pressure. The values of the pressure are respectively $p_{nom1} = 1\ bar$ and $p_{nom2} = 5\ bar$. The initial conditions are the initial temperature of the ice $T_{ice} = -4°C$ and the initial height of the liquid layer $h_0 = 70\ nm$. This last value, confirmed by the theory developed Persson [1], was evaluated experimentally, as suggested in [3]. The duration of the tests was $T = 5\ ms$. This value was defined considering a general length for the block of the winter tires of about $20\ mm$ and a sliding velocity of $v = 4\ \frac{m}{s}$. In the following paragraphs, the results for the two different value of pressure are showed and compared.

5.4.1.Friction coefficient for 1 bar of nominal pressure

The Figure 29 shows the results obtained in term of height of the liquid layer (on the left hand side) and the correspondent value of the friction coefficient. There are two different phases.

- The phase 1 represent the *squeeze-out* effect. The melting temperature of the ice are not reached consequently the height of the liquid layer decreases. Mathematically, this means that the value of the characteristic function $\mathcal{X}_{\{T_{ice(0,t)}<T_m\}}$ is 0 whereas, a certain amount of free space which can be filled by the water is still present, so $\mathcal{X}_{\{H_S(t)<H_V\}} = 1$. Applying these considerations to equation (5.23), a formula which describes the variation of the height of the liquid layer due to the *squeeze-out* effect is obtained (5.32).

$$\frac{dh(t)}{dt} = -\frac{8}{3\,\eta_{water}} \frac{p_{nom}}{\langle D_{asp}\rangle^2} h_{asp}(t)^3 , \quad for\ t > 0 \tag{5.32}$$

  From a physical point of view starting from the initial value of h_0, the cylinders representative of the roughness of the rubber surface act like brushes, taking away the initial amount of the liquid layer. Therefore, the friction coefficient increases its value.

- The phase 2 starts with a singularity point. In this point the melting temperature is reached, hence $\mathcal{X}_{\{T_{ice(0,t)}<T_m\}} = 1$. From this point, a new amount of water is produced leading to an increasing value of the height of the liquid layer. However, because the nominal pressure has a relative low value, the condition expressed by equation (5.22) is still true and so, the *squeeze-out* effect is still

present and thus $\mathcal{X}_{\{H_S(t)<H_V\}} = 1$. This means that there are two counterbalanced phenomena, therefore the growth rate of the curve is not very high, as shown by the equation (5.32):

$$\frac{dh(t)}{dt} = \frac{1}{\rho_{ice}\, L_{ice}}\left(k\,\eta_{water}\,\frac{v^2}{h(t)} - \lambda_{ice}\cdot\partial_z T_{ice}(z,t)_{|z=0}\right) - \frac{8}{3\,\eta_{water}}\,\frac{p_{nom}}{\langle D_{asp}\rangle^2}\,h_{asp}(t)^3, \quad for\ t>0 \tag{5.32}$$

This second phase negatively affects the friction performance of the rubber block considering that the higher the height of the liquid layer, the lower the friction coefficient.

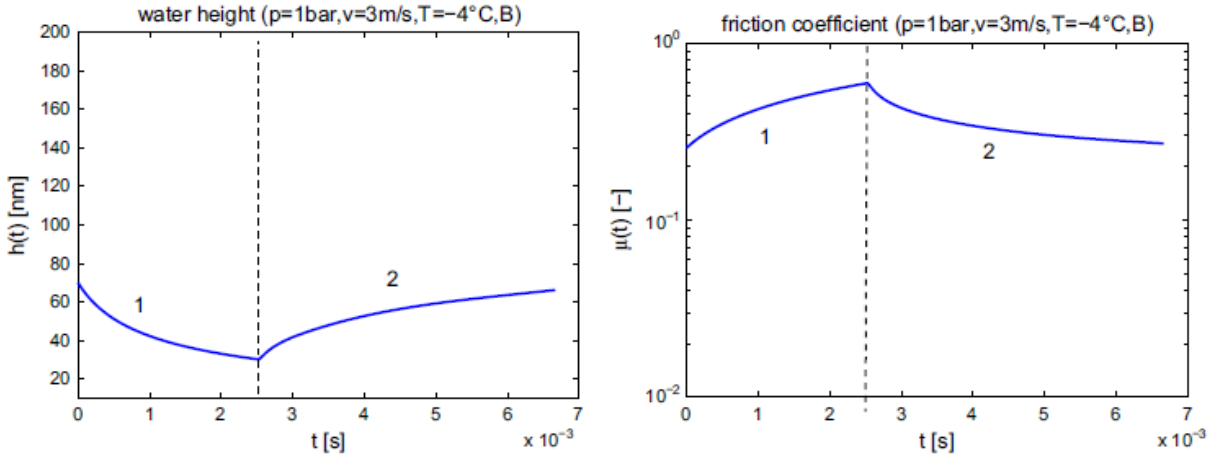

FIGURE 29: ON THE LEFT-HAND SIDE, THE HEIGHT OF LIQUID LAYER IS SHOWN. ON THE RIGHT-HAND SIDE, THE FRICTION COEFFICIENT. THE NOMINAL PRESSURE IS 1 BAR [3].

5.4.2.Friction coefficient for 5 bar of nominal pressure

The higher level of the nominal pressure leads to a completely different behaviour during the sliding contact. High pressure level affects the result in different aspects. Firstly, there is a big influence on the contact parameters and secondly, the amount of the deformation

work increases. As result of these considerations, a third phase is present as shown in Figure 32. More in detail:

- The phase 1 is considerably shorter than the one in the 1 bar simulation. The melting temperature is reached very quickly due to the higher amount of the friction energy produced, at least in this first phase.
- The duration along the time of the phase 2 is longer than the corresponding duration in the 1 bar simulation. For this reason, a longer steady-state period is obtained.
- The phase 3 is representative of the saturation effect which starts when $H_s(t) = H_V$ and so, $\mathcal{X}_{\{H_S(t)<H_V\}} = 0$. As a consequence, the negative contribution to the height of the liquid layer is switched-off. All the water that comes from the melting of the ice increases considerably the height of the liquid layer leading to an important fall of the value of the friction coefficient. These results can be explained with the equation (5.34):

$$\frac{dh(t)}{dt} = \frac{1}{\rho_{ice}\, L_{ice}}\left(k\, \eta_{water} \frac{v^2}{h(t)} - \lambda_{ice} \cdot \partial_z T_{ice}(z,t)_{|z=0}\right), \quad for\ t > 0 \tag{5.34}$$

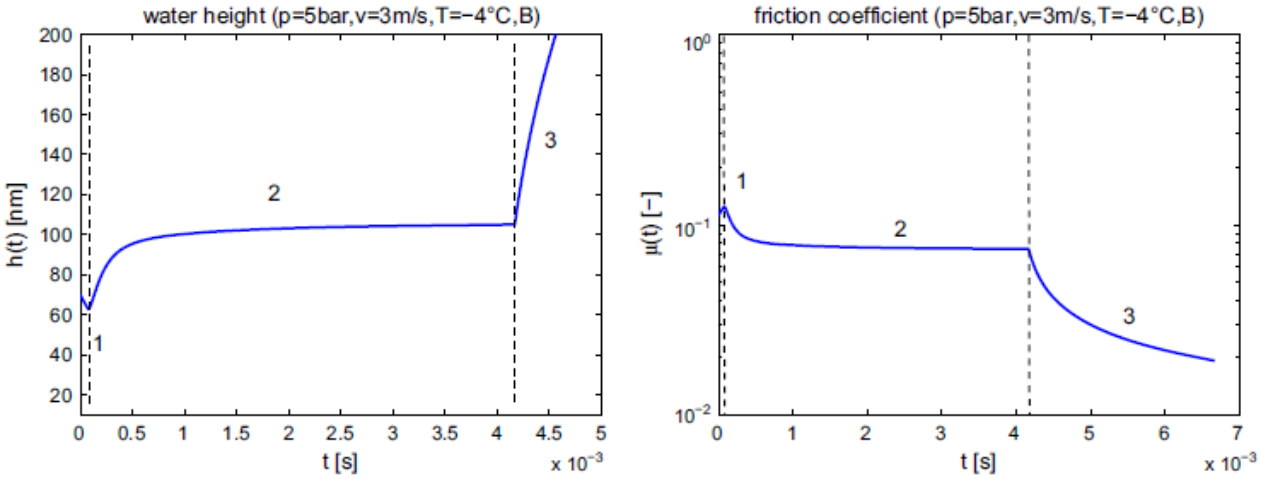

FIGURE 30: ON THE LEFT-HAND SIDE, THE HEIGHT OF LIQUID LAYER IS SHOWN. ON THE RIGHT-HAND SIDE, THE FRICTION COEFFICIENT. THE NOMINAL PRESSURE IS 5 BAR [3].

5.5. Validation procedure

In this section, the methodology proposed by Wiese et al. [3] for the validation of the results is showed. The device used for the experimental test is called High Speed Linear Friction Tester. A rubber sample is carried by a sliding runner on a ice surface under a defined condition of temperature and normal pressure. Figure 31 shows the test machine used in [3].

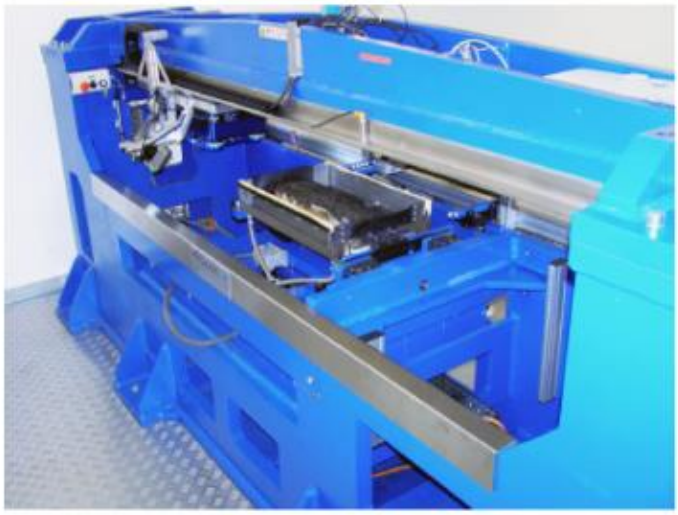

FIGURE 31: THE DEVICE USED FOR THE EVALUATION OF THE EXPERIMENTAL FRICTION COEFFICIENT, CALLED HIGH SPEED FRICTION TESTER [3].

The experimental friction coefficient is obtained as the ratio between the frictional force and the normal load in the stationary sliding phase. It is important to specify that, the term frictional force is meant the reaction force which the sliding runner of the device has to reach in order to move the rubber sample with the prescribed velocity. Figure 32 shows the time-dependent results obtained with this measurement device:

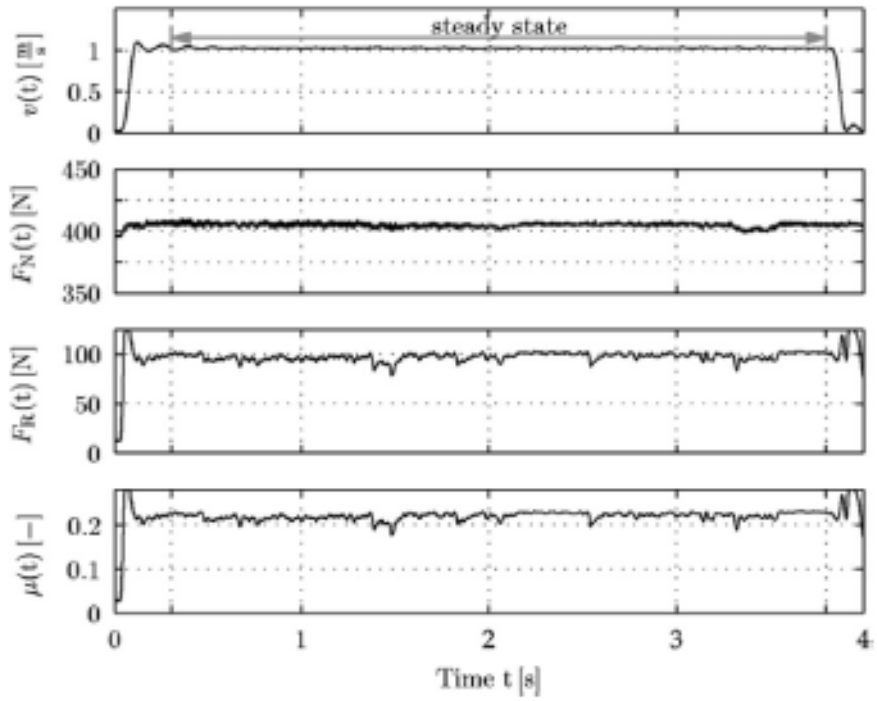

FIGURE 32: THE FIRST TWO CURVES REPRESENT THE OPERATIONAL PARAMETERS OF THE HIGH SPEED FRICTION TESTER, THE VELOCITY $v(t)$ AND THE NORMAL LOAD $F_N(t)$. THE LAST TWO CURVES, INSTEAD, REPRESENTS THE OUTPUT OF THE TEST, THE FRICTIONAL FORCE $F_R(t)$ AND THE FRICTION COEFFICIENT $\mu(t)$ [3].

The comparison between model's result and experimental data cannot be done by considering the absolute value of the friction coefficient because the macroscopic effects (e.g. the rubber block bending, the water wiping) are not considered. Consequently, the

numerical value could be shifted up or down in comparison to the real friction coefficient. Moreover, the model's result is a non-stationary friction coefficient whereas the test measurements can be carried out only in the steady-state condition. Choosing the time interval $[0, T]$ it is possible to define the average value of the friction coefficient as follow:

$$\mu_T = \langle \mu(t) \rangle_{[0,T]} \tag{5.35}$$

The equation (5.35) shows the high level of dependence that the averaged friction coefficient has with the sliding time T. This numerical value can be easily changed considering a different sliding time. Therefore, a qualitative comparison is carried out without considering the exact numerical value. The following comparison were made considering the average value of the frictional coefficient obtained with the model and the measured one. Different conditions of nominal pressure, velocity and temperature for a medium compound were considered.

5.5.1.Influence of nominal pressure

The Figure 33 shows the dependence of the friction coefficient with the pressure, for different ice temperatures. The comparison is made considering a medium stiffness rubber compound and a sliding velocity of 3 $\left(\frac{m}{s}\right)$. Both the experimental measurements and the model results show that frictional coefficient is a decreasing function in relations to the pressure. This is true for all the temperature values. In addition, the lower the temperature value the higher the dependency of the friction coefficient on the pressure.

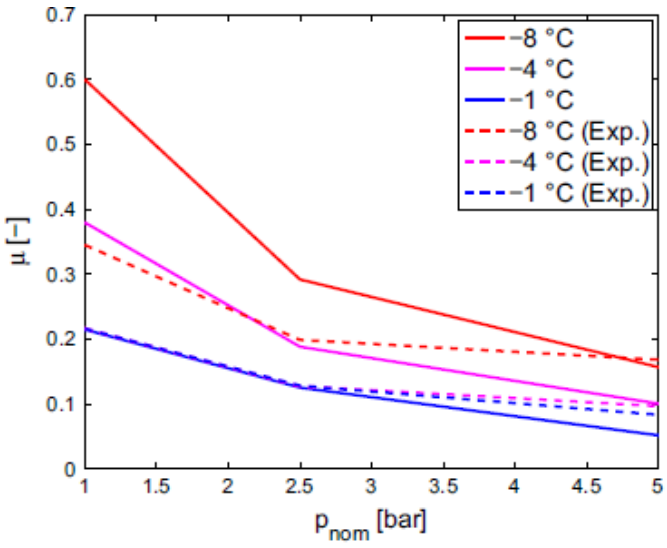

FIGURE 33: THE DIFFERENT VALUE OF THE FRICTION COEFFICIENT FOR DIFFERENT LEVEL OF NOMINAL PRESSURE FOR THE RUBBER COMPOUND B [3].

5.5.2.Influence of sliding velocity

This second analysis considers a medium rubber compound. The initial temperature of the ice is fixed to $-4°C$. Different tests are made with different pressure levels changing the sliding velocity. The results are showed in Figure 34.

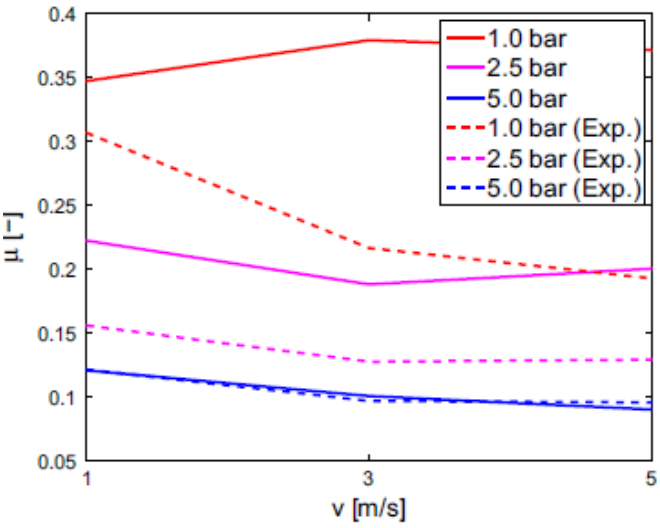

FIGURE 34: THE DIFFERENT VALUE OF THE FRICTION COEFFICIENT FOR DIFFERENT VALUE OF THE SLIDING VELOCITY FOR THE RUBBER COMPOUND B [3].

The model's result has also a good qualitative matching level for the test conducted with $p_{nom} = 1\,bar$. For low pressure value, the squeeze-out effect is less effective. Consequently, the melting temperature is reached relatively late. For this reason, the sliding phase with the melted ice is shorter than the one for the high pressure level, and the velocity effect is not so important.

5.5.3.Influence of the initial temperature of the ice

The same rubber compound with a sliding velocity of 3 $\left(\frac{m}{s}\right)$ is simulated by varying the value of the initial temperature of the ice for different pressure levels. The Figure 35 shows that both in simulation and in the experiments, the friction coefficient is a decreasing function of the temperature. With high temperatures a higher height of the water is obtained, and therefore a lower value of the friction coefficient.

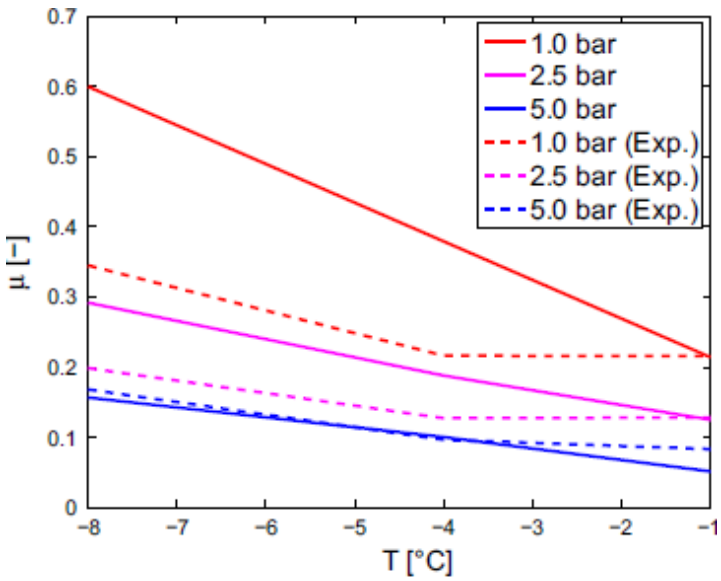

FIGURE 35: THE DIFFERENT VALUE OF THE FRICTION COEFFICIENT FOR DIFFERENT VALUE OF THE INITIAL TEMPERATURE OF THE ICE FOR THE RUBBER COMPOUND B [3].

5.6. Conclusion

An advanced viscous model for the evaluation of the friction coefficient during the sliding contact between rubber and ice was developed by Wiese et al. [3]. Starting from a microscopic approach, which includes both thermodynamic and hydrodynamic aspects, a non-stationary friction coefficient was obtained. The comparison between the model's result and the experimental results shows a good level of agreement, in particular from a qualitative point of view. For all these reasons, the last part of this master thesis work consists in the development of a FEM model for the simulation of the conditions described by this viscous model. A thermo-mechanical simulation will be used to study the sliding condition between the rubber and the ice. A customized sub-routine, according to the equation (5.23) was implemented in order to obtain, step by step, the friction coefficient that has to be used in the thermo-mechanical simulation. In addition, the macroscopic effect of the rubber block bending will be taken into account in the FE model developed in this thesis. This effect was not considered in the model developed by Wiese et al. [3]. This macroscopic effect can be very effective, because it has a direct influence on the pressure distribution on the contact interface. In the model proposed by Wiese et al. [3] it is neglected. A second macroscopic effect is the water wiping effect. It consists in a certain amount of water that goes out from the contact interface, spreading itself in the whole ice surface. A specific hydrodynamic module or, alternatively, a further modification of the constitutive equation (5.23) are required to capture this effect.

Chapter 6

6. Finite element model for rubber-ice sliding friction

6.1. Introduction

The last part of this master thesis work is dedicated to the development of a viscous model for the sliding friction between rubber and ice, based on the theory proposed by Wiese et al. [3]. To reproduce the frictional behavior during the sliding contact between rubber and ice with the same test conditions proposed in [3], the commercial finite element software *LS-DYNA* was chosen. The most innovative aspect of this work is the use of the finite element method to perform a thermo-structural analysis for the simulation of the contact between rubber and ice. In particular, both the thermal and the structural analysis are characterized by the calculation and the subsequent use of the non-stationary value of the friction coefficient. In the work of Wiese et al. [3], the FEM simulation was only used to determine the contact parameters while the sliding contact simulation was performed by solving the equation (5.23) without using finite element method. However, also if in this work are used different methods than those used in [3] for the evaluation of the frictional coefficient, the original division in two steps of the whole simulation used in [3], is maintained as shown in figure 36. The first one is the pre-load phase in which the static friction coefficient is used. In this phase, a normal load is applied on the rubber block and

the sliding velocity condition are subsequently established. With the transient analysis the real friction calculation starts.

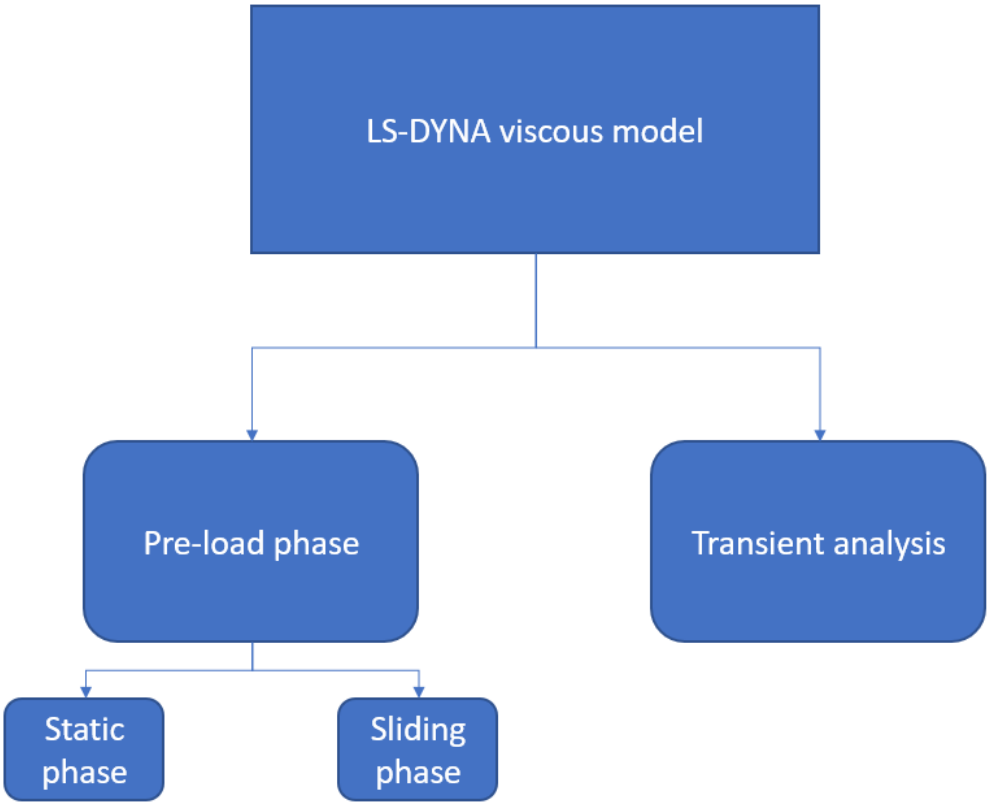

FIGURE 36: LS-DYNA SIMULATION SCHEME.

The pre-load phase consists in two stages, as shown in figure 37. The static contact simulation between the rubber block and the ice is represented by the images on the left and on the center of figure 36. In this phase of the simulation the normal load is applied on the upper surface of the rubber. After that, the sliding phase can start, as shown in the right hand side of the figure 36. The sliding velocity in y-direction is applied to the rubber block in order to reproduce the correct initial conditions for the evaluation of the non-stationary friction coefficient proposed in [3].

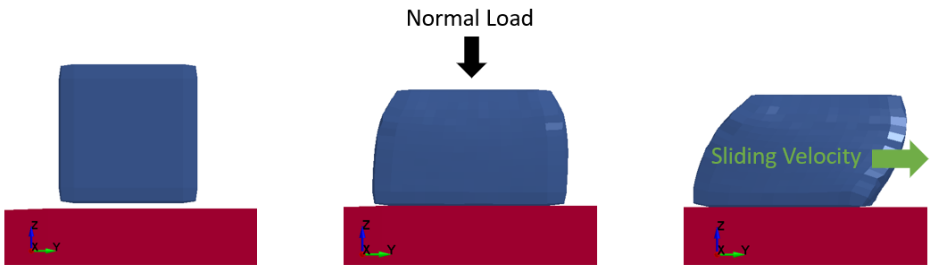

FIGURE 37: THE THREE DIFFERENT STAGES OF THE PRE-LOAD PHASE. ON THE LEFT HAND SIDE, THE INITIAL CONDITION IS SHOWN. IN THE CENTRE, THE APLLICATION OF THE NORMAL LOAD IS SHOWN. ON THE RIGHT HAND SIDE, THE SLIDING SIMULATION ARE REPRESENTED.

The static phase of the pre-load phase is detailed in figure 38. The left side of the figure 38 shows the initial condition of the static simulation in which, the rubber block (in blue) is not in contact with the ice block (in red). The right side of the figure 37 shows instead the deformed shape of the rubber block, under the action of the normal load, when the equilibrium condition is reached.

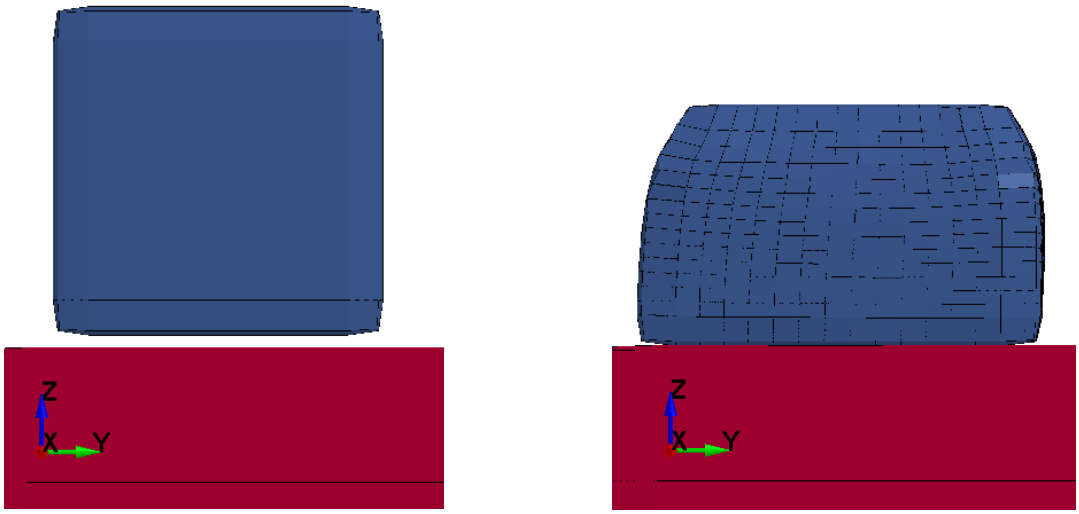

FIGURE 38: ON THE LEFT HAND SIDE, THE INITIAL CONDITION OF THE SIMULATION IS SHOWN. ON THE RIGHT HAND SIDE, THE DEFORMED SHAPE OF THE RUBBER BLOCK REACHED AT THE EQUILIBRIUM IS SHOWN.

During the subsequent sliding simulation, the strain level is responsible for the deformation work which is the first heat source of the problem. This amount of energy contributes to the determination of the height of the liquid layer and therefore to the coefficient of friction in the next transient phase. The bending level of the rubber block, representative of the amount of the available frictional energy under the sliding phase, is shown in figure 39.

FIGURE 39: BENDING OF THE RUBBER BLOCK DURING THE SLIDING SIMULATION

Then, in the next transient phase, the friction coefficient influences the thermo-mechanical simulation because the different value of the friction coefficient causes different levels of deformation during the sliding simulation. The figure 40 shows this effect. At different time during the simulation, the friction coefficient depends on the contact characteristic but also affects the thermo-mechanical simulation. In particular, it is possible to see that, while the first image on the left hand side is taken at time 0.8 (ms) with an high value of the friction coefficient, the image on the right is caught at 7 (ms), when the *saturation* effect is working with a consequent lower value of the friction

coefficient. Therefore, the deformed shape of the rubber block is representative of the contact characteristic, of the sliding simulation for a defined instant of time.

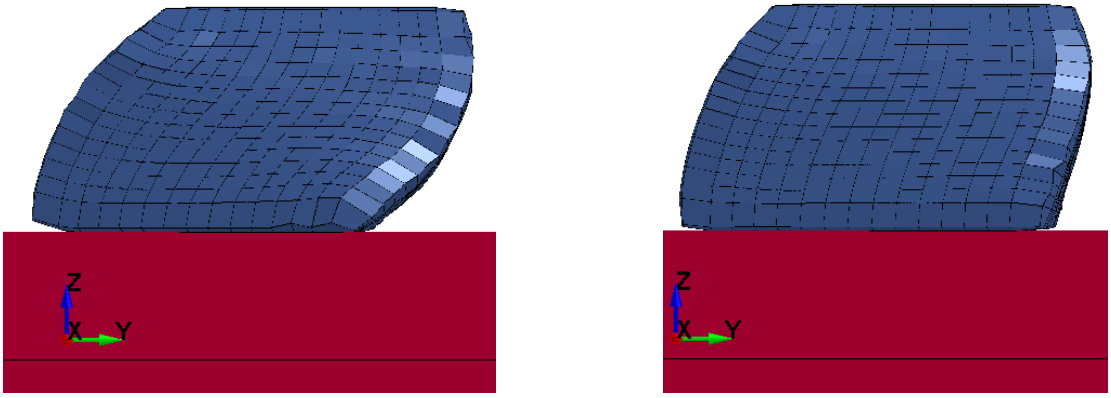

FIGURE 40: COMPARISON BETWEEN TWO DIFFERENT LEVEL OF DEFORMATION OF THE RUBBER BLOCK WITH DIFFERENT VALUE OF FRICTION COEFFICIENT. THE FRICTION COEFFICIENT FOR THE IMAGE ON THE LEFT SIDE IS 0.12 WHILE ON THE RIGHT SIDE IS 0.04.

Thus, there is a loop between the thermo-mechanical simulation and the calculation of the friction coefficient. Because of this, the whole model was built-up in two different sections. A sub-routine is completely dedicated to the frictional coefficient calculation by solving, step by step, the equation (5.23). A standard thermo-mechanical module of LS-DYNA take as input the current value of the friction coefficient and gives as output all the necessary information for the sub-routine calculation. Alternative approaches could be represented by meshless module, such as DEM (Discrete Element Method) module or SPH (Smooth Particles Hydrodynamics) module combined with an ALE (Arbitrary Lagrangian Eulerian) analysis. However, these two methods were not investigated, mainly because:

- The high risk of instability and the discontinuity in the definition of the equation of state are the main unsolved problems up to this moment.
- The magnitude of the dimensions involved such as, the initial height of the liquid layer is about $70 \cdot 10^{-9}\,(m)$. This means that the calculation time will be considerably massive especially thinking about a further extended analysis to the whole tire.

These two problematic aspects were overcome by using the LS-DYNA UDF module (User Define Features). In particular, the User Define Friction module allows to write a customized formula for the evaluation of the friction coefficient. By the mathematical modelling of the phase change of the ice, instability and discontinuity can be solved. All the necessary input data for the evaluation of the friction coefficient are provided by the thermo-mechanical simulation, which represents a virtual reproduction of the real test condition proposed in [3]. In addition, the calculation time is not affected by this numerical procedure.

6.2. Numerical formulation

The analytical formulation, represented by equations (5.23) and (5.24), was solved numerically. This is the simplest way to solve this set of equations. In addition, the solution can be written with a simple expression that can be implemented easily. The numerical method used to solve these equations was the Explicit Euler, [13]. In general, a derivative of a function $h(t)$ can be written as an incremental ratio, as showed in the equation (6.1).

$$\frac{dh(t)}{dt} = f(t) \longrightarrow \frac{h_{j+1} - h_j}{dt} = f(t) + \varepsilon(t) \tag{6.1}$$

Where the term $\varepsilon(t)$ represents the discretization error, dt is the chosen time step and $f(t)$ represent the mathematical expression of the derivative. In the first discretization stage the infinitesimal $dh(t)$ is written as a finite difference between the value of $h(t)$ at time $t + dt$ called h_{j+1} and the previous value at time t called h_j. It is possible to write the equation (6.2).

$$h_{j+1} = h_j + dt\left(f(t) + \varepsilon(t)\right) \tag{6.2}$$

Neglecting the discretization error, the value of the parameter, calculated in the next time-step, which represents the solution of the problem is a known entity. This procedure will be applied for the solution of the three phases of the equation (5.23).

6.2.1.Discretization of phase 1

The phase 1 represents the *squeeze-out* effect, modelled with the equation (5.32). To find the numerical solution, the terms of the equation (5.32) are associated to the terms in the equation (6.2) as follow.

- $h_{j+1} = h(t + dt)$

- $h_j = h(t)$

- $f(t) = -\frac{8}{3\,\eta_{water}} \frac{p_{nom}}{\langle D_{asp}\rangle^2} h(t)^3$

Hence, neglecting the discretization error, the solution will be:

$$h(t+dt) = h(t) - dt\left(\frac{8}{3\,\eta_{water}}\ \frac{p_{nom}}{\langle D_{asp}\rangle^2}\ h(t)^3\right) \tag{6.3}$$

The only time-dependent parameter is $h(t)$. For reason of formulation compactness, the other terms are putted together in a constant value:

$$h(t+dt) = h(t) - dt\ (K_3\ h(t)^3) \tag{6.4}$$

where

$$K_3 = \frac{8}{3\,\eta_{water}}\ \frac{p_{nom}}{\langle D_{asp}\rangle^2} \tag{6.5}$$

For the first step of the simulation, by using the initial condition (5.23), the solution will be:

$$h_1 = h_0 - dt\ (K_3\ h_0^3) \tag{6.6}$$

Where h_0 is a known value experimentally evaluated as said in [3].

6.2.2.Discretization of phase 2

The phase 2 is characterized by the presence of all the phenomena descripted in chapter 5. For this reason, its solution is the most complex in comparison to the other phases. The expression of the derivative function in this case is:

- $f(t) = \frac{1}{\rho_{ice}\,L_{ice}}\left(k\,\eta_{water}\frac{v^2}{h(t)} - \lambda_{ice}\cdot\partial_z T_{ice}(z,t)_{|z=0}\right) - \frac{8}{3\,\eta_{water}}\ \frac{p_{nom}}{\langle D_{asp}\rangle^2}\ h(t)^3$

Which becomes, solving the heat equation as shown in [5]:

$$f(t) = \frac{1}{\rho_{ice}\, L_{ice}}\left(k\, \eta_{water}\, \frac{v^2}{h(t)} - \lambda_{ice} \cdot \frac{T_m - T_0}{\sqrt{\pi\, \alpha\, t}}\right) - \frac{8}{3\, \eta_{water}}\ \frac{p_{nom}}{\langle D_{asp}\rangle^2}\ h(t)^3 \tag{6.7}$$

Two new terms K_1 and K_2, which allow to write in a simpler way the derivative expression, are introduced:

$$K_1 = \frac{1}{\rho_{ice}\, L_{ice}}\,(k\, \eta_{water}\, v^2) \tag{6.8}$$

$$K_2 = \frac{1}{\rho_{ice}\, L_{ice}}\left(\lambda_{ice} \cdot \frac{T_m - T_0}{\sqrt{\pi\, \alpha}}\right) \tag{6.9}$$

K_1 is composed only by constant terms, while K_2 can be considered as an effective constant value when the solution of the heat equation is obtained considering that the temperature of the ice will not overcome the melting temperature T_m. The equation (6.7) becomes:

$$f(t) = \frac{K_1}{h(t)} - \frac{K_2}{\sqrt{t}} - K_3\, h(t)^3 \tag{6.10}$$

And so, the numerical solution of the (5.32) will be:

$$h(t + dt) = h(t) + dt\left(\frac{K_1}{h(t)} - \frac{K_2}{\sqrt{t}} - K_3\, h(t)^3\right) \tag{6.11}$$

The equation (6.11) is used for the computation of the height of the liquid layer. This computation starts when the melting temperature is reached in the thermo-mechanical simulation. So, the first step of the simulation determined by the (5.33) will be:

$$h_1 = h_{0m} + dt\left(\frac{K_1}{h_{0m}} - \frac{K_2}{\sqrt{t_m}} - K_3\, h_{0m}^3\right) \tag{6.12}$$

Where $h_{0m} = h(t_m)$ represents the last value obtained by using the (6.4), at the time t_m in which the ice starts to melt.

6.2.3.Discretization of phase 3

In the last phase the *saturation* phenomenon is simulated. The expression of the derivative, in this case is:

- $f(t) = \frac{1}{\rho_{ice}\, L_{ice}}\left(k\, \eta_{water}\, \frac{v^2}{h(t)} - \lambda_{ice} \cdot \partial_z T_{ice}(z,t)_{|z=0}\right)$

Which becomes, by solving the heat equation:

$$f(t) = \frac{1}{\rho_{ice}\, L_{ice}}\left(k\, \eta_{water}\, \frac{v^2}{h(t)} - \lambda_{ice} \cdot \frac{T_m - T_0}{\sqrt{\pi\, \alpha\, t}}\right) \tag{6.13}$$

and, by using the previous defined quantities K_1 and K_2 it becomes:

$$f(t) = \frac{K_1}{h(t)} - \frac{K_2}{\sqrt{t}} \tag{6.14}$$

Therefore, the numerical solution of the (5.33) is:

$$h(t+dt) = h(t) + dt\left(\frac{K_1}{h(t)} - \frac{K_2}{\sqrt{t}}\right) \tag{6.15}$$

However, the problem in this case is to understand when the saturation effectively occurs. To do this, the numerical solution of the (5.22) was also obtained. In particular, the first step was to come-back to a differential equation from an integral formulation:

$$\frac{dH_S(t)}{dt} = \frac{8}{3\,\eta_{water}}\ \frac{p_{nom}}{\langle D_{asp}\rangle^2}\ h(t)^3 \tag{6.16}$$

This last expression is very similar to the one used for the phase 1. The derivative function is:

$$f(t) = \frac{8}{3\,\eta_{water}}\ \frac{p_{nom}}{\langle D_{asp}\rangle^2}\ h(t)^3 \tag{6.17}$$

And, applying the explicit method of Euler, the solution for this term is:

$$H_s(t+dt) = H_S(t) + dt\left(\frac{8}{3\,\eta_{water}}\ \frac{p_{nom}}{\langle D_{asp}\rangle^2}\ h(t)^3\right) \tag{6.18}$$

in this expression is also possible to see the presence of the constant K_3. Thus, in a more compact way it is possible to write:

$$H_s(t+dt) = H_S(t) + dt\ (K_3 \cdot h(t)^3) \tag{6.19}$$

This calculation was parallelly made also to the height of the liquid layer, because for the solution of the equation of the average height of the squeezed-out water $H_S(t)$, the value

at the current time-step of $h(t)$ is required. The initial condition for this last expression is:

$$H_s(0) = 0 \tag{6.20}$$

Which means that at the beginning of the simulation, the *squeeze-out* effect is not present. Therefore, during the first step of the simulation, the value of the average height of the squeezed-out water is:

$$H_{s_1} = dt\ (K_3 \cdot h_0^3) \tag{6.21}$$

6.2.4.Numerical solution with *Matlab*

Before to implement this whole procedure in the *LS-DYNA* subroutine, the equations were solved with a *Matlab* script and the obtained result were compared with those showed by Wiese et al. [3]. At first the comparison was made considering the simulation with a 1 bar of nominal pressure. The figure 41 shows a good level of agreement in particular for the phase 1. A higher difference between these two results is found in the phase two. This is manly due because, in the *Matlab* script, it was impossible to obtain the correct information about the simulation time and the temperature on the ice surface. This discrepancy will disappear in the FEM simulation, where all the necessary input data are available.

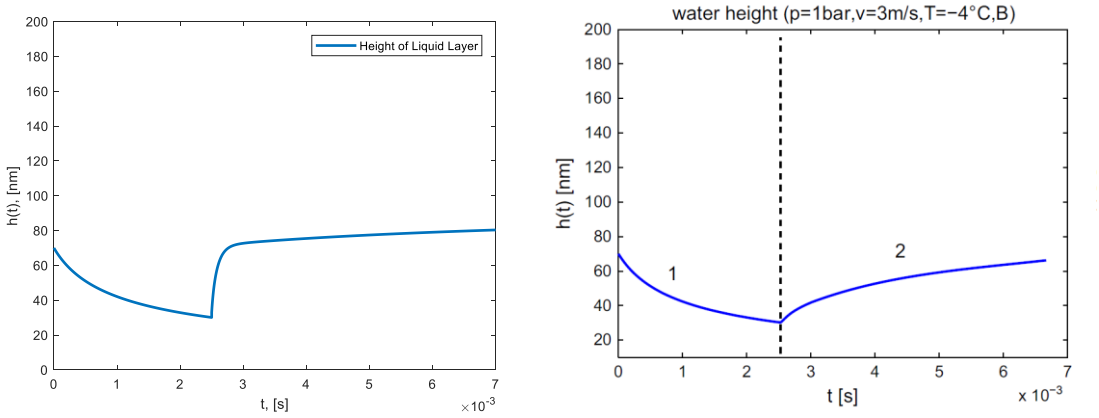

FIGURE 41: ON THE LEFT HAND SIDE, THE MATLAB RESULTS IS SHOWN. ON THE RIGHT HAND SIDE, THE RESULTS OBTAINED IN [3]. BOTH OF THESE PLOTS ARE REFERRED TO 1 BAR OF NOMINAL PRESSURE.

The figure 42 represents the graph of the average squeezed-out height of the water. The *saturation* effect is not present because the value of the pressure is low and the duration of the simulation is too short. The function has a monotonous trend because in the equation (6.19) there are only positive terms. The time at which the melting of the ice occurs is clearly shown by a change of the rate of growth of the curve. However, the prescribed value of the average height of the surface for the medium compound and for 1 bar of nominal pressure was not reached.

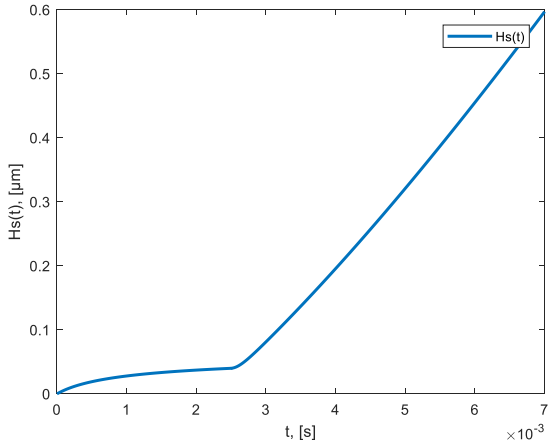

FIGURE 42: THE AVERAGE HEIGHT OF THE SQUEEZED-OUT WATER OBTAINED WITH MATLAB FOR 1 (BAR) OF NOMINAL PRESSURE.

The same comparison was also made with the 5 bar simulation, with similar results, as shown in figure 43.

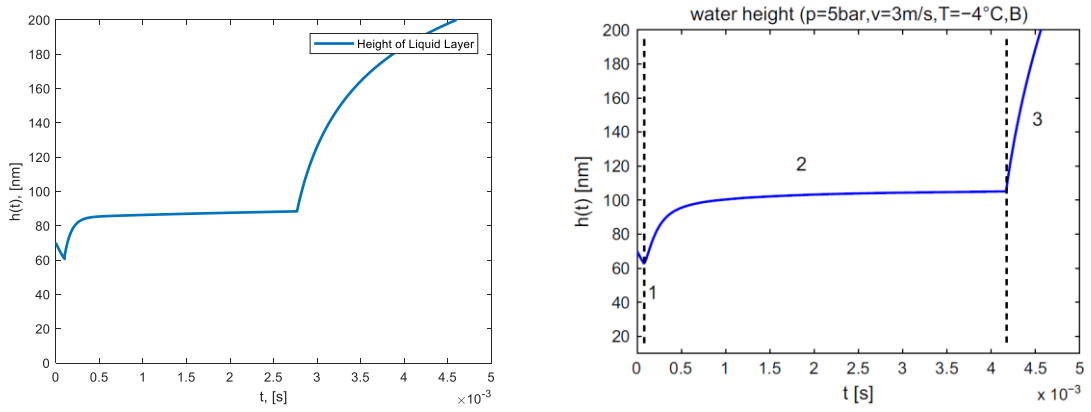

FIGURE 43: ON THE LEFT HAND SIDE, THE MATLAB RESULTS IS SHOWN. ON THE RIGHT HAND SIDE, THE RESULTS OBTAINED IN [3]. BOTH OF THESE PLOTS ARE REFERRED TO 5 BAR OF NOMINAL PRESSURE.

In figure 44, it is possible to observe when the *saturation* occurs. In the Hs(t) function there is a plateau range starting from the saturation point. It means that all the available space on the rubber surface is filled by the water and no more water can be squeezed-out.

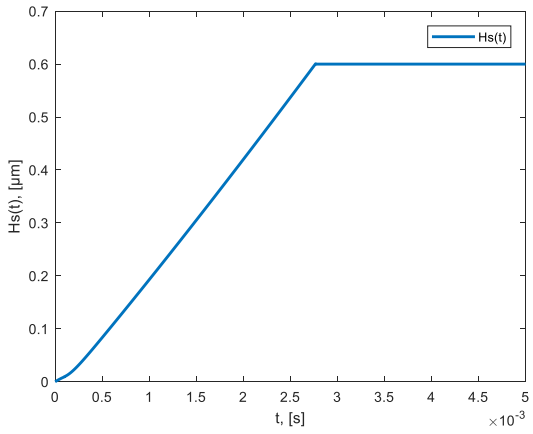

FIGURE 44: THE AVERAGE HEIGHT OF THE SQUEEZED-OUT WATER OBTAINED WITH MATLAB FOR 5 BAR OF NOMINAL PRESSURE.

6.3. LS-DYNA model organization

The complete LS-DYNA model is composed by two parts which work in parallel. The relationship between these two parts is showed in figure (45).

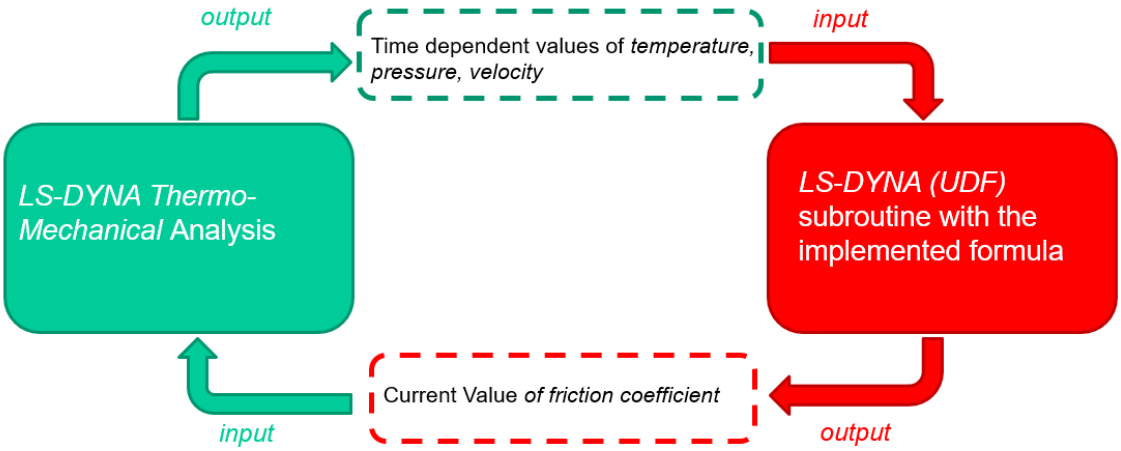

FIGURE 45: SCHEMATIC REPRESENTATION OF THE WHOLE LS-DYNA MODEL, WITH THE LOOP BETWEEN THE LS-DYNA THERMO-MECHANICAL SIMULATION AND THE CUSTOMIZED SUBROUTINE FOR THE CALCULATION OF THE FRICTIONAL COEFFICIENT.

Both these parts are necessary for the calculation of the friction coefficient. The thermo-mechanical part provides all the physical parameters necessary to the algorithm in the subroutine. The subroutine gives as output the current value of the friction coefficient which directly affects all the physical contact parameters. Both the load condition of 1 bar and 5 bar are simulated with this *LS-DYNA* model. To verify the accuracy of the finite element model the results were compared with the ones showed in [3]. Therefore, the material model and all the physical parameters chosen were the same suggested by Wiese et al. [3]. In the finite element model, the thermo-mechanical analysis is composed by two phases:

- The pre-load phase, which is performed using the LS-DYNA option called *dynamic relaxation.* The rubber block is loaded by a nominal pressure, then a boundary condition is assigned when the equilibrium is reached, which leads the sliding velocity of the rubber block to the desired value. The thermal contribute is neglected during this phase. Consequently, a constant value of the friction coefficient is assumed. For this reason, the subroutine calculation is switched off in the pre-load phase.
- The transient phase which is the main part of the whole simulation. The thermo-mechanical simulation and the *User Define Subroutine* start to work in parallel using the initial condition given by the previous pre-load phase.

The division is necessary to start the simulation with the same conditions of the test showed in [3] and consequently to compare the friction coefficient . The rubber block at the beginning of the simulation made in [3] had a constant value of velocity. This condition cannot be imposed as it is in the LS-DYNA simulation because it could give instability due to the high ramp of velocity. A pre-load phase allows to impose to the rubber block a smooth velocity ramp, consequently avoiding high peaks of acceleration.

6.3.1.Geometry and material of the thermo-mechanical model

From a geometrical point of view, the model was built up to reply the physical test condition described by Wiese et al. in [3]. In particular, the model was made up of two objects:

- The rubber block, with a nominal contact area of 1 mm^2
- The ice block, sufficiently long in y-direction for allowing the sliding process at the velocity and for the duration defined in the test.

The figure 48 shows the geometry of the model. To overcome numerical problem in the contact definition, the rubber block is not in contact with the ice in the initial condition. . The direction of the normal pressure coincides with the gravity one, which is $-z$ according to the reference system shown in figure 46, while in [3] is $+z$. The direction of the sliding velocity is along y, the same of the one chosen by Wiese et al. [3].

FIGURE 46: GEOMETRY OF THE LS-DYNA MODEL IN THE INITIAL CONDITION. THE RUBBER BLOCK IS IN BLUE WHILE THE ICE BLOCK IS IN RED.

The LS-DYNA thermo-mechanical analysis needs two different material models for the simulation: a material model for the mechanical part and a material model for the thermal part. The material models that were used in the simulation are:

- The LS-DYNA Mooney-Rivlin material, *MAT_MOONEY-RIVLIN_RUBBER, for the rubber block. The same parameters provided by Wiese et al. [3] for the compound B were used.
- The LS-DYNA rigid material, *MAT_RIGID, for the ice. The deformation of this part was considered negligible in these load conditions.
- The LS-DYNA thermal isotropic material, *MAT_THERMAL_ISOTROPIC, for both ice and rubber. This is the simplest thermal material model available in LS-

DYNA. It was chosen considering the thermal parameters available for the rubber and the ice.

Different choices were also made in the element formulation for the ice block and for the rubber block, in order to improve the accuracy of the results and to reduce the calculation time. In particular:

- For the rubber block, a tetrahedral formulation with one point of integration was adopted. This choice was made considering the high level of deformation under the sliding condition. The idea was to take advantage of the numerical limits of this kind of elements. It is well known as the tetrahedrons are more rigid than the other elements. This condition was used to overcome numerical problems which frequently occur during the sliding simulation.
- For the ice block, the hexahedral elements with a fully-integrated formulation were used.

6.3.2.Contact condition

In the contact between the ice and the rubber there is a significative difference of stiffness. In this particular simulation, there are two more aspects which made the condition even more difficult. The first one is the sliding condition. A lot of numerical instabilities occurred, especially in the leading edge of the rubber block which is affected by a higher level of deformation. The second problem is that a large amount of contact information have to be used in the sub-routine. Hence, the noise in the output parameter has to be reduced as much as possible. For example, if for a single time-step the contact condition failed, the numerical error will be carried for the whole simulation in both areas, the thermo-mechanical one and the subroutine. For the sliding contact, the optimal solution is the *Mortar* contact, particularly suitable for this contact condition.

Unfortunately, this kind of contact is not supported for a simulation with a user-defined subroutine. Hence, a classical type of contact was chosen, with the penalty-stiffness algorithm, named *surface to surface*. Both the ice block and the rubber block were covered with shell elements to avoid instability and contact failure, as well as to improve the accuracy of the contact output data (friction force, temperature rise etc.). For the shell elements the *MAT_NULL was adopted. In figure 47 it is possible to see the graphical effects of this modification. Another important advantage carried by the use of covering shell elements is that a fillet is automatically created at the edges of the blocks. This is particular useful because, with a sharp edge the detecting of the normal is very difficult and, a lot of numerical error can occur.

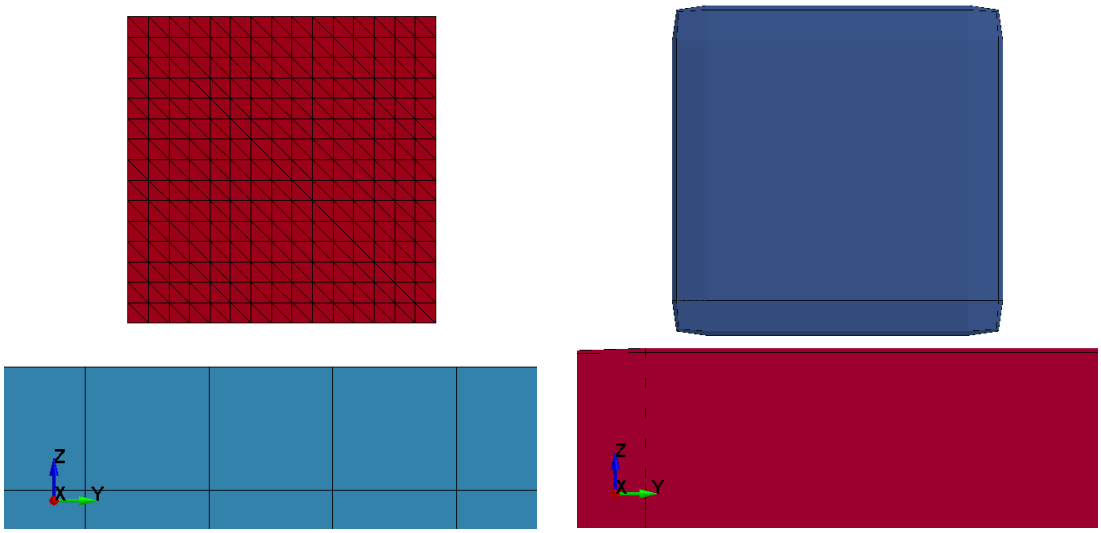

FIGURE 47: GRAPHICAL DIFFERENCE BETWEEN THE ORIGINAL TWO BLOCKS CONDITION AND THE MODIFIED CONDITION WITH SHELL ELEMENTS. ON THE LEFT HAND SIDE, THE RUBBER AND THE ICE BLOCK IN THE ORIGINAL CONFIGURATION. ON THE RIGHT HAND SIDE THE RUBBER AND THE ICE BLOCK COVERED BY THE SHELL ELEMENTS.

6.3.3.Load condition

The load condition is simulated, during the first part of the pre-load phase, applying the load on a rigid plate located near the upper surface of the rubber block. The plate is modelled with shell elements and using a rigid material. The value of the load is obtained by multiplying the nominal area of the contact for the nominal value of the pressure. The aim is to obtain a more realistic deformed shape of the rubber block under the normal pressure load and to have a simpler loading condition. There is no-contact between the rigid plate and the rubber block. The card **CONSTRAINED_EXTRA_NODE* was used to apply the kinematic condition between the two parts. The figure 48 shows the rigid plate on the rubber block.

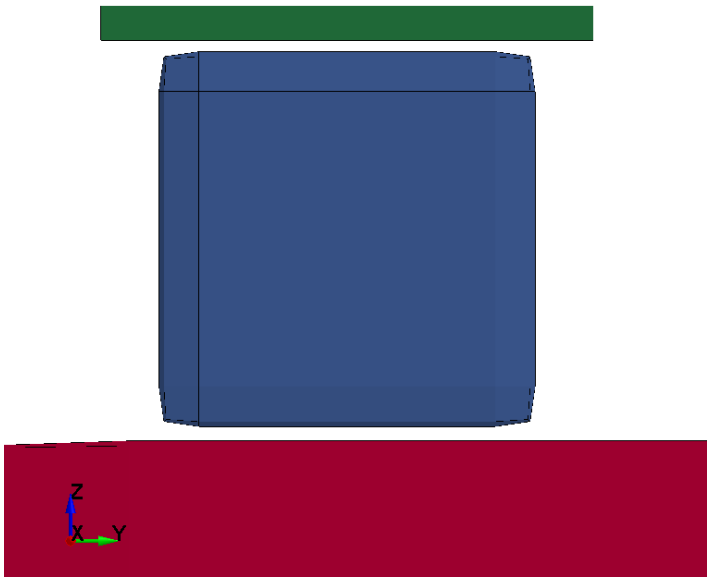

FIGURE 48: RIGID PLATE FOR THE LOAD APPLICATION IN THE INITIAL CONDITION.

6.4. LS-DYNA subroutine

The subroutine works using as input the information obtained with the thermo-mechanical simulation and, for every cycle, it gives as output the current value of friction coefficient, that is used for the next step of the thermo-mechanical simulation. The subroutine consists in a Fortran compiled file, which is recalled, step by step, by the principal *LS-DYNA* code. This is done using a *LS-DYNA* card, called **USER_INTERFACE_FRICTION*. The numerical formulation descripted in the paragraph 6.2, is written in Fortran language. One of the most difficult aspect of writing the subroutine was to adapt the numerical formulation to the LS-DYNA available variables. Not all the necessary parameters to solve the equations shown in paragraph 6.2 were avaialble. For this reason, the numerical formulation was adapted considering the provided input deck of parameters. The calculation of the frictional coefficient has to start during the transient-phase and not in the pre-load one, because in the transient-phase the static friction coefficient is necessary. For this reason, a timing procedure based on the number of cycle of the simulation was developed. With the variable *num* it was possible to recognise the number of time-step of the pre-load phase. When the current time-step number is bigger than the number indicated with the variable *num*, the friction coefficient calculation can start. The effective use of this variable is explained in the following paragraphs.

6.4.1. User define variables and parameters

Two different type of variables are effectively used in the subroutine. The first type of variables are the *User defined friction parameters* $u_c(n_c)$. These friction parameters are defined in the card *USER_INTERFACE_FRICTION*. They are the value of the constant

parameters such as the melting temperature of the ice, the initial temperature, the thermal parameters and so on. For this reason, they are input entity for the subroutine, which are used in the calculation without changing their value. With the symbol n_c the number of these parameters are indicated. In this case, 13 parameters are used. The table 4 shows these entities and the relative value.

Symbol	$u_c(n_c)$	Value and S.I. ( )
rho_{ice}	$u_c(1)$	$916\ \left(\frac{kg}{m^3}\right)$
L_{ice}	$u_c(2)$	$330000\left(\frac{J}{kg}\right)$
λ_{ice}	$u_c(3)$	$2.25\ \left(\frac{W}{m\,K}\right)$
η_{water}	$u_c(4)$	$0.0018\ (Pa \cdot s)$
h_0	$u_c(5)$	$70 \cdot 10^{-9}\ (m)$
c_{ice}	$u_c(6)$	$2220\ \left(\frac{J}{kg\,K}\right)$
α_{ice}	$u_c(7)$	$1.105 \cdot 10^{-6}\ \left(\frac{m^2}{s}\right)$
T_0	$u_c(8)$	$269.15\ (K)$
T_m	$u_c(9)$	$273.15\ (K)$
k	$u_c(10)$	$(-)$
D	$u_c(11)$	(m)
H_v	$u_c(12)$	(m)
f_{st}	$u_c(13)$	$0.1\ (-)$

TABLE 4: USER DEFINED FRICTION PARAMETERS WITH SYMBOL, NUMBERING AND THE INDICATION OF THE NUMERICAL VALUE WITH THE RELATIVE UNIT SYSTEM.

The numerical value of the contact parameters is strictly dependent on the process variables, such as the nominal pressure and the rubber compound. Their numerical values are reported in the following paragraphs. The other type of variables used in the subroutine are the *User defined history friction variables* $u_h(n_h)$. These variables are essential for the script. The numerical explicit method chosen for the solution of the equation (5.22) needs the information at the previous time step to calculate the current value of the variables of interest. This means that a vector in which are stored all the necessary information for each cycle of the simulation has to be created in the subroutine. The dimension of this vector is very large. This aspect affects the calculation time and the memory request for the output file. The *User defined history friction variables* allow to avoid this problem because they give the opportunity to store the variables, working as an input for the next step and as an output for the current step. The numerical value of these variables is overwritten cycle by cycle. In particular, the entities that are associated to this kind of variables are the height of liquid layer, the average height of the squeezed-out water and the friction coefficient.

6.4.2. Stability condition

The user define friction subroutine starts working when the contact between the ice and the rubber is detected. When the rubber block is sliding on the ice surface, it can be possible that some nodes can lose the contact with the ice, for reasons principally related to the definition of the contact algorithm. In this case, the subroutine cannot receive the correct input data and consequently it cannot provide results. These results are stored for each cycle in the user-defined friction variables, consequently the non-contact situations bring to the failure of the entire simulation. For this reason, the numerical formulation considered more than one nodes. The aim of this choice is to avoid the non-contact

situation that leads to a failure into the subroutine script. When one or more nodes are no longer in contact, the formula refers to that/those that are still in contact. However, this procedure introduces a level of inaccuracy of the results, by the fact that the final friction coefficient is the average between the values evaluated for the considered nodes. It is thus necessary to consider as few nodes as possible. The nodes that belong to the leading edge are the most representative of the real temperature condition. However, these nodes are also the ones with the highest risk of non-contact situation. The rubber block has high deformation in that area. The number of nodes used for this calculation was 3. It was defined after a series of attempt. The nodes chosen for calculation are showed in figure 49.

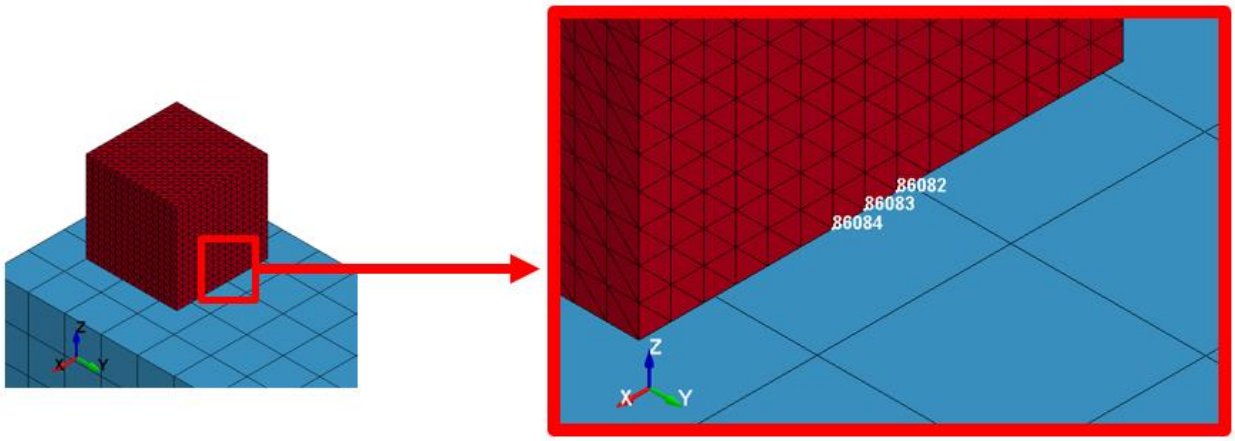

FIGURE 49: CHOSEN NODES FOR THE STABILITY CONDITION ON THE LEADING EDGE OF THE RUBBER BLOCK.

6.4.3.Subroutine code

In the subroutine code the numerical solution of the constitutive equation (5.23) proposed by Wiese et al [3] is implemented. The input parameters are given to the subroutine using

the *user define friction parameters*. The results of each calculation step are given to the thermo-mechanical simulation. The subroutine code is divided in four sections:

1. The initialization of the variables
2. The algorithm for the numerical solution of the constitutive equation for each node
3. The stability condition for each node
4. The calculation of the average friction coefficient

The basic structure of the subroutine code is shown more in detail in the sub-sections below. All the figures present in the following discussion are referred to one node, because the structure is the same for the others. The chosen node is the 86083 shown in figure 49. The following explanations about the structure of the subroutine refer to Appendix A.

Initial condition

The initial condition section consists in three parts.

- Assignment the value of the *user define friction parameters* to the variables involved, such as all the material parameters. The height of the liquid layer, during the pre-load phase has to be also stored in order to maintain the correct initial condition for the first time-step of calculation. These conditions consist in the instructions written in lines 6432,6433,6434 and 6441.
- Detection of the interested node and the calculation timing. The calculation starts when the pre-load phase is ended. This condition is represented by the two *if* conditions at lines 6438 and 6439.
- Even if the calculation is not started and the pre-load phase is not ended, the height of the liquid layer and of the average height of the squeezed-out water have to be stored for the subsequent initial conditions. For this reason, their value was

assigned to the *user defined history friction variables*. The lines 6444,6445 and 6446 are representative of this last condition.

Algorithm for the height of liquid layer

This section of the subroutine contains the numerical solution of the equation (5.23) showed in section 6. Considering the temperature of the node which comes from the thermo-mechanical simulation and the value of the average height of the squeezed-out water which comes from the previous time-step calculation, it is possible to switch in the correct expression of the solution. The effective calculation starts with an *else* condition, which is referred to the previous *if* -statement. The if statement indicates the end of the pre-load phase. It is possible to see the different solution formulations and the formula for the average height of the liquid layer.

- The line 6456 contains the instructions for the calculation of the height of the squeezed-out water for the selected node, as described in paragraph 6 with the equation (6.19).
- The *if*-statement for the *saturation* condition refers to the average height of the squeezed-out water and not for a single node. This is because the non-contact condition can be present at every time-step with a consequent fail of the calculation. This condition is shown at line 6458.
- The second *if*-statement refers to the temperature, at line 6461. If the melting temperature is not reached, the formula for the calculation of the height of the liquid layer is the (6.4), line 6464, else the correct formulation will be the (6.11), line 6468.

- If the average height of the squeezed-out water becomes equal to the average height of the free surface, the calculation switch to the formula which represents the *saturation* effect (6.15), line 6473

Stability condition

The stability condition allows to have a normal termination of the simulation. The condition consists to exclude the nodes where a non-contact situation is detected from the calculation. This was made by using two coefficients, for the node 86083, called AA and mm, with the possibility to have value 0 or 1. If the variable assumes a non-physical value the coefficient associated to that variable is 0, in the other cases it is 1. When the value of the parameter is 0, the variable associated to the node is excluded to the calculation of the average height of liquid layer and so, excluded in the calculation of the friction coefficient. This condition starts at line 6477 and finishes at line 6498.

Calculation of the average friction coefficient

In this part of the subroutine, the calculation concerns the average height of the liquid layer hh, the average height of the squeezed-out water for the three chosen nodes H_{SS} and the average friction coefficient mu_{av}. This section of the subroutine starts the calculation when the pre-load phase is ended, and this condition is expressed by the first *if*-statement at line 6597. If the number of cycle is less than the parameter *num*, which indicates the number of cycles of the pre-load phase, the variables hh, H_{ss} and mu_{av} are set to the initial values. If the number of cycle is greater than the *num* the averaging procedure can start as shown in lines 6606 and 6607. The average friction coefficient mu_{av} has the same expression showed in the equation (5.30). In this case the average value hh is used instead of the single value of the height of liquid layer h, in order to avoid the non-contact situation. An additional *if*-condition is added to the calculation of the average squeezed-

out water. When the value which correspond to the saturation effect is reached, the value of $H_{SS}(t)$ cannot change anymore. This is expressed in line 6610. All these average entities are stored in the *user define history friction variables* and they are used as starting value for the calculation of the next time-step. The numerical coefficient mentioned before for each node avoid numerical failure of the simulation. The last command (line 6623) associates the calculated value of the friction coefficient to the name of the variable effectively used in the original *LS-DYNA* code $fstt$. This condition starts at line 6594 and finishes 6623.

6.5. Simulation results

In this section the results obtained with the *LS-DYNA* model are showed. Two different tests are conducted with different level of pressure as proposed by Wiese et al. [3]. At the end of this paragraph the results obtained with this *LS-DYNA* model will be compared to the data obtained in [3]. The parameters used for the simulations of the two tests are the same and their values are showed in table 6.

Operational parameters	**Value**
Duration of the simulation	$7 \cdot 10^{-3}\ (s)$
Sliding velocity	$3\ (m/s)$
Initial temperature	$-4\ (°C)$

TABLE 5: OPERATIONAL PARAMETERS FOR THE LS-DYNA SIMULATION

The rubber compound is also the same for both the simulations. The mechanical properties and the Mooney-Rivlin parameters for the rubber compound with medium stiffness are the same suggested in [3]. The table 7 shows these entities:

Material parameters	Value
Young modulus E	1.64 (MPa)
Density ρ	1100 $(kg/m\text{^}3)$
Poisson modulus ν	0.495 $(-)$
C_{10}	0.1662 (MPa)
C_{01}	0.1068 (MPa)
D_1	0.0737 (MPa)

TABLE 6: MATERIAL PARAMETERS FOR MEDIUM RUBBER COMPOUND

6.5.1.Simulation with 1 bar of nominal pressure

The contact parameters in this case are showed in table 8.

Parameters	$\boldsymbol{p_{nom} = 1\ (bar)}$
$\boldsymbol{k}$	0.266 $(-)$
$\boldsymbol{D}$	$29.0 \cdot 10^{-6}\ (m)$
$\boldsymbol{H_v}$	$2.86 \cdot 10^{-6}\ (m)$

TABLE 7: CONTACT PARAMETERS FOR THE LS-DYNA SIMULATION WITH 1 BAR OF NOMINAL PRESSURE.

The figure 50 shows the results of this simulation in terms of friction coefficient. Two phases are shown. In the first phase, where the squeeze-out effect is present, the friction coefficient has high value. In the second phase with the melting of the in which a downward trend of the friction coefficient is shown.

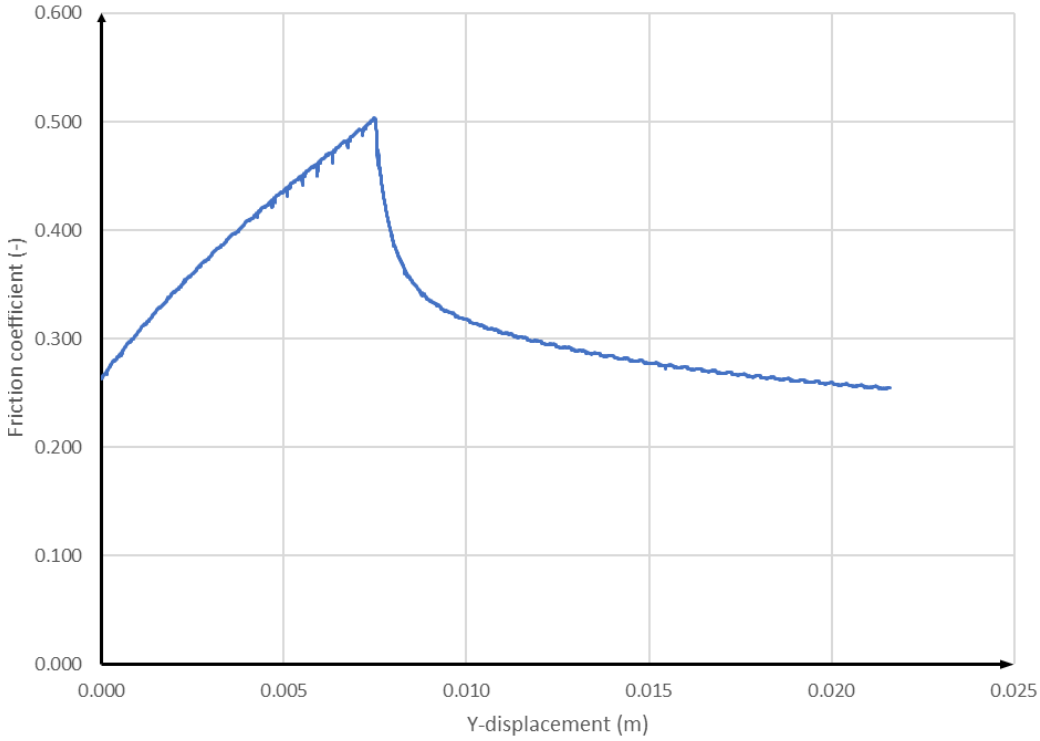

FIGURE 50 FRICTION COEFFICIENT AS A FUNCTION OF THE DISPLACEMENT WITH A NOMINAL PRESSURE OF 1 BAR

The results in term of the friction coefficient and the related bending level of the rubber block, during the whole simulation, are shown in figure 51. Different values of the friction coefficient affect the deformation of the rubber block. The higher the friction coefficient, the higher the bending of the rubber block. In the lower part of the figure 51 the relationship between the shape of the rubber block and the friction coefficient is detailed. This image considers only the phase 1, when the squeeze-out phenomena is the principal effect. On the y-axis it is possible to see the value of the friction coefficient whereas in the x-axis there is the relative value of the displacement. The highest value of the friction coefficient is about 0.5. The deformation (bending) of the rubber block at that point is the highest. This is due to the strict relation between the thermo-mechanical simulation and the subroutine script.

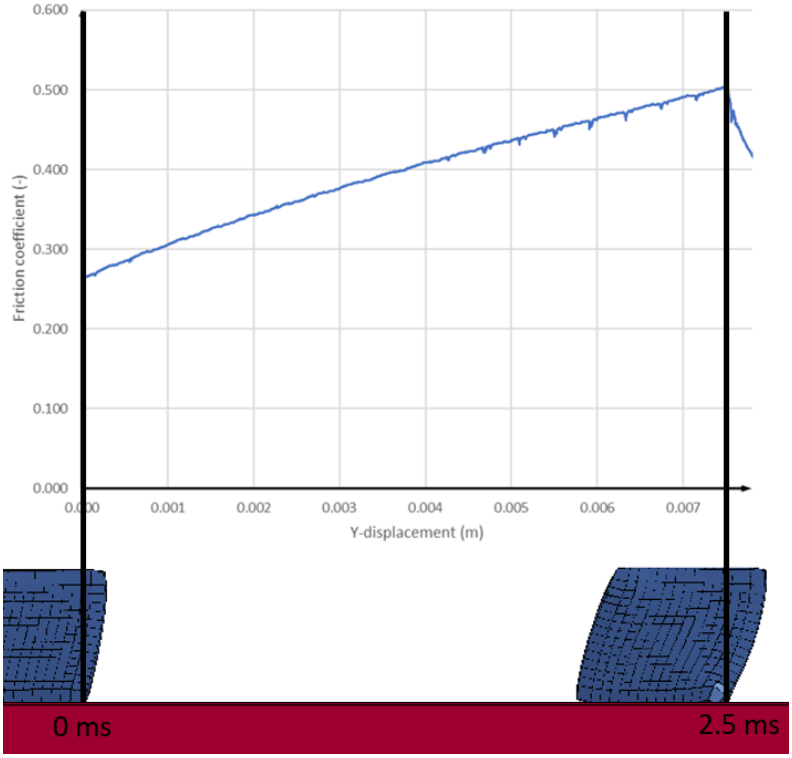

FIGURE 51: IN THE UPPER PART THE FRICTION COEFFICIENT IN FUNCTION OF THE DISPLACEMENT IS SHOWN, IN THE LOWER PART THE RUBBER BLOCK DEFORMED AT THE BEGINNING AND AT THE END OF THE SIMULATION IS SHOWN. THE CONDITION WITH THE SQUEEZE-OUT EFFECT FOR A NOMINAL PRESSURE OF 1 BAR IS CONSIDERED.

The reverse condition is showed in figure 52, which represents the second part of the same test. In this phase the melting temperature was reached and the effect of the squeeze-out is not so important. For this reason, the value of the friction coefficient drops. The bending level of the rubber block decreases as the y-displacement increases.

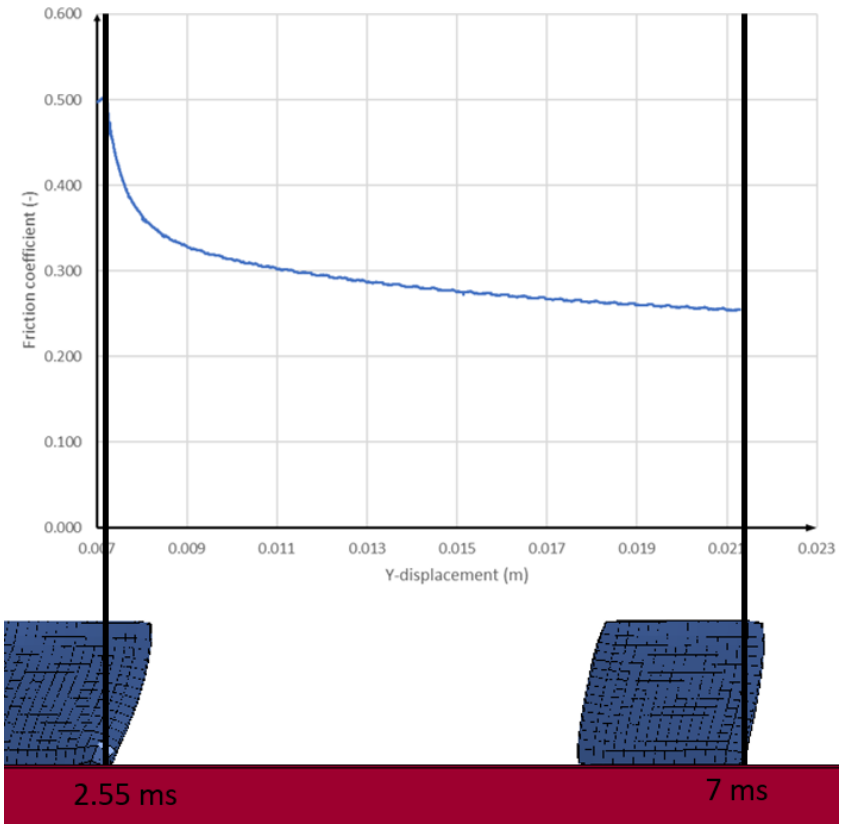

FIGURE 52: IN THE UPPER PART THE FRICTION COEFFICIENT IN FUNCTION OF THE DISPLACEMENT IS SHOWN, IN THE LOWER PART THE RUBBER BLOCK DEFORMED AT THE BEGINNING AND AT THE END OF THE SIMULATION IS SHOWN. THE CONDITION WITH THE SQUEEZE-OUT EFFECT AND THE MELTING OF THE ICE FOR A NOMINAL PRESSURE OF 1 BAR IS CONSIDERED.

6.5.2.Simulation with 5 bar of nominal pressure

The contact parameters for this simulation are showed in table 9.

Parameters	$\boldsymbol{p_{nom} = 5\ (bar)}$
$\boldsymbol{k}$	$0.105\ (-)$
$\boldsymbol{D}$	$46.5 \cdot 10^{-6}\ (m)$
$\boldsymbol{H_v}$	$5.6 \cdot 10^{-7}\ (m)$

TABLE 8: CONTACT PARAMETERS FOR THE LS-DYNA SIMULATION WITH 5 BAR OF NOMINAL PRESSURE

In this case the level of pressure and the duration of the simulation allow to take into consideration all the phenomena described in the chapter 5. In the figure 53 the friction coefficient as a function of the sliding displacement is shown. It is possible to distinguish three different phases. The first two phases were also present in the result of the previous simulation (1 bar of nominal pressure). In this case there is also a third effect, the *saturation*. A fast decrease of the friction coefficient is due to this effect.

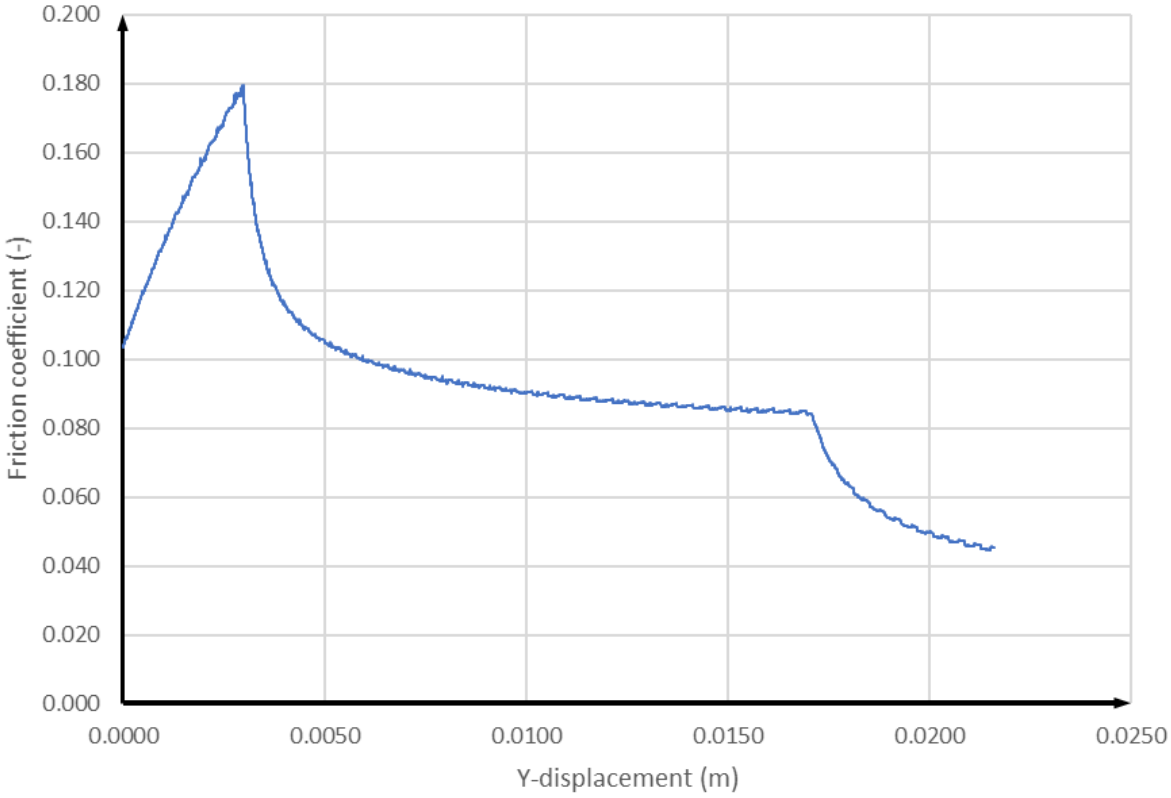

FIGURE 53: FRICTION COEFFICIENT AS A FUNCTION OF THE DISPLACEMENT WITH A NOMINAL PRESSURE OF 5 BAR

In this case the deformation of the rubber is quite high. The absolute value of the friction coefficient is, in general, lower than the previous case (1 bar of nominal pressure). The higher level of the pressure leads to the melting temperature in a considerably shorter time. However, the load condition and the friction coefficient cause an extreme

deformation for the rubber block. Here the stability condition defined in the subroutine was very useful because the non-contact situation is more frequent. The high level of the deformation of the rubber block in the first phase with the *squeeze-out* effect is shown in figure 54.

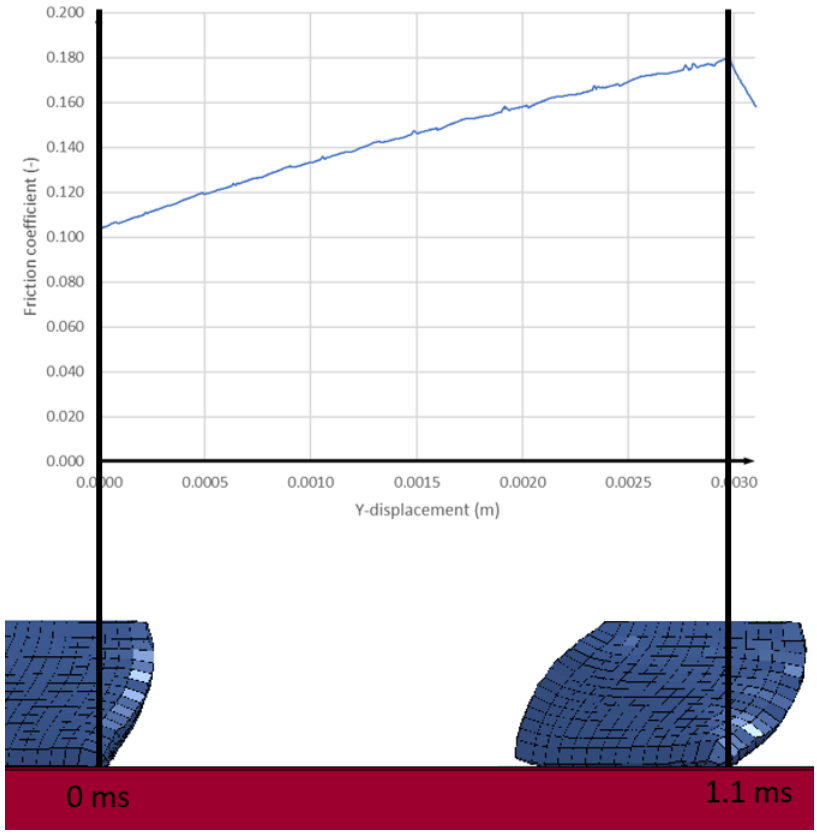

FIGURE 54: IN THE UPPER PART THE FRICTION COEFFICIENT IN FUNCTION OF THE DISPLACEMENT IS SHOWN, IN THE LOWER PART THE RUBBER BLOCK DEFORMED AT THE BEGINNING AND AT THE END OF THE SIMULATION IS SHOWN. THE CONDITION WITH THE SQUEEZE-OUT EFFECT FOR A NOMINAL PRESSURE OF 5 BAR IS CONSIDERED

In the next phase, with the melting of the ice, the deformation is lower. In this second phase, the non-contact situations are less frequent. In the figure 55 the bending behaviour of the rubber block in relation to the value of the friction coefficient is shown.

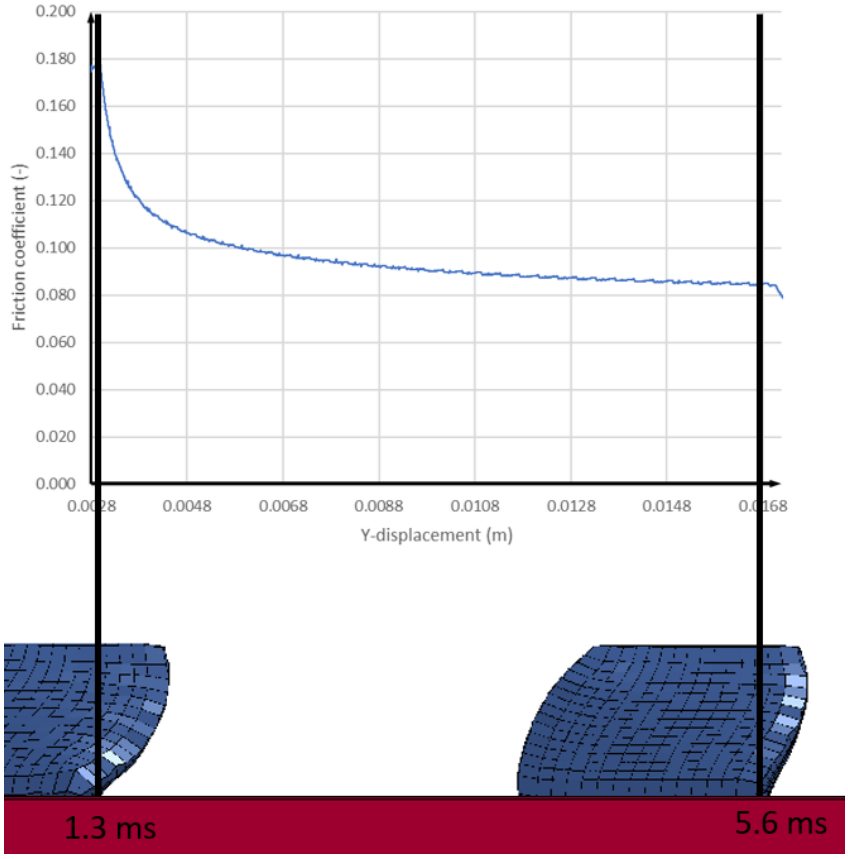

FIGURE 55: IN THE UPPER PART THE FRICTION COEFFICIENT IN FUNCTION OF THE DISPLACEMENT IS SHOWN, IN THE LOWER PART THE RUBBER BLOCK DEFORMED AT THE BEGINNING AND AT THE END OF THE SIMULATION IS SHOWN. THE CONDITION WITH THE SQUEEZE-OUT EFFECT AND THE MELTING OF THE ICE FOR A NOMINAL PRESSURE OF 5 BAR IS CONSIDERED

The third phase is characterized by the saturation effect. This causes which leads to a steep fall of the value of the friction coefficient. This is due to the big amount of the water made by the melting of the ice which cannot be stored anymore because all the free space in the rubber surface is filled. The deformation of the rubber block is representative of this behaviour. The figure 56 shows a deformation of the rubber related to the drop of the friction coefficient.

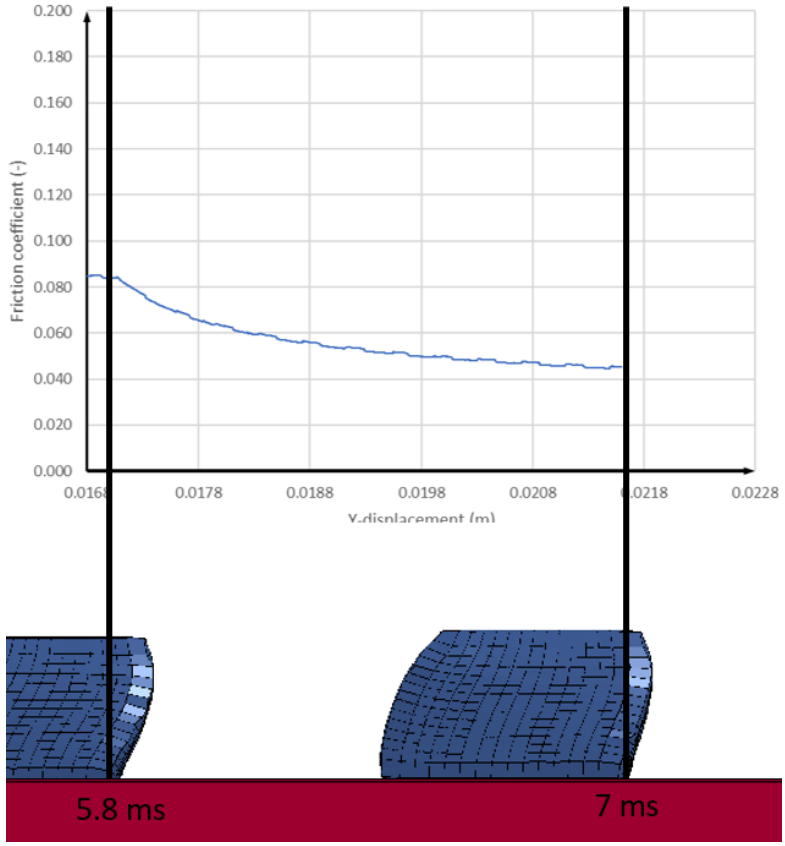

FIGURE 56: IN THE UPPER PART THE FRICTION COEFFICIENT IN FUNCTION OF THE DISPLACEMENT IS SHOWN, IN THE LOWER PART THE RUBBER BLOCK DEFORMED AT THE BEGINNING AND AT THE END OF THE SIMULATION IS SHOWN. THE CONDITION WITH THE SATURATION EFFECT FOR A NOMINAL PRESSURE OF 5 BAR IS CONSIDERED

6.5.3. Comparison between the LS-DYNA model and the Wiese model

In this section, a comparison between the results obtained with the simulation performed with LS-DYNA and the results obtained by Wiese et al. [3] are proposed for a nominal pressure of 1 and 5 bar. In both the simulations there is a certain level of discrepancy. This is due to the uncertainness about the thermal property of the rubber compound and for the ice. These uncertainness lead to a different timing between the simulation and the results proposed by Wiese et al. [3].

Nominal pressure of 1 bar

The simulation with the value of 1 bar is shown in figure 57. The absolute value of the friction coefficient is in good agreement with the paper result. The time at which the melting temperature is reached is also very similar (about 2.5 ms). At this time, the peak of the friction coefficient obtained with the *LS-DYNA* simulation is 0.51 while in the paper it is about 0.55.

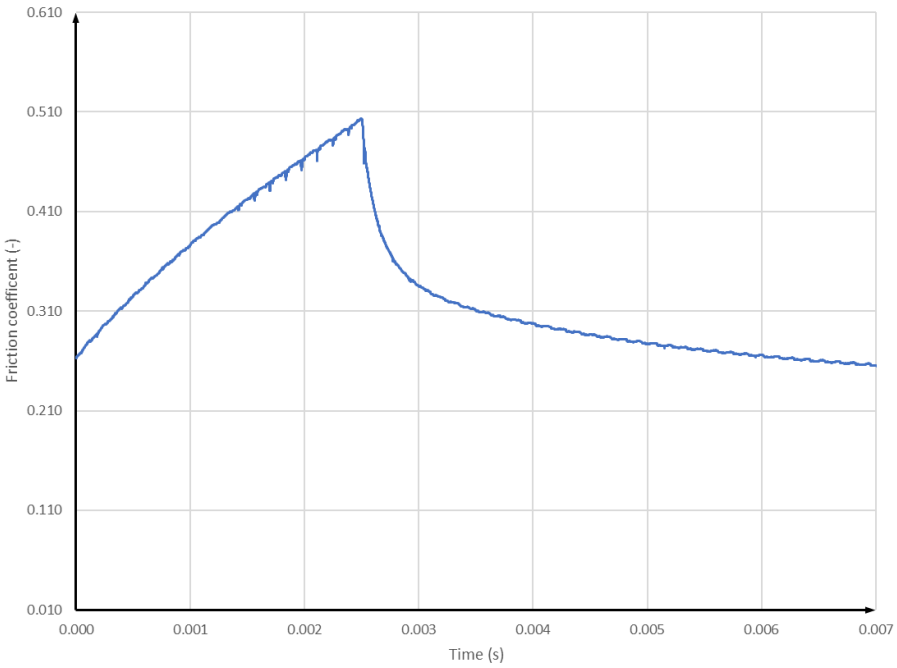

FIGURE 57: FRICTION COEFFICIENT VERSUS TIME FOR 1 BAR OF NOMINAL PRESSURE OBTAINED WITH LS-DYNA

The result showed in [3] are in logarithmic scale. For this reason, the same graph of the figure 58 is represented in logarithmic scale, in order to be compared with the paper result. The shape of the two curves, that is the general trend of the curves is also very similar. The uncertainness on the material parameters lead to have a little degree of anticipation on the time at which the melting temperature is reached. This means that, the absolute value of the friction coefficient will be lower than the one obtained in [3]. These effects

are shown in figure 58 where the red curve represents the *LS-DYNA* model's results while the blue curve is representative of the results obtained in [3].

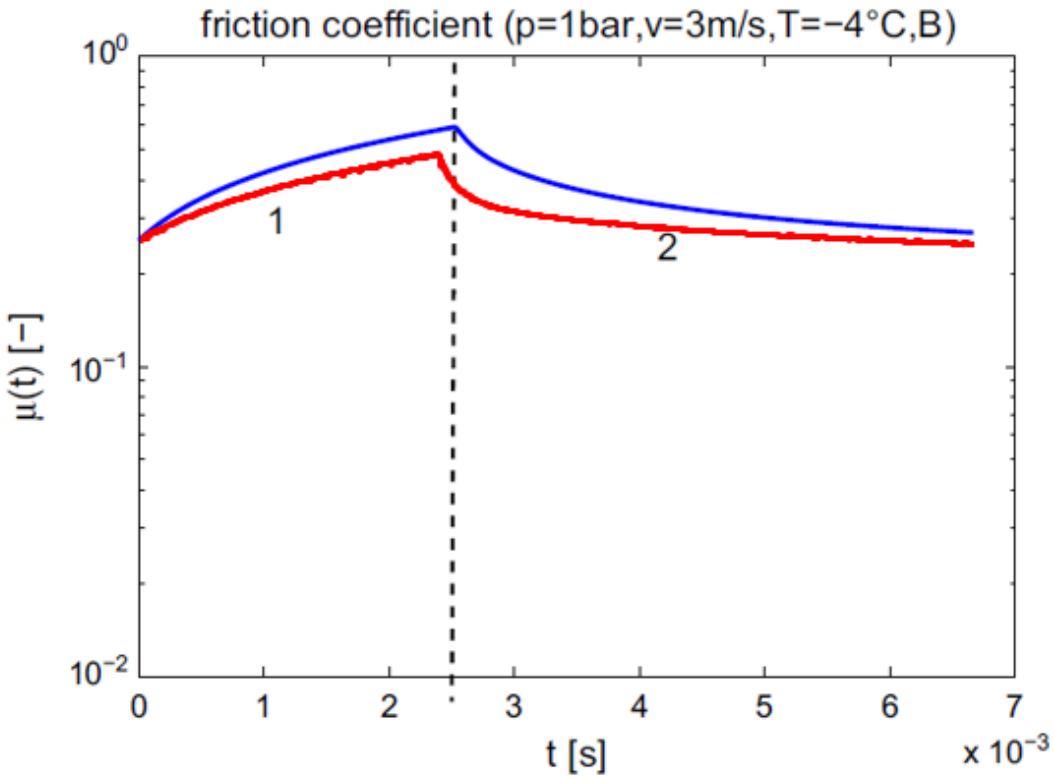

FIGURE 58: OVERLAPPING OF THE LS-DYNA MODEL'S RESULTS CURVE (IN RED) AND THE WIESE'S RESULTS (IN BLUE) [3] FOR 1 BAR OF NOMINAL PRESSURE.

Nominal pressure of 5 bar

The comparison shows also some differences in this case. The melting temperature is reached with a 1 *ms* of delay respect to the results obtained by Wiese et al. [3]. This delay affects also the absolute maximum value of the friction coefficient obtained in the LS-DYNA simulation, which is higher than the one obtained in [3]. This is due to the squeeze-out phase which has a longer duration. The reasons of these differences are mainly due to the uncertainty about the correct value of the thermal parameters of the ice and of the rubber. Moreover, the material model does not take into account the

viscoelastic effects of the deformation of the rubber. The figure 59 shows the friction coefficient obtained with LS-DYNA in function of the time.

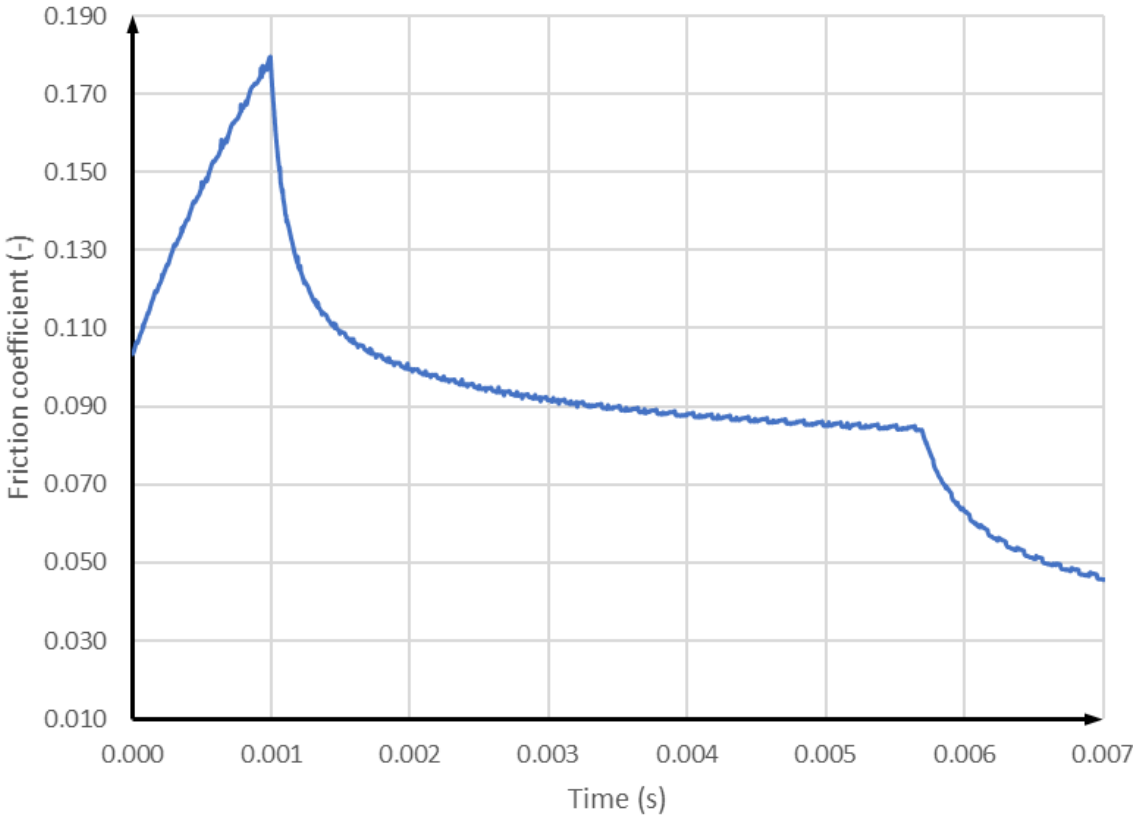

FIGURE 59: FRICTION COEFFICIENT VERSUS TIME FOR 5 BAR OF NOMINAL PRESSURE OBTAINED WITH LS-DYNA

In the figure 60, the comparison between the LS-DYNA results and the results showed in [3], is proposed in logarithmic scale. Similarly to the 1 bar simulation, also in this case the uncertainness on the material parameters influence the timing of the simulation. The effect of the time-delay is represented in figure 60 where it is possible to see that, a different melting time leads to have a different saturation time and so, the absolute value of the friction coefficient has a certain level of discrepancy.

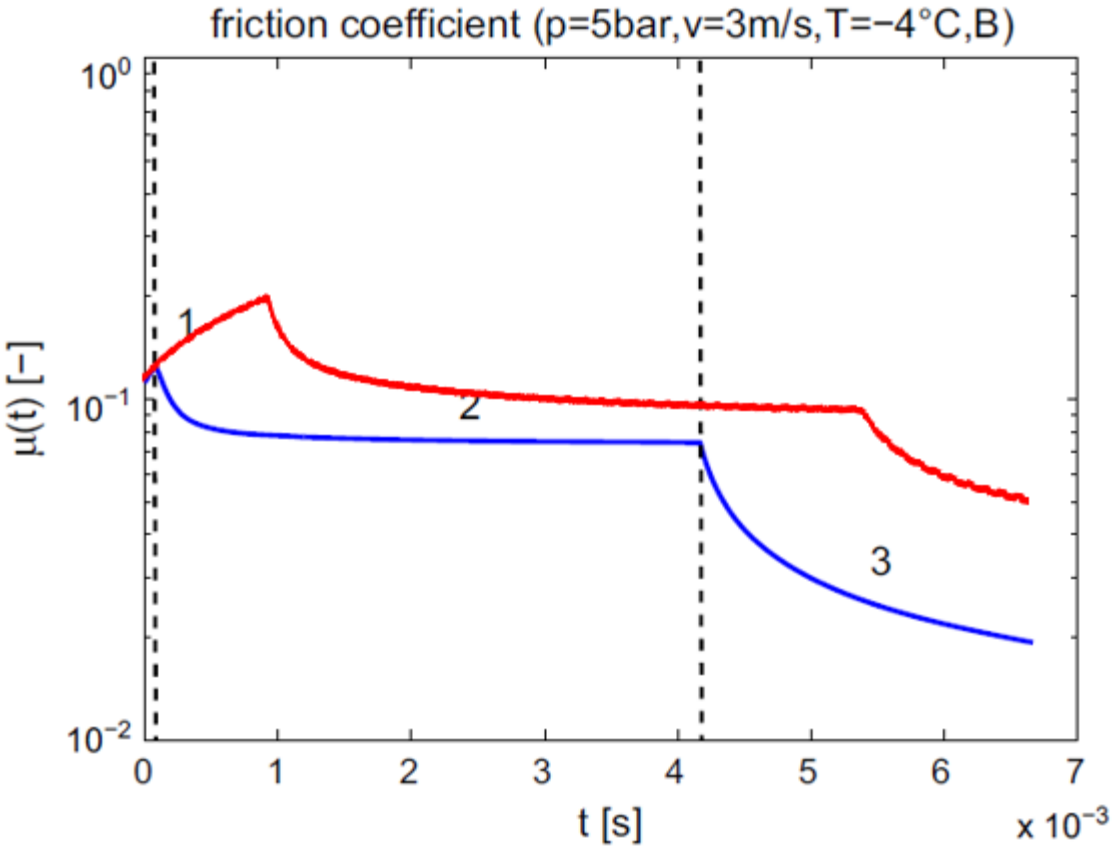

FIGURE 60: OVERLAPPING OF THE LS-DYNA MODEL'S RESULTS CURVE (IN RED) AND THE WIESE'S RESULTS (IN BLUE) [3] FOR 5 BAR OF NOMINAL PRESSURE.

Chapter 7

7. Conclusion

A *LS-DYNA* model was developed to simulate the contact between the tire and the icy road condition. The simulation of this contact situation is very challenging, considering the number and the type of the involved physical phenomena. In particular, the worst condition for the tire is when the adherence is lost and the rolling is replace by the sliding motion. At this point, melting of the ice and related hydrodynamic effects occur. To take into account these effects, a small block sample of the whole tire is considered as subject of the FEM model. To simulate the microscopic sliding behaviour of this rubber block on the ice, a customized subroutine was developed. The results obtained with the FEM model show a good agreement with the models proposed in literature. A short delay (1 ms) of the melting point of the ice is the unique discrepancy obtained between the numerical model developed in this work and that of Wiese et al. [3]. The methodology proposed for a single rubber block could be implemented considering more complex geometries. The calculation described in this work can be applied to each node of the model in contact between the two parts. This aspect can be useful if only a particular area on the contact patch should be studied. Future developments could be represented by the possibility to include also the macroscopic hydrodynamic effects. Moreover, a material model for the rubber, where the viscoelastic effects are taken into account should be used. As final step, the application of this methodology to a whole tire could be associated with a specific ALE modulus for the hydrodynamic behaviour in order to study the effect of the shape of the tread.

Appendix A

Subroutine script

Lines: from 6259 to 6301

```
      subroutine usrfrc(fstt,fdyn,uc,nc,prs,temp,v,vx,vy,vz,uh,nh,
     . crv,nnpcrv,nosl,
     . ictype,side,time,ncycle,dt2,fric1,fric2,fric3,fric4,lsv,idele8,
     . sfac1,sfac2,insv,fni,areas,stfk,ix1,ix2,ix3,ix4,aream,
     . rn1,rn2,rn3,ue,ne,uhnew)
c
c*******************************************************************
c|  Livermore Software Technology Corporation  (LSTC)              |
c|  ------------------------------------------------------------  |
c|  Copyright 1987-2008 Livermore Software Tech. Corp             |
c|  All rights reserved                                           |
c*******************************************************************
c
c     user subroutine for interface friction control (mpp)
c
c     Purpose: To define static and dynamic frictional
c              coefficients for a slave node
c
c     Variables:
c
c     fstt            = static frictional coefficient (output)
c     fdyn            = dynamic frictional coefficient (output)
c     uc(nc)          = user defined friction parameters (input)
c     nc              = number of user defined friction parameters (input)
c     prs             = interface pressure (input)
c     temp            = temperature (input, available for coupled analysis)
c                       ... not yet supported for SOFT=4
c     v               = magnitude of relative tangential velocity (input)
c     vx,vy,vz        = components of relative tangential velocity (input)
c     uh(nh)          = user defined friction history variables (input/output)
c     uhnew(nh)       = user defined friction history variables (input/output)
c     nh              = number of user defined friction history variables (input)
c     crv             = curve array (input)
c     nnpcrv          = # of discretization points per crv()
c     nosl            = number of sliding interface (input)
c     ictype          = contact type (input)
c     side            = 'master' for 1st pass or 'slave' for 2nd pass (input)
c     time            = current solution time (input)
c     ncycle          = number of current cycle (input)
c     dt2             = time step size at n+1/2 (input)
c     fric1           = static friction coefficient FS from keyword (input)
c     fric2           = dynamic friction coefficient FD from keyword (input)
c     fric3           = decay constant DC from keyword (input)
```

Lines: from 6302 to 6346

```
c     fric4           = viscous friction coefficient VC from keyword (input)
c     lsv             = master segment number (input)
c     idele8          = external user element number of master segment (input)
c     sfac1           = Coulomb friction scale factor FSF from keyword (input)
c     sfac2           = Viscous friction scale factor VSF from keyword (input)
c     insv            = slave node user id (input) only for output purpose
c     fni             = normal force (input)
c     areas           = slave node area (input)
c     stfk            = penalty stiffness (input)
c     ix1,ix2,ix3,ix4 = master segment nodes - internal node numbers (input)
c                       (external user node numbers: ix1ext=lqfinv8(ix1,1) ...)
c     aream           = master segment area (input)
c     rn1,rn2,rn3     = x,y,z components of master segment normal (input)
c     ue(ne)          = user defined friction element data (input)
c                       (not yet supported for SOFT=4)
c                         1 - plastic strain
c                         2 - yield stress (materials 24,36,37,106,224,243,244)
c                         3,4,5 - x,y,z components of material direction
c                                 (materials 36,103,133,243)
c     ne              = number of user defined friction element variables (input)
c     Hs(nt)          = average squeezed-out water height
c     h(nt)           = water height
c     mu(nt)          =friction coefficient
c     nt              = number of timestep
      implicit none
      include 'nlqparm'
      real*8 fstt,fdyn
      integer*8 lqfinv
      external lqfinv
      integer*8 nc,nh,nosl,ictype,ncycle,lsv,insv,ix1,ix2,ix3,ix4
      integer*8 ne,nt
      real*8 uc(nc),uh(nh),uhnew(nh),ue(ne)
      real*8 prs,temp,v,time,dt2,fric1,fric2,fric3,fric4,sfac1,sfac2,
     .     fni,areas,stfk,aream,rn1,rn2,rn3,vx,vy,vz,mu,Hs,h,num
      real*8 press,rho,L,lambda,eta,h0,c,alpha,T0,Tm,pnom1,
     .     k1,D1,Hv1,Cost1,Cost2,Cost3,dt,xx,vv,h2,Hs2,mu2,h3,Hs3,
     .     mu3,AA,BB,CC,DD,EE,FF,hh,muav,Hss,h4,h5,h6,mu4,mu5,mu6,
     .     Hs4,Hs5,Hs6,h7,h8,h9,mu7,mu8,mu9,Hs7,Hs8,Hs9,GG,II,LL,mm,
     .     nn,oo,pp,qq,rr,ss,tt,uu,ww,www
      real*8 crv(lq1,2,*)
      integer*8 nnpcrv(*)
      character*(*) side
      integer*8 idele8
      real*8 pi
      parameter (pi=3.14)
```

Lines: from 6399 to 6441

```
      num=19500
      vv=3
c      Cost1=k1*eta*v**2/(rho*L)
      Cost1=uc(10)*uc(4)*vv**2/(uc(1)*uc(2))
c
c
c      Cost2=lambda*(Tm-T0)/(rho*L*(pi*alpha)**0.5)
      Cost2=uc(3)*(uc(9)-uc(8))/(uc(1)*uc(2)*(pi*uc(7))**0.5)
c      press=fni/areas
      press=1e5
c     Cost3=8*press/(3*eta*D1**2)
      Cost3=8*press/(3*uc(4)*uc(11)**2)
c
c     Time-step from LS-Dyna, does it possible to know the
c     name of this parameter?
c      dt=tfin/N
c      dt2-->da usare!
c
c
c
c
c
c
c
c
c     Initial Condition
c
c
c
c     node 86083
c
c     Initial Condition
c
      eta=uc(4)
      k1 =uc(10)
      Hv1=uc(12)
c
c
c
      if (insv.eq.86083) then
      if(ncycle.LT.num)then
c
        h=uc(5)
```

Lines: from 6442 to 6486

```
c
c
        uh(1)=h
        Hs=0
        uh(2)=Hs
c
c
      else
        Hs=uh(2)
        h=uh(1)
        mu=uh(3)
c
c     Algorithm for the Height of Liquid Layer
c
      Hs=Hs+dt2*Cost3*(h**3)
c
      if(Hss.LT.uc(12))then
c
c
      if(temp.LT.uc(9))then
c
c
          h=h-dt2*(Cost3*h**3)
c
c
      else
          h=h+dt2*((Cost1/h)-(Cost2/((time)**0.5))-(Cost3*h**3))
      endif
c
c
      else
         h=h+dt2*((Cost1/h)-(Cost2/((time)**0.5)))
      endif
      endif
c
c     Stability Condition
c
c
      if(h.eq.0)then
      AA=0
      else
      AA=1
      endif
c
c
```

Lines: from 6847 to 6530

```
6487        if(h.gt.1)then
6488        h=0
6489        AA=0
6490        endif
6491  c
6492  c
6493        if(hs.eq.0)then
6494        mm=0
6495        else
6496        mm=1
6497        endif
6498        endif
6499  c
6500  c
6501  c  node 86084
6502  c
6503  c
6504        if (insv.eq.86084) then
6505        if(ncycle.LT.num)then
6506          h2=70e-9
6507          uh(4)=h2
6508          Hs2=0
6509          uh(5)=Hs2
6510        else
6511          Hs2=uh(2)
6512          h2=uh(1)
6513          mu2=uh(3)
6514  c
6515  c     Algorithm for Friction Coefficient
6516        Hs2=Hs2+dt2*Cost3*(h2**3)
6517        if(Hss.LT.uc(12))then
6518        if(xx.LT.uc(9))then
6519            h2=h2-dt2*(Cost3*h2**3)
6520        else
6521            h2=h2+dt2*((Cost1/h2)-(Cost2/((time)**0.5))-(Cost3*h2**3))
6522        endif
6523        else
6524           h2=h2+dt2*((Cost1/h2)-(Cost2/((time)**0.5)))
6525        endif
6526        endif
6527        if(h2.eq.0)then
6528        BB=0
6529        else
6530        BB=1
```

Lines: from 6531 to 6575

```
6531        endif
6532        if(h2.gt.1)then
6533        h2=0
6534        BB=0
6535        endif
6536  c
6537        if(hs2.eq.0)then
6538        nn=0
6539        else
6540        nn=1
6541        endif
6542        endif
6543  c
6544  c
6545  c
6546  c
6547  c
6548  c
6549  c  nodo 86082
6550  c
6551  c
6552        if (insv.eq.86082) then
6553        if(ncycle.LT.num)then
6554          h3=70e-9
6555          uh(7)=h3
6556          Hs3=0
6557          uh(8)=Hs3
6558        else
6559          Hs3=uh(2)
6560          h3=uh(1)
6561          mu3=uh(3)
6562  c
6563  c     Algorithm for Friction Coefficient
6564        Hs3=Hs3+dt2*Cost3*(h3**3)
6565        if(Hss.LT.uc(12))then
6566        if(xx.LT.uc(9))then
6567           h3=h3-dt2*(Cost3*h3**3)
6568        else
6569           h3=h3+dt2*((Cost1/h3)-(Cost2/((time)**0.5))-(Cost3*h3**3))
6570        endif
6571        else
6572          h3=h3+dt2*((Cost1/h3)-(Cost2/((time)**0.5)))
6573        endif
6574        endif
6575        if(h3.eq.0)then
```

Lines: from 6576 to 6620

```
6576        CC=0
6577        else
6578        CC=1
6579        endif
6580        if(h3.gt.1)then
6581        h3=0
6582        CC=0
6583        endif
6584        if(hs3.eq.0)then
6585        oo=0
6586        else
6587        oo=1
6588        endif
6589        endif
6590  c
6591  c
6592  c
6593  c
6594  c     Average Friction Coefficient
6595  c
6596  c
6597        if(ncycle.LT.num)then
6598  c
6599  c
6600        hss=70e-9
6601        muav=uc(13)
6602  c
6603        else
6604  c
6605  c
6606        hh=(h+h2+h3)/(AA+BB+CC)
6607        muav=k1*eta*vv/(press*hh)
6608  c
6609  c
6610        if(Hss.LT.uc(12))then
6611        Hss=(Hs+Hs2+Hs3)/mm+nn+oo
6612        else
6613        Hss=uc(12)
6614        endif
6615        endif
6616        endif
6617  c
6618        uh(1)=hh
6619        uh(2)=Hss
6620  c
```

Lines: from 6621 to 6652

```
6621        uh(3)=muav
6622  c
6623        fstt=muav
6624  c
6625        if (insv.eq.86083.and.mod(ncycle,1).eq.0) then
6626          write(11,*) 'h',hh,'Hs',Hss,'mu',muav,'cycle',ncycle,'temp',xx
6627        endif
6628        if (insv.eq.86083.and.mod(ncycle,1).eq.0) then
6629          write(111,*) 'h',h,h2,h3,'cyc',ncycle
6630        endif
6631        if (insv.eq.86083.and.mod(ncycle,1).eq.0) then
6632          write(1,*) Hss,www,hs,hs2,hs3,ncycle
6633        endif
6634        if (insv.eq.86083.and.mod(ncycle,1).eq.0) then
6635          write(2,*) ww,www,mm,nn,oo,ncycle
6636        endif
6637        if (insv.eq.86083.and.mod(ncycle,1).eq.0) then
6638          write(3,*) 'h',hh,'Hs',Hss,'mu',muav,'press',press,prs,ncycle
6639        endif
6640  c
6641  c     set coefficients to keyword values
6642  c
6643  c     fstt=fric1
6644  c     fdyn=fric2
6645  c
6646  c     define frictional coefficients as function of temperature via load curve
6647  c
6648  c     call crvval(crv,uc(1),temp,fstt,fdyn)
6649  c     fdyn=fstt
6650  c
6651        return
6652        end
```

Bibliography

[1] Persson BNJ. Theory of rubber friction and contact. J Chem Phys 2001;115 (8):3840–61.

[2] Tuononen, A. J., Kriston, A. & Persson, B. Multiscale physics of rubber-ice friction. *The J. Chem. Phys.* **145**, 114703 (2016).

[3] C. Klapproth, T. M. Kessel, K. Wiese, and B. Wies, "An advanced viscous model for rubber–ice-friction," Tribol. Int. **99**, 169–181 (2016).

[4] A. K. Bhoopalam, C. Sandu, and S. Teheri, "A tire-ice model (TIM) for traction estimation," Journal of Terramechanics **66**, 1–12 (2016).

[5] Kessel TM, Mundl R, Wies B, Wiese K. An analytical thermodynamical approach to friction of rubber on ice.TireSciTechnol2012;40(2):124–50..

[6] B.N.J. Persson, E. Tosatti: The effect of surface roughness on the adhesion of elastic solids, J. Chem. Phys. **115**, 5597–5610 (2001).

[7] Scaraggi M, Persson BNJ. General contact mechanics theory for randomly rough surfaces with application to rubber friction.

[8] O. Lahayne, B. Pichler, R. Reihsner, J. B. Suh, D. S. Kim, S. K. Nam, H. S. Paek, B. Lorenz, and B. N. J. Persson, "Rubber friction on ice: Experiments and modeling," Tribology Lett.

[9] Kishore Bhoopalam, A. 2015. Pneumatic Tire Performance on Ice. Faculty of the Virginia Polytechnic Institute and State University. Luettu 20.3.2018

[10] The Engineering ToolBox <http://www.engineeringtoolbox.com/ice-thermal-

properties-d_576.html>.

[11] Smithers Rapra <https://www.smithersrapra.com/testing-services/by-sector/automotive/tire-testing/footprint>.

[12] Carslaw HS, Jaeger JC. Conduction of heat in solids. Oxford: Oxford Press; 1959.

[13] C. Canuto, Modelli e Metodi Numerici-2013.

[14] LS-DYNA Manual R10.0 Vol I, Vol II